TESIS DOCTORAL

THE HISTORY OF A SURFACE IN A SINGLE LASER SHOT: FROM ULTRAFAST CARRIERS EXCITATION TO PLASMA EMISSION, FADING, AND BEYOND

Irene María Carrasco García

Directores: Javier Laserna Vázquez y José Miguel Vadillo Pérez

UNIVERSIDAD DE MÁLAGA

Facultad de Ciencias

Programa de Doctorado en Química y Tecnologías Químicas, Materiales y Nanotecnología

UNIVERSIDAD DE MÁLAGA

Málaga 2020

UNIVERSIDAD
DE MÁLAGA

AUTOR: Irene María Carrasco García

http://orcid.org/0000-0002-4677-0997

UNIVERSIDAD
DE MÁLAGA

DOCTORAL THESIS

UNIVERSIDAD DE MÁLAGA

THE HISTORY OF A SURFACE IN A SINGLE LASER SHOT: FROM ULTRAFAST CARRIERS EXCITATION TO PLASMA EMISSION, FADING, AND BEYOND

By

IRENE MARÍA CARRASCO GARCÍA

THESIS SUBMITTED IN PARTIAL FULFILMENT OF THE REQUIREMENTS TO APPLY FOR THE DEGREE OF DOCTOR

Departamento de Química Analítica

Facultad de Ciencias

Universidad de Málaga

Málaga, 2020

THE HISTORY OF A SURFACE IN A SINGLE LASER SHOT: FROM ULTRAFAST CARRIERS EXCITATION TO PLASMA EMISSION, FADING, AND BEYOND

por **IRENE MARÍA CARRASCO GARCÍA**

José Javier Laserna Vázquez
Catedrático de Universidad
Departamento de Química Analítica
Universidad de Málaga

José Miguel Vadillo Pérez
Catedrático de Universidad
Departamento de Química Analítica
Universidad de Málaga

Memoria de Tesis presentada para optar al título de Doctor

Irene María Carrasco García

Málaga, 2020

JOSÉ JAVIER LASERNA VÁZQUEZ, Catedrático del Química Analítica de la Universidad de Málaga y **JOSÉ MIGUEL VADILLO PÉREZ**, Catedrático de Química Analítica de la Universidad de Málaga

CERTIFICAN

Que **IRENE MARÍA CARRASCO GARCÍA** ha realizado bajo su dirección la presente Tesis Doctoral titulada "**THE HISTORY OF A SURFACE IN A SINGLE SHOT: FROM ULTRAFAST CARRIERS EXCITATION TO PLASMA EMISSION, FADING, AND BEYOND**" en el Laboratorio Láser del Departamento de Química Analítica de la Universidad de Málaga, y que el conjunto de publicaciones aportadas para avalar el trabajo científico no han sido utilizadas en Tesis anteriores, reuniendo a nuestro juicio los requisitos necesarios y autorizando, por ello, su presentación para optar al grado de Doctor.

Y para que así conste a los efectos oportunos firman las presente, en Málaga a 2020

Prof. José Javier Laserna Vázquez   Prof. José Miguel Vadillo Pérez

UNIVERSIDAD
DE MÁLAGA

UNIVERSIDAD
DE MÁLAGA

ANDALUCÍA TECH
Campus de Excelencia Internacional

Vicerrectorado Estudios de Posgrado
Servicio de Posgrado y Escuela de Doctorado

DECLARACIÓN DE AUTORÍA Y ORIGINALIDAD DE LA TESIS PRESENTADA PARA OBTENER EL TÍTULO DE DOCTOR

D./Dña IRENE MARÍA CARRASCO GARCÍA

Estudiante del programa de doctorado QUÍMICA Y TECNOLOGÍAS QUÍMICAS. MATERIALES Y NANOTECNOLOGÍA de la Universidad de Málaga, autor/a de la tesis, presentada para la obtención del título de doctor por la Universidad de Málaga, titulada: THE HISTORY OF A SURFACE IN A SINGLE LASER SHOT: FROM ULTRAFAST CARRIERS EXCITATION TO PLASMA EMISSION, FADING, AND BEYOND

Realizada bajo la tutorización de JOSÉ MIGUEL VADILLO PÉREZ y dirección de JOSÉ JAVIER LASERNA VÁZQUEZ (si tuviera varios directores deberá hacer constar el nombre de todos)

DECLARO QUE:

La tesis presentada es una obra original que no infringe los derechos de propiedad intelectual ni los derechos de propiedad industrial u otros, conforme al ordenamiento jurídico vigente (Real Decreto Legislativo 1/1996, de 12 de abril, por el que se aprueba el texto refundido de la Ley de Propiedad Intelectual, regularizando, aclarando y armonizando las disposiciones legales vigentes sobre la materia), modificado por la Ley 2/2019, de 1 de marzo.

Igualmente asumo,ante a la Universidad de Málaga y ante cualquier otra instancia, la responsabilidad que pudiera derivarse en caso de plagio de contenidosen la tesis presentada, conforme al ordenamiento jurídico vigente.

En Málaga, a 20 deFEBRERO de 2020

Fdo.:IRENE MARÍA CARRASCO GARCÍA

EFQM AENOR   BUREAU VERITAS   bequal

Edificio Pabellón de Gobierno, Campus El Ejido,
29071
Tel.: 952 13 10 28 / 952 13 14 61 / 952 13 71 10
E-mail: doctorado@uma.es

TESIS DOCTORAL POR COMPENDIO DE PUBLICACIONES

En cumplimiento con los requisitos especificados en el Reglamento de Doctorado de la Universidad de Málaga, la presente Tesis Doctoral ha sido autorizada por los Directores de Tesis y el Órgano Responsable del Programa de Doctorado para ser presentada en el formato de "compendio de publicaciones".

Las referencias de los artículos en los que el doctorando figura como primer o segundo autor y que avalan la presente Tesis Doctoral se detallan a continuación de acuerdo con su orden cronológico de publicación:

- I. Carrasco-García, J. M. Vadillo, J. J. Laserna, Visualization of surface transformations during laser ablation of solids by femtosecond pump–probe time-resolved microscopy, Spectrochim. Acta Part B 113 (2015) 30–36.
- I. Carrasco-García, J. M. Vadillo, J. J. Laserna, Monitoring the dynamics of the surface deformation prior to the onset of plasma emission during femtosecond laser ablation of noble metals by time-resolved reflectivity microscopy, Spectrochim. Acta Part B 131 (2017) 1–7.
- I. M. Carrasco-García, J. M. Vadillo, J. J. Laserna, Wavelength and energy dependence on ablation dynamics under femtosecond laser pulses observed by time-resolved pump–probe microscopy, Spectrochim. Acta Part B 158 (2019) 105634.
- I. Carrasco-García, J. M. Vadillo, J. J. Laserna, Onset of optical emission in femtosecond laser-induced plasmas and its correlation with surface dynamics monitored by pump–probe time-resolved microscopy, J. Anal. At. Spectrom. 34 (2019) 2119.

AGRADECIMIENTOS

Aunque no lo parezca, creo que ésta es la parte más difícil. Hay mucha gente a la que agradecer el apoyo que me han ofrecido durante la investigación y redacción de esta tesis, y muy poco espacio para decirles todo a todos.

En primer lugar, quiero dar las gracias a mi director Javier Laserna por la oportunidad que me ofreció para realizar esta tesis en el Laboratorio Láser. He recibido muchos consejos, he aprendido muchísimo y lo he disfrutado. Gracias a mi codirector de tesis José Miguel Vadillo. Me llevo muchas lecciones aprendidas sobre muchos aspectos, de los que espero poner en práctica.

Quiero dar las gracias por la financiación para desarrollar el proyecto en el que se enmarcan los trabajos presentados en esta Tesis, ofrecida por el Ministerio de Economía, Competitividad e Industria de España. Esta ayuda se corresponde con las Ayudas para la Formación de Personal Investigador (FPI) asociadas al proyecto CTQ2011-24433.

Gracias al profesor John T. Costello y Paddy Hayden. La estancia en la DCU bajo su equipo -fue increíble. Es toda una experiencia salir de tu zona de confort y trabajar con otros grupos para crecer, aprender cómo se trabaja en otros grupos y técnicas nuevas. Gracias además por el trato y la atención que nos dieron a Antonio y a mí.

Gracias a Valentín Guadaño, por todas las horas que has pasado ayudando a resolver problemas con el equipo. Lo que he aprendido a nivel de funcionamiento del equipo es increíble. La forma en que explicabas todo ha sido fundamental para poder desarrollar estos experimentos.

Gracias a todos mis compañeros del Laboratorio Láser que me han prestado ayuda en todo momento. Tomás y Fran, gracias por esos consejos sobre cómo funcionan los dispositivos más quisquillosos, las risas, la experiencia. Patricia, Luisa, Belén, y Carmunchita sois mis estrellitas guías. Me habéis tratado como si fuera una hermana vuestra.

Gracias a María del Mar Pérez y Ana Yebra, del grupo de Óptica de Biomateriales de la Universidad de Granada. Con vosotras empecé a investigar, así que en este trabajo hay una contribución vuestra, la semilla de la curiosidad. Todo lo que he aprendido como profesoras mías espero que lo ponga en práctica a la hora de ganar experiencia tratando con los demás. Me he llevado tanto cariño de vosotras que es imposible olvidar lo que he aprendido y lo bien que me he sentido.

Al equipo de la red BOOTES, resultado de la colaboración entre el Instituto de Astrofísica de Andalucía (IAA-CSIC), la unidad del CSIC asociada a la Universidad de Málaga y muchas otras instituciones. En especial Alberto Castro. La oportunidad que he tenido de investigar en los Gamma Ray Burst con personas tan maravillosas como los miembros, no tiene precio. Aprendo de todo con Emilio, Carlos, Alberto y Youndong, y estoy deseando que siga así.

Gracias a mi familia. Todo el agradecimiento es poco para describir el apoyo que he recibido en todo momento. Muchos fines de semana analizando imágenes en el salón mientras veíamos "Big Bang" o "El precio de la historia", y poco a poco tuvimos que cambiar por "Los Minions" y "Los Vengadores". Cuánta paciencia y comprensión me habéis dado. Incluso quienes no están "presentes" en estos momentos, nunca habéis dejado de acompañarme, y sé que siempre me apoyáis. En especial le tengo que dar las gracias a Antonio. Eres la luz de mi vida. Una sonrisa, un abrazo o un beso tuyo te "recarga las pilas" al máximo. Me has acompañado muchas horas dentro de mí, y luego a mi lado. Todo esfuerzo es poco para agradecerte la felicidad que me aportas, sobre todo cuando voy a recogerte y escucho ese "¡Mamá!" que hasta a las monitoras les encanta.

Olalla y Edu. Tantas "ensalsadas" que nos hemos dado para celebrar los buenos momentos. Ahora tenemos excusa para una más. Pero no pueden faltar Mari Cruz, ni mi antipartícula Trini. A Sara González. Ni siquiera un océano es capaz de separarnos, y que no falte mi peque Sara Husein. A mis "Puretas del Caribe"; Rafa, Ana, María y Sadia. Como el vino, mejoramos con los años, y vamos cogiendo experiencia y compartiendo momentos. Gracias a David por todos los momentos en los que me ha ayudado y revisado la redacción, y toda la amistad que me das. Gracias a Lucie, mi "mazetita" favorita. Después de tantos años seguimos siendo amigas. Cris. Irene, Salomecita. Pasan los años y aquí seguimos. La idea de los "desagradecimientos" es completamente original. María, Desirée. Más de 30 años de amistad, se dice pronto. He crecido con vosotras y siempre me habéis animado incluso sin pedirlo.

Por supuesto, y no menos importante, a Toastmasters Málaga y mis "Toasties" de otros clubes. Me habéis ayudado, aconsejado. No sabía todas las cosas buenas que podía sacar de mí. Gracias a vosotros he perdido el miedo a hablar en público, he ganado confianza, y ahora soy consciente de que puedo mejorar todavía más. No puedo nombraros a todos por desgracia, porque nos estamos haciendo una familia muy grande, pero no puedo evitar no nombrar la inspiración infinita de Claudia, quien además me ha ayudado tanto con mis

dudas en el estilo de la redacción, o las evaluaciones que me dan mi mentora Laura, Magda, Rea o Vincent.
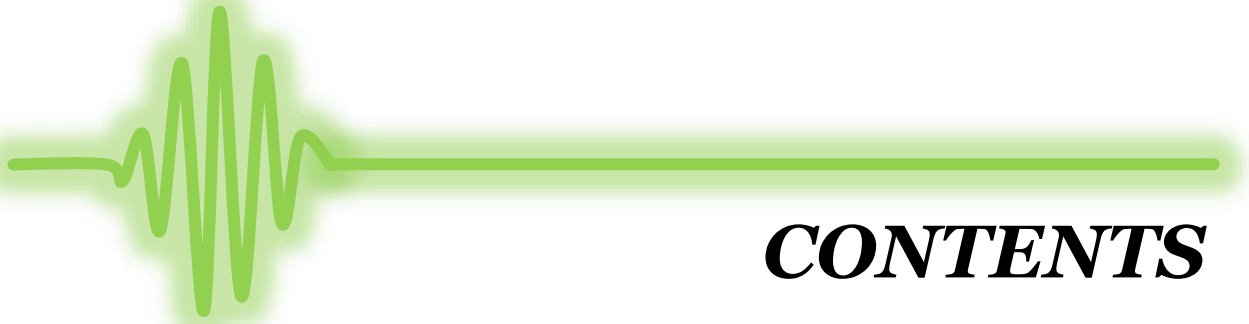
CONTENTS
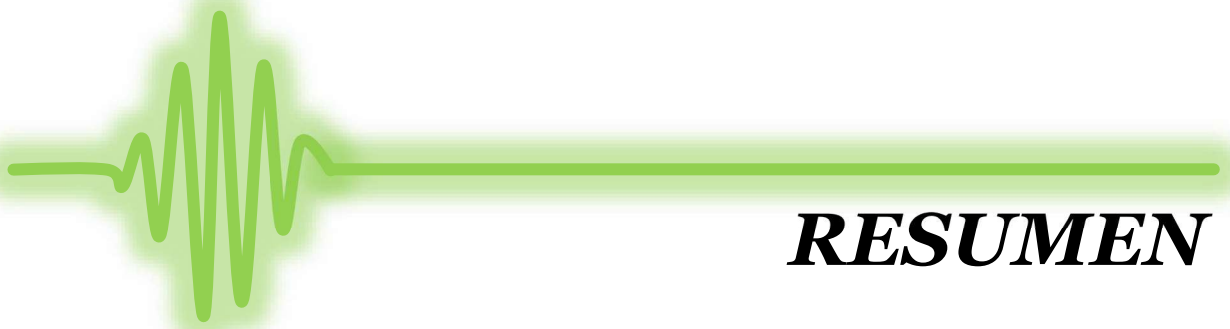
RESUMEN

En cumplimiento con los estatutos de Doctorado de la Universidad de Málaga, se incluye un resumen de este trabajo. Se introducen los aspectos fundamentales que han apoyado la base para desarrollar los estudios incluidos en esta Tesis Doctoral, y por consiguiente una breve descripción de los resultados más significativos.

El desarrollo de la tecnología asociada a la emisión láser ha abierto nuevas y variadas aplicaciones, como restauración del patrimonio histórico y cultural, procesos de mecanizado en la industria, o cirugía. El éxito observado en los resultados experimentales ha incrementado el interés en la investigación de nuevas aplicaciones y una mayor eficiencia. En la mayoría de las aplicaciones en las que la luz láser está involucrada, el proceso fundamental resultante de la interacción con un material es la ablación. La ablación consiste en eliminar una cierta cantidad de material, que puede incluir un rango de varios átomos, hasta suficiente masa para provocar un cráter o daño observable en la superficie de la muestra. Esta cantidad de masa dependerá de características como la luz láser irradiada, la naturaleza del material, y las condiciones experimentales requeridas en relación con los resultados esperados en la aplicación seleccionada.

Entre las características de la luz láser que pueden influir en la interacción láser-materia, se puede destacar la fuerte relevancia de la longitud de onda del láser, la fluencia del láser, o el ancho del pulso. Están involucrados en los procesos morfológicos del material, de acuerdo con sus propiedades físicas y químicas, y en caso de que se supere un cierto umbral de energía, se produce la ablación del material. En condiciones experimentales satisfactorias, la masa ablacionada se vaporiza, alcanzando altas temperaturas que terminan en la formación de plasma. Hay otras condiciones experimentales que se pueden considerar cuando se produce la ablación en los materiales, como la presión ambiental o la composición de la atmósfera circundante al material irradiado. Estas condiciones también pueden influir en la formación y evolución del plasma como resultado de la interacción de las especies del plasma excitadas con los componentes de la atmósfera circundante.

En este sentido, una de las técnicas que ha obtenido una impactante repercusión en investigación para aplicaciones ha sido la espectroscopia de plasmas inducidos por láser (LIBS, Laser-induced breakdown spectroscopy). Esta técnica utiliza una fuente láser para inducir la ablación de materiales y producir plasmas, que pueden proporcionar una valiosa información cuantitativa y cualitativa de las muestras de interés. La técnica LIBS ofrece

varias ventajas y versatilidad respecto a otras técnicas analíticas. Entre estas características cabe destacar que no es necesaria una preparación previa de la muestra y que permite realizar análisis de materiales tanto en laboratorios o incluso a una distancia del láser o detector.

Del mismo modo que se ha incrementado el número de campos de investigación en los cuales su pueden encontrar equipos láser como componentes activos de la configuración experimental, los avances tecnológicos han desarrollado grandes avances en los sistemas de emisión láser, alcanzando anchos de pulso láser realmente estrechos en el dominio del tiempo. Hace algunas décadas, la implementación de la técnica de "chirped pulse amplification" (CPA) condujo a una reducción del ancho temporal de los pulsos láser hasta un intervalo de tiempo situado en el rango de los femtosegundos. Para obtener estos pulsos ultracortos de forma efectiva, la técnica CPA se aplica en tres pasos que se encuentran implementados en una cabina amplificadora. En primer lugar, se inyecta en la cabina un pulso semilla de una fuente láser, que es estirado por un sistema óptico dispersivo en esta etapa. El estiramiento es seguido por la segunda etapa, que consiste en la amplificación gracias a la adición de una segunda fuente láser que se agrega sincrónicamente con el primer pulso láser. Finalmente, el pulso es comprimido en la tercera etapa por otro medio dispersivo que compensa el estiramiento, y obtiene como resultado un pulso láser ultracorto. Los resultados experimentales que se muestran en esta Tesis se han llevado a cabo con un sistema láser de femtosegundo, con un cristal titanio-zafiro como medio de ganancia.

La ventaja fundamental de los láseres de femtosegundo con respecto a los pulsos láser más largos es que casi toda la energía del pulso láser se deposita en la muestra y ha terminado antes de que se produzca cualquier proceso de relajación de la red cristalina. Esto significa que los mecanismos de transporte de energía como fusión o ablación no se rigen por la conducción térmica en la muestra, al contrario que la irradiación con pulsos láser más largos. Esto ha dado lugar a una mejora de algunas aplicaciones, entre las que caben destacar un mecanizado más preciso con una zona más pequeña afectada por el calor y cráteres bien definidos, así como se ha informado de un umbral de ablación más bajo en los materiales. La ausencia de interacción láser-plasma después de la irradiación con altas energías utilizando láseres de femtosegundo ha reportado algunos resultados interesantes. Se ha monitorizado que la emisión de continuo en los primeros instantes de vida de plasma es menor, y una diferente propagación de especies excitadas en la pluma del plasma. Por otro lado, los plasmas producidos con láser de femtosegundo tienen una temperatura más baja que los producidos con pulsos láser más anchos. Estos motivos requieren por tanto una

explicación física completamente diferente del transporte de energía, que afecta tanto al campo electromagnético del pulso láser como los procesos producidos en la muestra.

Cuando el láser alcanza la muestra, el primer proceso que acaece es la excitación de los electrones de la muestra. En el caso de los metales, los electrones de la superficie recibirán un aumento de su energía por parte del campo electromagnético del pulso láser. En semiconductores y dieléctricos, si la energía del pulso es suficiente para superar la banda de energía prohibida de su red, los electrones de la banda de valencia se excitan a la banda de conducción. En todos los casos, esta excitación conlleva un aumento de la densidad electrónica en la superficie de la muestra que puede tomar un intervalo entre cientos de femtosegundos hasta algunos picosegundos. Seguido por la excitación de electrones, comienza la desexcitación del subsistema electrónico, pero en ese momento, el pulso láser ya ha terminado y no hay energía adicional suministrada a la muestra. Esto significa que la fusión del material irradiado se inicia durante la desexcitación de electrones ya sea por colisiones con otros electrones o con los fonones de la red cristalina.

Estas colisiones se propagan hacia el interior de la muestra como una onda mecánica que pierde su energía progresivamente con cada colisión hasta que desaparece y se genera la interfaz entre el material fundido y el material sólido. Esta onda mecánica deja tras de sí un volumen de material fundido que genera una onda térmica. Cuando esta onda térmica llega a la interfaz entre el material fundido y el material sólido, se refleja y se propaga hacia la superficie de la muestra. Durante el camino de vuelta, se propaga a través del material fundido, lo empuja hacia afuera e induce la formación de un gradiente de densidad en el volumen fundido. Este gradiente de densidad deja como resultado de progresiva formación una mezcla de material líquido-vapor. Mientras tanto la interfaz material-aire permanece como una capa muy delgada sólido-líquido de varios nanómetros de profundidad, ya que no ha sido alcanzado por la onda térmica reflejada.

A medida que el material fundido expande hacia la superficie por la onda reflejada, empuja a la capa más externa de material sólido-líquido, y experimenta una deformación gradual, con la forma de una cúpula. La curvatura de la cúpula aumenta a medida que la mezcla gas-líquido se expande hasta que finalmente se rompe, y todo el material encapsulado se expulsa en dirección perpendicular a la superficie de la muestra. Este material se encuentra a una temperatura extremadamente alta por lo que está en estado de plasma y compuesto por átomos excitados, electrones, iones y moléculas que se expanden con un haz de forma cilíndrica y hacia adelante. A medida que este plasma se expande, las especies excitadas se desexcitan mediante procesos de recombinación o colisiones con partículas de la atmósfera

circundante y se observa la formación de un espectro de emisión continua. La expansión e interacción del plasma con la atmósfera disminuye progresivamente su temperatura y densidad, y las líneas de emisión características de cada material emergen de la emisión continua. La intensidad de estas líneas de emisión alcanzará un máximo, y finalmente su intensidad disminuye hasta que el material ablacionado se enfría.

Esta descripción es el resultado de la combinación de un abundante número de estudios inter y multidisciplinarios, incluyendo modelos teóricos y resultados experimentales obtenidos mediante diferentes técnicas. Se puede destacar desde el punto de vista experimental la contribución de técnicas de imagen como interferometría, shadowgrafía o microscopía de sonda-prueba. Estas técnicas tienen en común que utilizan un primer pulso láser con alta energía o pulso de prueba. Un segundo pulso láser débil, también conocido como pulso de sonda, interroga el área de interés y se registra la imagen obtenida. Si la luz de la sonda se retrasa en intervalos temporales respecto al pulso de prueba, estas técnicas se pueden utilizar para estudios con resolución temporal. La shadowgrafía ofrece una vista lateral de la evolución que sigue la pluma de plasma después de la eyección del material. Por otro lado, la interferometría se puede utilizar tanto para las vistas laterales como delanteras del objetivo y ofrece información relevante de acuerdo con el cambio de fase de la luz de la sonda después de interrogar el plasma.

La microscopía sonda-prueba nos permite mientras tanto visualizar la dinámica de las alteraciones morfológicas inducidas en la superficie de los materiales a partir de su excitación. Esta técnica utiliza el pulso de prueba e inicia el proceso de ablación en la muestra. El pulso de sonda es lo suficientemente débil como para evitar cualquier daño adicional en el objetivo, y actúa como una lámpara de flash que ilumina el área donde el pulso de prueba ha irradiado la muestra previamente. Cuando el haz de sonda se retrasa con respecto al haz de prueba, refleja el efecto del pulso de prueba en los intervalos temporales de interés, y se dirige a un detector que registra la luz del haz de sonda reflejada en la muestra. Sin embargo, los dispositivos de grabación de imágenes convencionales suelen tener un tiempo de exposición demasiado largo en comparación con la escala temporal de los procesos en la ablación con láser de femtosegundo. Este efecto indeseado se compensa ya que el ancho de los pulsos de sonda son lo suficientemente estrechos y la muestra no recibe iluminación adicional. Por tanto, el tiempo de exposición efectivo de la cámara queda limitado por el ancho del pulso de la sonda. Los láseres femtosegundos son entonces un candidato ideal para obtener una evolución temporal muy precisa de estos procesos dinámicos en la ablación de un material.

La configuración experimental desarrollada para los estudios presentados en esta Tesis doctoral se describe en detalle en la Introducción y Capítulos. Sin embargo, es útil una breve descripción para el lector como un enfoque introductorio. La configuración de los experimentos de sonda-prueba utiliza un sistema láser Ti:sapphire que suministra pulsos de 35 fs FWHM centrados a una longitud de onda 800 nm, con una energía media de 3,5 mJ. Los pulsos láser suministrados por el equipo se dividieron en dos utilizando un divisor de haz. Este divisor de haz envía un 80% de la energía láser como pulsos de prueba, y el otro 20% se utiliza como haz de sonda. La energía depositada por los pulsos de prueba en la muestra inicia el proceso de ablación y es controlada por un atenuador óptico colocado en el camino óptico del haz de prueba. El haz de la sonda sigue un camino óptico diferente, donde se duplica su frecuencia. Durante la conversión de frecuencia se produce una pérdida de energía que contribuye en el control de la energía del haz de sonda para evitar cualquier daño en la superficie del objetivo.

El haz de la sonda, una vez convertido a 400 nm, se conduce perpendicularmente a la superficie de la muestra y pasa a través de un objetivo de microscopio vigilando que la luz de sonda no se enfoque en el objetivo. El haz de sonda ilumina la muestra y se refleja. En su camino de regreso, pasa a través del objetivo del microscopio de nuevo, y se dirige a una cámara CMOS con un filtro de paso de banda centrado en la longitud de onda del pulso sonda. Una condición indispensable en estas medidas era obtener imágenes de eventos con un único pulso de prueba. Para garantizar esta condición, se colocó un obturador mecánico en el camino óptico del haz de prueba y se sincronizó con la apertura del obturador de la cámara utilizando un generador de pulsos. Este sistema era finalmente dirigido por una señal electrónica interna del equipo láser para obtener una sincronización completa del experimento. Una vez que la cámara graba la luz reflejada de un evento sonda-prueba la muestra se mueve a una nueva área limpia gracias a una etapa que permite el movimiento en tres direcciones.

Las imágenes grabadas por la cámara se pueden procesar para obtener información, ya que se puede establecer una relación entre la intensidad de los píxeles de las imágenes con los procesos morfológicos inducidos en la superficie del objetivo. Como las imágenes grabadas muestran variaciones de reflectividad de la muestra, se pueden asociar a la dinámica de ablación de la muestra y asignar un intervalo temporal a cada mecanismo observado.

Todo este procedimiento experimental carecerá de éxito si no se establece una precisa sincronización temporal entre los dos haces de sonda-prueba que establezca el inicio de los procesos de ablación. En este sentido, el tiempo cero entre los haces de prueba y sonda se

considera cuando ambos haces llegan a la muestra simultáneamente y no se observan alteraciones morfológicas. Los detalles de cómo se llevó a cabo este procedimiento de sincronización se presentan en esta Tesis, y una vez que se logró, se realizaron estudios de tiempo resueltos que lograron una resolución temporal de 100 fs. Como resultado, se pueden establecer mediante el registro temporal de las imágenes obtenidas la relación entre las etapas del proceso de ablación con las alteraciones de la reflectividad observadas en las imágenes adquiridas. Los principales procesos que se han descrito previamente en este resumen quedan descritos a través de las imágenes como se relata a continuación.

Durante la excitación, la densidad de electrones en la superficie de la muestra aumenta, y las propiedades ópticas del material varían de acuerdo con este efecto en una escala temporal de hasta unos pocos picosegundos. Cuando el pulso de la sonda ilumina la muestra en estos primeros instantes, se observa un aumento gradual de la reflectividad de la muestra en comparación con su reflectividad natural. Estas diferencias en el aumento de la reflectividad son intrínsecas a las propiedades materiales y se observarán diferentes valores, así como diferencias temporales en durante la excitación de las muestras. El aumento de la reflectividad se ha documentado en una amplia variedad de materiales, y estudiado qué parámetros de los pulsos de femtosegundo pueden influir en la evolución de la superficie. Los resultados en películas delgadas de oro y plata depositadas sobre sustrato de cuarzo no mostraron diferencias temporales significativas en la duración de la fase de excitación en función de la fluencia del pulso de prueba. Por otro lado, la energía del fotón de los pulsos de la prueba sí reveló fuertes diferencias durante la excitación en películas de oro. Esto fue el resultado de una excitación más fuerte de electrones con longitudes de onda más cortas. Se puede resumir que se requiere un mayor número de fotones cuando las muestras se irradian con longitudes de onda más largas para inducir su excitación.

La fusión se considera cuando comienza la desexcitación de los electrones. El mecanismo fundamental es liderado por colisiones con otros electrones y fonones en la red cristalina como se ha mencionado anteriormente. Como el pulso láser ha terminado en este momento no hay contribución de energía externa y se asocia al comienzo de la ablación. Esto significa que la densidad de electrones en la superficie en esta etapa disminuye y es seguida por una consecuente disminución de la reflectividad. Cuando la fusión aflora también se induce un cambio en las propiedades físicas de la muestra. En este aspecto, la reflectividad alcanza valores negativos en comparación con su valor nativo. Los resultados obtenidos con la técnica de sonda-prueba muestran un oscurecimiento gradual desde el centro hasta el exterior del área irradiada cuando se ilumina con el haz de sonda en estos retrasos. En este momento, el frente de fusión se propaga hacia el interior de la muestra, y el área irradiada

con el pulso de prueba se vuelve más oscura que el resto de la muestra. De la misma manera que la excitación, la fusión depende de las propiedades físicas y químicas del objetivo. Un aumento en la fluencia aplicada no dio lugar a diferencias temporales significativas con respecto a la aparición de la fusión de acuerdo con los resultados observados en oro y plata. Sin embargo, se reportó de una caída más rápida de la reflectividad de la muestra, ya que la longitud de onda de prueba seleccionada es más corta, y por tanto un mayor número de electrones puede ser excitado. El aumento de la población de electrones excitados contribuye a una mayor tasa de colisión de electrones y electrones y huecos y, en consecuencia, a una fusión más rápida de la muestra.

El frente de fusión se propaga hasta que se refleja por la interfaz con el material no fundido, y se acciona el mecanismo de expansión del material fundido. En este momento se generan vacíos y mezcla de líquido-gas en el material fundido, y se inicia la deformación de la superficie de la capa líquido-sólida. Si la muestra se ilumina con pulsos de sonda en esta etapa de la ablación, pasará a través del material en diferentes estados, como se ha descrito previamente. Esta expansión crea un sistema multicapa con diferentes constantes ópticas, e índices de refracción, lo que conduce a múltiples reflexiones y transmisiones de la luz de sonda cuando entra en este sistema. Si la superficie irradiada de la muestra no presenta rugosidad o defectos considerables, se desarrolla un patrón de interferencias debido a la interacción de los pulsos láser de sonda.

Debido a la simetría axial del objetivo inducida por la geometría los pulsos de prueba, el patrón de interferencias resultante de la interacción del haz de sonda con la muestra se conoce como anillos de Newton. Sin embargo, como se ha descrito, la mezcla de volumen de líquido-gas empuja hacia fuera la cúpula de material sólido-líquido de la superficie, y su curvatura evoluciona con el tiempo. Cuando el sistema es iluminado por pulsos de sonda en diferentes retardos durante esta etapa de la ablación, el patrón de interferencias se modificará como consecuencia de la deformación progresiva y curvatura de la cúpula, y se obtiene un patrón de interferencia en evolución. Esta evolución se corresponde con un aumento del número de anillos de Newton con el tiempo mientras que su espaciado disminuye. El lapso entre la irradiación del pulso de prueba y el inicio de los anillos de Newton depende no sólo de las propiedades ópticas del objetivo, las condiciones experimentales también juegan un papel importante. Contrario a las evidencias observadas durante la excitación y fusión, los resultados experimentales realizados en silicio mostraron diferencias con el aumento de la fluencia del haz de prueba. El análisis de las micrografías mostró que el aumento de la fluencia implicaba un inicio más temprano de los sucesivos anillos de Newton, así como su número creció, y el espaciado disminuyó. Se obtuvieron

resultados similares en películas delgadas de oro y plata, aunque cada material mostró un tiempo característico en la aparición del patrón de anillos. Además, los índices de refracción del material tienen un efecto en el contraste y la visualización de las interferencias.

La contribución de la longitud de onda del haz de prueba es también merecedora de mención. Se ha observado que la irradiación con mayor energía de fotones en los pulsos de prueba dio lugar a un desarrollo más rápido de los anillos de Newton cuando la luz de sonda se mantuvo en 400 nm. Esta evolución más rápida está en concordancia con el efecto de una mayor excitación electrónica con longitudes de onda más cortas. La energía transferida a la red cristalina inducida se derrite más rápido, y durante la expansión, se obtiene una deformación más rápida de la cúpula sólido-líquido.

Los estudios realizados con diferentes longitudes de onda de prueba abrieron interrogantes sobre el impacto de diferentes longitudes de onda del haz de sonda, ya que las propiedades ópticas de los materiales tienen una respuesta diferente según la longitud de onda incidente. Estudios anteriores demostraron que los anillos de Newton consistían en un patrón de interferencia por iluminación con diferentes longitudes de onda de sonda. Por lo tanto, la anchura de los de los anillos y su contraste son función de las propiedades ópticas de los materiales y su estado bajo la longitud de onda de luz de la sonda. Sin embargo, había poca información sobre el efecto de la longitud de onda de luz de la sonda durante la excitación y fusión. Para evaluar este impacto, se realizó una modificación en el montaje experimental sonda-prueba utilizando pulsos de prueba a 400 nm y pulsos de sonda a 800 nm en la misma muestra. Este experimento se utilizó para visualizar la contribución de la longitud de onda de la sonda a la dinámica de la superficie. Sorprendentemente no se observó el aumento de la reflectividad esperado en oposición a dos resultados significativos. Por un lado, el aumento de la reflectividad que se podía observar cuando la muestra se irradiaba a energías idénticas utilizando la luz de prueba a 800 nm y la luz de sonda a 400 nm. Por otro lado, las mediciones de sonda-prueba utilizando 400 nm tanto para haces prueba como de sonda mostraron también un aumento de la reflectividad durante la excitación a energías de prueba más bajas. Estos resultados fueron explicados debido a la reflectividad natural del material estudiado (oro). La reflectividad en el oro es de aproximadamente 37% bajo 400 nm de luz, mientras que es de 98% bajo 800 nm de luz. Esto significa que el aumento de la densidad de electrones en la superficie no podría apreciarse debido a la alta reflectividad de la luz de la sonda a 800 nm.

La mezcla gas-líquido durante su expansión sigue empujando hacia afuera a la cúpula, y su deformación evoluciona, hasta que se ésta se rompe, y este material es entonces expulsado.

En este momento se puede observar un patrón de interferencias residual y muy estrecho en la periferia de la zona irradiada, mientras que la zona central del cráter se puede ver con una estructura diferente en comparación con la muestra no irradiada. En esta etapa, el material ablacionado que ha sido expulsado está en estados vaporizados y plasma dejando un cráter en la muestra. Sin embargo, se podría obtener más información sobre su dinámica de resolidificación en esta etapa utilizando la técnica de sonda-prueba, como el daño permanente producido por la ablación adecuada a la forma de la zona excitada y la formación de los anillos de Newton.

Una vez que el material vaporizado es expulsado empieza su expansión libre en estado plasma, con la emisión de continuo y más tarde las líneas de emisión características del material como se ha mencionado anteriormente. La evolución de la pluma de plasma sin embargo, no se puede estudiar con precisión con la técnica de sonda-prueba, aunque se pueden utilizar otras técnicas de imagen como la shadowgrafía o la interferometría. Aunque estas técnicas proporcionan información útil para revelar la evolución de la pluma de plasma y su interacción con el ambiente circundante, no proporciona información sobre la formación y evolución de las especies excitadas en el plasma.

En este sentido, la espectroscopia de rotura inducida por láser (LIBS) es capaz de suministrar la información relacionada con las líneas de emisión de especies excitadas a distintos niveles, tanto atómicas como moleculares, y cubre simultáneamente una amplia resolución temporal y espectral. El uso de detectores que puedan ser sincronizados a un generador de pulsos permite ajustarlos con un retraso de interés, por lo que la evolución del plasma y las características de su especie se pueden resolver temporalmente. Sin embargo, a menudo se centran en observar espectros de emisión de plasmas, y su ventana de adquisición se retrasa después de que la emisión de continuo se ha desvanecido. La ventaja de los láseres de femtosegundo ha reducido la vida útil de esta emisión continua y es posible estudiar la emisión de plasma en momentos más tempranos que los requeridos para plasmas inducidos con pulsos láser más largos. Además, la menor temperatura de los plasmas producidos por láser de femtosegundo ha mejorado la observación de las bandas moleculares, que ha sido profundamente estudiada con varias técnicas. Se ha observado que las moléculas pueden seguir diferentes vías de formación, como fragmentación o recombinación con el ambiente, según la estructura y composición de las muestras. También se ha observado que la molécula CN presentaba la máxima intensidad a diferentes retrasos según si el nitrógeno estaba presente o no en la composición de la muestra, pero no se ha determinado una diferencia temporal en la observación de esta banda molecular cuando es originada por diferentes vías.

Esto significa que hay poca información sobre la relación que vincula la dinámica en la morfología de una muestra tras su irradiación con pulsos láser de alta potencia, su ablación y su posterior plasma. Entonces, el tiempo que pasa entre la interacción de las especies excitadas de un plasma y la atmósfera circundante, para convertir la emisión continua en líneas de emisión espectral, se puede considerar una pregunta abierta. Estos fenómenos ocurren en una escala de tiempo que requiere una alta precisión temporal, pero no son accesibles a algunos detectores. Las mediciones espectrales pueden verse afectadas debido a tiempos de retardo intrínsecos a la fluctuación electrónica de los dispositivos y a una forma de pulso TTL no ideal de los tiempos de subida y cierre del obturador de los detectores.

Para esclarecer cómo se relacionan estos fenómenos, se propuso una aproximación que combinaba dos técnicas. Por un lado, la microscopía de sonda-prueba con resolución de femtosegundo ofrece su robustez y su alta precisión temporal durante los primeros 2 nanosegundos. Por otro lado, la espectroscopía LIBS se aplicó para estudiar nuevos retrasos y obtener información adicional.

Para lograr este propósito, un sensor iCCD acoplado a un espectrógrafo se conectó al mismo generador de pulsos que regulaba la apertura de la cámara CMOS y el obturador mecánico implementado en la configuración experimental del montaje experimental sonda-prueba. Por tanto, todos los dispositivos electrónicos se regían por el pulso TTL interno generado por el sistema electrónico del láser.

Bajo esta configuración, el equipo electrónico del láser entrega un pulso TTL que se envía al generador de pulsos, y es seguido por la salida de un pulso láser desde la cavidad amplificadora. El retardo de todos los componentes conectados a él se selecciona para que estén abiertos o en adquisición de señales cuando se genera el siguiente pulso láser. En este punto del experimento, el obturador mecánico está abierto, y un evento de un solo disparo se puede grabar con la cámara CMOS y el iCCD de manera simultánea.

A pesar de que todos los sensores estaban conectados a la misma fuente de disparo, también se requería un tiempo cero global para establecer el comienzo de los fenómenos de ablación en una muestra. Según este propósito, el mejor candidato para llevar a cabo esta calibración temporal era el silicio. Este material presenta una respuesta rápida tras la irradiación con la luz de prueba, ya que la excitación de los electrones se puede observar a un retraso de 100 fs entre los haces de prueba y sonda. Además, la aparición del primer anillo de Newton se observa en torno a los 100 ps y se obtiene un patrón de anillos de Newton bien contrastado en menos de 500 ps de retraso.

El primer paso consistió entonces en una sincronización de la configuración experimental de la bomba-sonda que se explica en la Tesis presentada. Una vez que se estableció el tiempo-cero en el experimento de sonda-prueba, el sensor iCCD también se sincronizó con el montaje experimental, y estas mediciones se pueden a continuación monitorizar con precisión en el tiempo con las alteraciones morfológicas observadas en la superficie de la muestra. El tiempo de exposición de la iCCD se estableció de manera que se abría mucho antes de la llegada del haz de prueba en el objetivo. Con este enfoque, se podría registrar la formación de emisiones continuas y la posterior aparición de líneas de emisión aumentando gradualmente el retraso del obturador de la iCCD en pasos que alcanzaron un rango temporal de subnanosegundos. Por lo tanto, la ventana de puerta estrecha se puede obtener independientemente de la anchura de la puerta del sensor si se restan dos espectros consecutivos en el tiempo.

Las medidas que combinaban la microscopía de sonda-prueba y LIBS con la muestra de silicio, tenían el espectrógrafo centrado en un rango espectral entre 375 y 415 nm. Esta ventana espectral permite la monitorización de la línea Si (I) a 390.55 nm y Si (II) a 385.60 nm. El procesamiento de los datos espectrales expuso que no hay evidencias de emisión espectral antes de 2 ns, ya que el material expulsado todavía está en expansión, pero el inicio de la señal de emisión de la línea Si (I) puede establecerse a un retraso de 6 ns. Por otro lado, la línea Si (II) no pudo observarse satisfactoriamente hasta un retardo mayor, ya que era mucho más débil que la línea Si (I). La temperatura del plasma es más baja en los plasmas inducidos por láser de femtosegundo y la ausencia de interacción láser-plasma son las razones fundamentales para observar una línea iónica debilitada. Por otro lado, la propagación de la pluma, con una fuerte componente normal durante las etapas iniciales de expansión también podría contribuir a una señal más débil de la línea iónica, como se explica en el capítulo 4.

La observación de la formación de líneas de emisión de un material ablacionado también supuso su aplicación para el estudio de la formación de la emisión molecular, que se observa con LIBS a intervalos temporales más largos que la emisión iónica y atómica. Se seleccionaron dos polímeros utilizando la misma configuración experimental que en las medidas de silicio para estudiar la formación de la evolución molecular de CN. El modo fundamental de las moléculas de CN se centra en 388,20 nm, por lo que no fue necesario cambiar la adquisición de la ventana espectral. Los polímeros considerados en estas mediciones fueron el teflón, que no contiene átomos de nitrógeno en su estructura molecular y nylon, que contiene nitrógeno. Esto significa que las adquisiciones espectrales de CN realizadas en Teflón sólo pueden atribuirse a mecanismos de recombinación de

átomos de carbono con moléculas de nitrógeno en la atmósfera ambiente, mientras que el nylon puede mostrar la emisión de CN debido a la fragmentación directa de moléculas.

La comparación de ambas mediciones resueltas temporalmente mostró diferencias en la evolución espectral de CN, así como los resultados obtenidos con silicio. No se observaron resultados significativos antes de 10 ns, cuando se podía distinguir la emisión de CN de nylon debido a la fragmentación directa. El teflón en oposición no mostró una señal de calidad aceptable hasta 20 ns después de la irradiación láser. Esta diferencia temporal está de acuerdo con el mecanismo de recombinación con átomos de la atmósfera de alrededor y de carbono seguidos en Teflón en sus espectros moleculares.

También se han presentado en esta Tesis algunos anexos que reflejan estudios adicionales y suplementarios relacionados con diferentes temas sobre plasmas inducidos por láser, que podrían desarrollarse para futuros estudios.

Uno de estos estudios se realizó en el Centro Nacional de Ciencia y Tecnología del Plasma, en la Dublin City University, Irlanda, durante la estancia de investigación concedida por el Ministerio de Economía de España. Se estudió el comportamiento de los plasmas de colisión producidos por láser utilizando un sistema láser de nanosegundos.

Se pueden encontrar dos escenarios opuestos extremos cuando dos plasmas chocan: capa de estancamiento o interpenetración, y dependen fuertemente de las condiciones experimentales. Durante la interpenetración, las especies de cada plasma comparten el espacio entre ambos plasmas. Pero bajo ciertas condiciones, las especies de los plasmas interactúan y crean una capa de especies excitadas que expulsa el material (capa de estancamiento). Algunos de los parámetros relevantes que pueden determinar el comportamiento de los plasmas que colisionan son la masa atómica del objetivo, la distancia entre los dos plasmas y la energía cinética de las especies excitadas. A pesar de que hay estudios centrados en el efecto de la masa atómica, fue de interés para estudiar el comportamiento de las colisiones de plasmas en un metal pesado como el estaño. Para obtener un estudio detallado se estudiaron los rastros obtenidos con una copa Faraday a diferentes energías, y estos resultados se compararon con los observados cuando se formaron plasmas individuales o "semillas". También se estudió la influencia de las mismas energías cuando un pulso láser de sonda UV se retrasó con respecto a los plasmas que colisionan, mientras que la distancia entre los plasmas de semillas se mantuvo fija en todos los estudios de caso. Todas estas mediciones también se registraron utilizando un sensor iCCD para que las imágenes integradas se compararan con los resultados de la copa Faraday.

El segundo anexo hizo un primer enfoque experimental en la aplicación de la microscopía de bomba-sonda para estudiar el efecto de la ablación láser de femtosegundo en los tejidos oculares. La ablación de los tejidos implica una combinación más compleja de procesos debido a la estructura de los tejidos biológicos y su alto contenido de agua, por lo que sigue siendo un área de estudio desafiante. Es de interés la aplicación de láseres de femtosegundo en estas situaciones ya que la transferencia de energía es diferente a la impulsada por pulsos más largos, lo que puede reducir la zona de tejidos afectada por el calor y los consiguientes efectos térmicos.

En este estudio se eligieron tres tejidos de un ojo porcino (córnea, esclerótica y lente), que son los tejidos oculares más comunes involucrados en la cirugía. Fueron estudiados bajo microscopía de sonda-prueba para visualizar si estos tejidos siguen una evolución temporal similar a la reportada para dieléctricos o compuestos orgánicos. Era evidente que la transparencia y la estructura de estos tejidos implicaban un papel significativo durante los procesos de ablación. Las fuertes diferencias que se han observado para los tres tejidos evidencian la necesidad de aumentar un conocimiento detallado de los mecanismos de ablación en los tejidos. Una configuración experimental mejorada adaptada para visualizar los tejidos biológicos también contribuiría a una mejor comprensión si se combina con técnicas espectroscópicas y de imagen adicionales.

Para concluir, los estudios de investigación que se presentan en esta Tesis doctoral han dado lugar a un notable aumento del conocimiento relativo a la dinámica superficial transitoria de la materia bajo irradiación de pulsos láseres ultracortos, lo que resulta en la formación final de plasmas. Además, se ha demostrado una mejora apreciable en los procedimientos experimentales relativos a estudios de ablación láser ultrarrápidos y espectroscopia de descomposición inducida por láser.
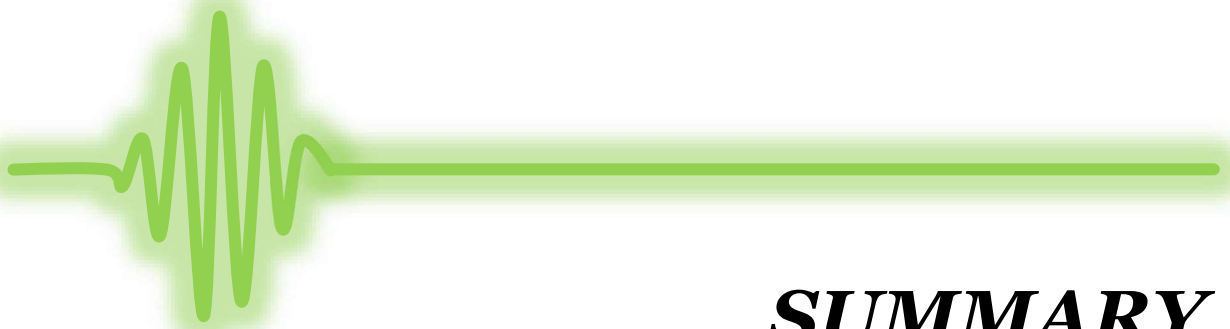
SUMMARY

SUMMARY

In fulfilment with the doctoral statements of the University of Málaga, a summary of this work is included. The fundamental aspects which have supported the basis to develop the studies included in this doctoral dissertation have been introduced, as hence a brief description of the significant results.

The development of technology associated to laser emission has opened new and spread variety of applications, from restoration of cultural heritage, to machining processes in industry or surgery applications. The successful observation of experimental results has enhanced the interest in researching newer applications and higher efficiency. In most applications in which laser light is involved, the fundamental process resulting from the interaction with a material is ablation. Ablation consists in removing a certain quantity of material, which can include a range from several atoms, up to enough mass to impress an observable crater or damage on the sample surface. This amount of mass will depend on the characteristics of the irradiated laser light, the nature of the material and required experimental conditions concerning to expected results in the selected application.

Among the characteristics of laser light which can influence in laser-matter interaction, the laser wavelength, the laser fluence, or the pulse width can be remarked as the most relevant. They are involved in the morphological processes of the material, according to its physical and chemical properties, and in case a certain energy threshold is overcome, material ablation occurs. Under satisfying experimental conditions, the ablated mass is vaporized, reaching high temperatures which ends in plasma formation. Other experimental conditions can be considered when ablation is being induced on materials, as the ambient pressure or composition of surrounding atmosphere to the irradiated material. They can also influence in the formation and evolution of plasmas as plasma species react with the constituents of the surrounding atmosphere.

In this sense, one of the applications that has resulted in a major repercussion in research applications has been laser-induced breakdown spectroscopy (LIBS). This technique uses a laser source to induce ablation of materials and produce plasmas, which can provide valuable quantitative and qualitative information of the samples of interest. LIBS offers several advantages and versatility respect to other analytical techniques. It can be highlighted that sample preparation is no necessary and allows performing material analysis in laboratories or even at a distance from the laser or detector.

In parallel to the increasing number of research fields which laser systems can be found as components of the experimental set up, technology advances have achieved improvements in laser systems, reaching extremely narrow laser pulse widths. Some decades ago, the development of Chirped Pulse Amplification technique (CPA) was proposed and resulted in a reduction of the temporal width of pulsed lasers up to a timescale in the range of femtoseconds. To obtain effectively such ultrashort pulses, CPA is performed in three steps. In the first stage, a seed pulse from a laser source is stretched by a dispersive optical system. Stretching is followed by amplification and a second laser source is added synchronously with the stretched laser pulse. Finally, the amplified pulse is compressed by another dispersive medium which compensates the stretching, and the ultrashort laser pulse can be then delivered. The experimental results which are shown in this dissertation have been carried out with a femtosecond laser system, with a Ti:sapphire crystal as a gain medium.

The fundamental advantage of femtosecond lasers respect to longer laser pulses is that almost all the energy of the laser pulse is deposited on the sample and has ended before any relaxation process of the phonon lattice occurs. This means that energy transport mechanisms as melting or ablation are not governed by thermal conduction in the sample, in opposition to irradiation with longer laser pulses. As a result, an improvement of some laser applications has been observed. More precise machining with a smaller heat-affected zone and well-defined craters, as well as a lower ablation threshold in materials have been reported as more advantageous results using ultrashort laser pulses. In addition, the absence of laser-plasma interaction after irradiation with high energies using femtosecond lasers has reported some interesting results. Lower continuum emission signal, and a different propagation of excited species of the plasma plume can be mentioned. On the other hand, laser-produced plasmas with femtosecond lasers has reported a lower temperature than the usual values with longer pulses. Then a completely different physical explanation of energy transport is required, which covers from the electromagnetic field of the laser pulse to the target due to this new scenario.

When the laser reaches the target, the first process in laser-matter interaction consists in excitation of electrons of the sample. In case of metals, the electrons on the surface will receive an increase of energy from the electromagnetic field of the laser pulse. In semiconductors and dielectrics, if the pulse energy is enough to overpass the band-gap energy of the atoms, electrons from the valence band are promoted to the conduction band. In all cases, this excitation leads to an increase of the electron density on the surface of the target which can take from hundreds of femtoseconds to some picoseconds. Followed by electron excitation, de-excitation of the electronic subsystem starts, but by that time, the

laser pulse has ended and there is no additional energy supplied to the target. This means that melting is initiated during electron de-excitation by collisions with other electrons or with the lattice.

These collisions propagate downwards to the sample as a mechanical wave which loses its energy progressively with each collision until it finally vanishes and the interface between molten and bulk material is generated. This mechanical wave leaves behind its propagation molten material which generates a thermal wave. When this thermal wave reaches the interface between molten and bulk material, is reflected and propagates upwards the surface through molten material. The propagation of the reflected wave pushes the molten material outwards and induces the formation of a density gradient in the molten volume. This density gradient leaves behind its propagation a liquid-vapor mixture of material while the material-air interface remains as a very thin solid-liquid layer of several nanometers depth, as it has not been reached by the reflected thermal wave.

As molten material expands and pushes the external solid-liquid layer, this layer experiments a gradual deformation, with the shape of a cupola or dome. The curvature of the dome increases with the expansion of the gas-liquid mixture until it finally breaks, and all the encapsulated material is ejected normal to the surface of the target. This material is in plasma state with a high temperature and composed by excited atoms, electrons, ions and molecules which expands with cylindrical shape and forward biased propagation. As this plasma expands, excited species are de-excited by recombination processes or collisions with particles of the surrounding atmosphere and continuum emission is emerged. The expansion and interaction of plasma with the atmosphere decreases its temperature and density, and emission lines characteristic of each material emerge from continuum emission. The intensity of these emission lines reaches a maximum, and then their intensity is decreased until the ablated material cools.

This description is outcome from the combination of an exhaustive number of inter and multidisciplinary studies, which include both theoretical models and experimental results obtained from different techniques. In this experimental frame, the contribution of imaging techniques as interferometry, shadowgraphy or pump-probe microscopy must be remarked. These techniques have in common that they use a first laser pulse with high energy or pump pulse. A second weak laser pulse, also known as probe pulse, interrogates the area of interest and the obtained image is recorded. If the probe light is delayed in steps respect to the pump pulse, these techniques can be used for time-resolved studies. Shadowgraphy offers a side view of the evolution followed by the plasma plume after material ejection. On the other

hand, interferometry can be used both for side and front views of the target and offers relevant information according to the phase shift of the probe light after interrogating the plasma.

Pump-probe microscopy allows us visualizing the dynamics of morphological alterations induced on the surface of materials from its excitation. This technique uses a high energy pump pulse to initiate the process of ablation on the sample. Another pulse, or probe pulse, is weak enough to avoid any additional damage on the target, acts as a flashlight and illuminates the area where the pump pulse irradiated the sample previously. The probe beam is delayed respect to the pump beam, reflects the effect of the pump pulse at the delays of interest, and is directed to a detector which records the light. However, conventional image recording devices usually have long exposure time compare to the timescale of the processes in femtosecond laser ablation. When laser pulses width is narrow enough and are used as flashlight, the exposure of the image will be limited by the probe pulse width. Femtosecond lasers are then an ideal candidate for obtaining a strongly accurate temporal evolution of these dynamic processes.

The experimental set up developed for the studies presented in this Doctoral thesis are described in detail in the Introduction and Publications. Nevertheless, it is useful a brief description to the reader as an introductory approach. The configuration of pump-probe experiments used a Ti:sapphire laser system which supplied 35 fs FWHM pulses centred at 800 nm with an average energy of 3.5 mJ. The laser pulses delivered by the laser system were divided into two using a beam splitter. This beam splitter sent an 80% of the laser energy as pump pulses, and the other 20% was used as probe beam. The energy deposited by the pump pulses onto the target initiated the ablation process and was controlled by an optical attenuator set on the optical path beam. The probe beam followed a different optical path beam, and frequency doubled, which lost energy during frequency conversion and could be then controlled to avoid any damage on the surface of the target.

On the other hand, the probe beam, once it was converted to 400 nm, was driven perpendicularly to the surface of the target, and passed through a microscope objective taking care of not being focused onto the target. The probe beam then illuminated the sample and was reflected. On its way back, it passed through the microscope objective again, and was directed to a CMOS camera with a band pass filter centred at the probe wavelength. The band pass filter centred at the probe wavelength was in the experimental set up to avoid any contribution from early plasma emission.

A highly relevant step in this experimental procedure consisted in obtaining single shot events in the measurements to avoid effects of multishot irradiation. To ensure this condition, a mechanical shutter was set on the pump beam optical path and was synchronized to the exposure time of the camera using a pulse delay generator. This system was finally governed by the internal trigger signal of the laser system to obtain a complete synchronization of the experiment. The camera then only records the reflected light of a single pulse irradiation and afterwards the sample is moved to a new clean area.

The recorded images by the camera can be processed to obtain information, as the intensity of the pixels can be related to the morphological processes induced in the surface of the target. As the images recorded show reflectivity variations of the sample, they can be attached at the ablation dynamics and a time lapse can be associated to each mechanism.

Once the experimental set-up was implemented, a good temporal synchronization was necessary as it was a crucial part of the experiment, otherwise a temporal record of ablation processes could not be established. In this sense, time-zero delay between pump and probe beams was considered when both beams arrived at the sample simultaneously, so no morphological alterations would be observed. The details of how this synchronization procedure was accomplished is presented in this dissertation, and once it was achieved, time-resolved studies which were performed, achieving a temporal resolution of 100 fs.

During excitation, electron density on the surface of the sample increases, and the optical properties of the material varies in agreement to this effect in a short timescale up to few picoseconds. When the probe pulse illuminates the sample at these earliest delays, it is observed a gradual increase of the reflectivity of the sample, compared to its natural reflectivity. This increase of the reflectivity is a consequence of the variation of the electron population on the surface of the sample, and optical properties of materials are varied. These differences in increase of the reflectivity are intrinsic to the material properties and different values will be observed, as well as temporal differences in the excitation of samples. This increase of reflectivity has been reported in a wide variety of materials, and it was studied which parameters of femtosecond laser pulses could influence on the evolution of surface dynamics. Results in gold and silver thin films deposited on fused silica bulk showed that the higher the pump pulse fluence reported a similar behaviour for both materials regardless the applied fluence showing no significant temporal differences. On the other hand, the energy of the photon of pump pulses revealed strong differences during excitation in gold films. This was the result of a stronger excitation of electrons with shorter

wavelengths. It can be followed that it is required a higher number of photons when samples are irradiated with longer wavelengths to induce its excitation.

Melting is considered when de-excitation of electrons starts. The fundamental mechanism is leaded by collisions with other electrons and phonons in the lattice has started as it has been mentioned previously. As the laser pulse has ended by this time there is no external energy contribution and it is associated to the initialization of ablation. This means that the electron density at this stage decreases and is followed by a consequent decrease of the reflectivity. When melting overcomes is also induced a change in the physical properties of the sample. Reflectivity then reaches negative values compared to its native value. In this stage, a gradual darkening which propagates from the centre of the target to outwards the irradiated area is reported when pump-probe technique is applied. By this time, the melting front propagates inwards the target, and the irradiated area with the pump pulse grows darker than the rest of the sample. In the same way to excitation, melting depends on the physical and chemical properties of the target. An increase on the applied fluence did not result in significant temporal differences respect to the onset of melting according to the results observed in gold and silver. Nevertheless, a faster decay of the reflectivity of the sample was reported when shorter pump wavelengths were applied, as a greater number of electrons could be excited. The increased population of excited electrons contribute to a higher electron-electron and electron-phonon collision rate and consequently, a faster melting of the sample.

The melting front propagates inwards the irradiated volume until it reaches the bulk-molten material interface and is reflected. Once the melting front is reflected by the interface with bulk sample, expansion of molten material is driven by this mechanism. By this time voids and liquid-gas mixture is generated due to the outwards propagation of the wave, or expansion front, and deformation of the liquid-solid layer surface is started consequently. This expansion creates a multilayer system with the liquid-gas mixture behind the expansion front and a solid liquid layer in front of the expansion front. This multilayer system then presents different optical constants, and refractive indices. When the sample is illuminated with probe pulses at this stage, the probe beam travels through this multilayer system which leads to multiple reflexions and transmissions. If the irradiated surface of the sample is smooth and does not present considerable roughness or defects, an interference pattern is developed due to the interaction of probe laser pulses with this system.

The interference pattern observed will present a Newton's rings pattern due to the axial symmetry of the target induced by pump pulses. However, the gas-liquid mixture and the

expansion front keep on pushing out the external layer of the target, which results in a progressive curvature of the dome with time. When this system is enlightened by probe pulses at different delays of this stage, the optical path of the probe beam inside the target is continuously modified by the progressive deformation of the dome. This results in an evolving pattern where the number of Newton's rings increases with time, whilst their spacing decreases. The time lapse between pump irradiation and the onset of Newton's rings depends not only on the optical properties of the target, but also the experimental conditions play a significant role. Experimental results performed in silicon showed differences, contrary to the evidences observed during excitation and melting. Pump-probe micrographs reported that a growing fluence implied an earlier onset of the successive Newton's rings, as well as their number grew, and their width decreased. Similar results were obtained in gold and silver thin films; each material showed a characteristic time in the apparition of the rings pattern. These materials nonetheless did not show significant temporal differences in the development of these rings when the fluence was increased as observed in silicon. This behaviour is explained as an increase of the pump fluence provided more energy to the electronic subsystem during excitation which was transferred to the lattice, and liquid-gas mixture expands and pushes the dome faster. Furthermore, the contrast of the interferences are determined by the refractive indices of materials and can affect to the visualization of this pattern.

The contribution of the pump wavelength is also merely of mention. Irradiation with higher pump photon energy resulted in a faster development of Newton's rings when experimental measurements with probe light kept at 400 nm were performed. This faster evolution is in accordance to the effect of the higher electronic excitation reported with shorter wavelengths. The transferred energy to the lattice induced melting faster, and during expansion, and a faster deformation of the solid-liquid dome is obtained.

The performed studies using different pump wavelengths speculated about the impact of different probe wavelengths, as the optical properties of materials have a different response according to the wavelength. Previous studies demonstrated that Newton's rings consisted in an interference pattern by illumination with different probe wavelengths. Therefore, the width of fringes and their contrast are function of the optical properties of materials and their state at a certain probe wavelength. Nevertheless, there was little information about the effect of the probe light wavelength during excitation and melting. It was performed a modification to evaluate this impact, on the pump-probe experimental using pump pulses at 400 nm and probe pulses at 800 nm. This experiment aimed to visualize the contribution of the probe wavelength to the surface dynamics. The increase of the reflectivity was

surprisingly not observed, in opposition to two previous significant results. On one hand the increase of reflectivity which could be observed when the sample was irradiated at identical energies using pump light at 800 nm and probe light at 400 nm. On the other hand, pump-probe measurements using 400 nm both for pump and probe beams showed also an increase of reflectivity during excitation at lower pump energies. These results were explained due to the natural reflectivity of the material (gold). The reflectivity in gold is about 37% under 400 nm light, while it is of 98% under 800 nm light. This means that the increase of electron density on the surface could not be appreciated due to the high reflectivity of probe light at 800 nm.

As the gas-liquid mixture keeps pushing outwards the dome, its deformation evolves too, until the dome finally breaks, and the gas-liquid mixture is then ejected. By this time, a residual and very narrow interference pattern is observed in the periphery of the irradiated area, and the central of the crater can be seen with a different structure compared to the non-irradiated sample and the dark central area is no longer observed. The ablated material which has been ejected is now in vapor and plasma states and a crater has been formed on the sample. However, further information about resolidification dynamics at this stage could be obtained using pump-probe technique, as the permanent damage produced by ablation suited to the shape of the excited area and the formation of Newton's rings.

The ejected material starts its expansion in plasma state, with the consequent continuum background and further emission lines as it has been mentioned previously. The evolution of the plasma plume cannot be precisely studied with pump-probe technique, but it can be used other imaging techniques as shadowgraphy or interferometry. Although these techniques provide helpful information in revealing the evolution of the plasma plume and its interaction with the ambient, they do not provide information about the formation and evolution of the emission spectrum of materials.

On the other hand, laser induced-breakdown spectroscopy (LIBS) can supply information related to the emission lines of excited species and covers broad temporal and spectral resolution simultaneously. The use of gated detectors connected to a trigger source can be adjusted at a delay of interest, and the evolution of plasma as well as the characteristics of their species can be then temporally resolved. However, LIBS is often focused on observing emission spectra from plasmas, and its acquisition window is then delayed after the continuum background has fainted or vanished. The featuring advantages of femtosecond lasers has reduced the lifetime of this continuum emission, and it is possible to study plasma emission at earlier times than the presented with plasmas induced with longer laser pulses.

Additionally, the lower temperature of femtosecond laser-produced plasmas has improved observation of molecular signatures, which has been deeply studied with several techniques. Molecules can follow different routes of formation, as fragmentation or recombination with ambient, according to the structure and composition of samples, as shown by experimental results. Indeed, the CN molecule presented maximum intensity at different delays when nitrogen was presented or not in the target composition, but a temporal difference of molecular band originated by different routes have not been established according to this condition.

This means that there is little information about the relation which links the surface dynamics of a sample after its irradiation with high power laser pulses and laser-produced plasmas. The time spent by the plasma plume during its interaction among excited species and the atmosphere to convert continuum background light into spectral emission lines can be still considered an open question. These phenomena occur at a timescale which a high accuracy and temporal precision are required but are not reachable to some detectors. Spectral measurements can be affected due to delay times intrinsic to electronic jitter of devices and a non-ideal TTL pulse shape of the rise and closure times of the shutter of detectors.

To elucidate how these phenomena are related, an experimental set up which combined two techniques was proposed. On one hand, femtosecond pump-probe microscopy offered its robustness and its highly accurate temporal precision during the first 2 nanoseconds. On the other hand, LIBS would be applied to study further delays and obtain additional information.

To accomplish this purpose, an iCCD coupled to a spectrograph was connected to the same pulse delay generator which triggered the CMOS camera and the mechanical shutter implemented in the pump-probe experimental set-up. Then, all the electronic devices were governed by the internal TTL pulse generated by the laser system.

Under this configuration, the laser system delivered a TTL pulse which is sent to the delay pulse generator, and it is followed by the output of a laser pulse from the regenerative amplifier. The delay of all components connected to it is selected to open when the next laser pulse is delivered: the mechanical shutter is open, and an a single-shot event can be recorded with the CMOS camera and the iCCD.

Despite all sensors were connected to the same trigger source, they also required a temporal synchronization to establish a global zero-time delay. According to this purpose, silicon was the best candidate as target study. Silicon presented a fast response of pump irradiation,

and excitation of the electrons can be observed at a delay of 100 fs between pump and probe beams. Furthermore, it is observed a well contrasted Newton's rings pattern in less than 500 ps delay.

The first step developed for the experimental set up was the synchronization of the pump-probe experimental set-up which is explained in the present dissertation. Once the time-zero was established in the pump-probe experiment, the iCCD was also synchronized to the experiment, and these measurements can be then related accurately in time to the morphological alterations observed in the surface of the sample. The gate width of the iCCD was fixed, and it was opened much earlier than the arrival of the pump beam on the target. With this approach, the formation of continuum emission and the formation of emission lines could be recorded increasing gradually the delay of the iCCD shutter in steps which reached sub-nanosecond temporal range. The narrow gate window can be hence obtained independently of the gate width of the sensor if two consecutive spectra in time are subtracted.

Measurements combining pump-probe microscopy and LIBS with the target study, silicon, had the spectrograph centred at the spectral range between 375 and 415 nm. This spectral window let the monitorization of Si (I) line at 390.55 nm and Si (II) at 385.60 nm. The processing of the spectral data exposed that there is no evidence of spectral emission before 2 ns, as the ejected material is still under expansion, but the onset of Si (I) could be established at a delay of 6 ns. On the other hand, the Si (II) line could not be satisfyingly observed until further delays as it was much weaker than the Si (I) line. The lower plasma temperature of femtosecond laser plasmas and the absence of laser-plasma interaction are the fundamental reasons to observe a fainted ionic line. On the other hand, the forward biased propagation of the plume during initial stages of expansion could also contribute to a weaker signal of the ionic line, as it is explained in Publication 4.

The observation of the formation of emission lines of an ablated material could be also applied later in the formation of molecular emission, which is observed with LIBS at longer times than ionic and atomic emission. It was selected two polymers using the same configuration for silicon to study the formation of CN molecular evolution. The fundamental mode of CN molecules is centred at 388.20 nm, so it was no necessary to change the spectral window acquisition. The polymers considered in these measurements were Teflon, which does not contain nitrogen atoms in its molecular structure and nylon, which does contain nitrogen. This means that CN spectral acquisitions performed in Teflon can be only attributed to recombination mechanisms of carbon atoms with nitrogen molecules in the

ambient atmosphere, while nylon can show CN emission due to direct fragmentation of molecules.

Comparison of both temporally resolved measurements showed differences on the spectral evolution of silicon and CN. Significant results could not be observed earlier up to 10 ns, when CN emission from nylon could be distinguished from continuum emission due to direct fragmentation. In opposition, Teflon could not be observed until 20 ns after laser irradiation. This temporal difference agreed with the recombination mechanism with ambient and carbon atoms followed in Teflon in its molecular spectra.

There have been also presented in this dissertation some Annexes which reflect additional and supplementary studies related to different topics on laser-induced plasmas, which could be developed for future studies.

One of these studies was carried out in the National Centre for Plasma Science and Technology, in Dublin City University, Ireland, during the research stay granted by the Ministry of Economy of Spain. It was studied the behaviour of laser-produced colliding plasmas using a nanosecond laser system.

It can be found two extreme opposite scenarios when two plasmas collide: stagnation layer or interpenetration, and they strongly depend on the experimental conditions. During interpenetration, the species from each plasma share the space between both plasmas. But under certain conditions, the species from the plasmas interact and creates a layer of excited species which ejects material (stagnation layer). Some of the relevant parameters which can determine the behaviour of colliding plasmas are the atomic mass of the target, the distance between the two plasmas and the kinetic energy of the excited species. Despite there are studies focused on the effect of the atomic mass, it was of interest studying the behaviour of colliding plasmas in a heavy metal as tin. To obtain a detailed study, the traces obtained with a Faraday cup at different energies were studied, and these results were compared to the observed when single or "seed" plasmas were formed. The influence of the same energies when a UV probe laser pulse was delayed respect to the colliding plasmas was also studied, keeping a fixed distance between seed plasmas in all the case studies. All these measurements were also recorded using an iCCD for integrated imaging to be compared with results from the Faraday cup.

The second annex made a first experimental approach in the application of pump-probe microscopy to study the effect of femtosecond laser ablation on ocular tissues. Ablation of tissues involves a more complex combination of processes due to the structure of biological tissues and their high content of water, so it is still a challenging area of study. It is of interest

the application of femtosecond lasers in these situations as the energy transfer is different than the driven by longer pulses, which can reduce the heat affected zone of tissues and the consequent thermal effects.

In this study three tissues from a porcine eye were chosen (cornea, sclera and lens), which are the most common ocular tissues involved in surgery. They were studied under pump-probe microscopy to visualize if these tissues followed a similar temporal evolution than the reported for dielectrics or organic compounds. It was evident that the transparency and structure of these tissues implied a significant role during ablation processes. The strong differences which have been observed for the three tissues evidenced the necessity of increasing a detailed knowledge of ablation mechanisms in tissues. An improved experimental set up adapted to visualize biological tissues would also contribute to a better comprehension if it is combined with additional spectroscopic and imaging techniques.

To conclude, the research studies which are presented in this doctoral dissertation have resulted in a notable increase of knowledge concerning to transient surface dynamics of matter under ultrashort laser pulse irradiation, which results in the final formation of plasmas. Furthermore, it has been proven an appreciable improvement in experimental procedures concerning to ultrafast laser ablation studies and laser-induced breakdown spectroscopy.

OBJECTIVES

OBJECTIVES

The development of laser systems has resulted in an exponential increase in the number of applications where they can be found, as their implementation can be suited to any situation, from industrial machining to surgery with precise resolution. Many of the applications where laser light is involved have ablation as a process in common among them, in which a certain amount of material is heated and removed from the sample. It can cover from several atoms and gentle ablation to remove a considerable quantity of mass. If the ablated mass overcomes a certain temperature, then it will be ablated as plasma state. The amount of mass removed depends on the characteristics of the laser pulse during ablation namely energy, wavelength or pulse width, which are continually controlled and improved.

One of the most remarkable achievements developed in laser technology consisted in the chirp pulse amplification (CPA). This technique reduces the laser pulse width up to femtosecond timescales, so the laser pulse ends before any relaxation process of the irradiated material takes place. This shortening in the pulse width has proven to obtain smaller heat affected zone (HAZ), and a completely different evolution and expansion of induced plasmas is observed. These distinguished features need therefore to be described under a new physical approach.

Nevertheless, there is not a complete description of femtosecond laser ablation as a whole picture. It is undergone by a complex and multiple optical, electromagnetic and chemical discipline. However, it is of high relevance the complete description of femtosecond laser ablation and the determination of the characteristic temporal ranges where the ablation processes are observed is of powerful help.

The experimental results obtained during the development of the presented Doctoral Thesis are led to understand the morphological processes induced on a sample upon femtosecond laser irradiation. Then, it can be established a relation between the surface dynamics and plasma formation to determine when the formation of emission lines start.

To accomplish these purposes, the first objective consisted of the design and development of a time-resolved pump-probe microscope using a femtosecond laser system based on a Ti:sapphire medium. This experimental set up easily reaches a temporal resolution of 100 fs with high precision, so visualization of surface dynamics due to laser-matter interaction processes can be studied and recorded.

One of the goals of this work looked for the relation between irradiation with femtosecond laser pulses and the evolution of morphological processes on materials according to their nature to establish the fundamental differences under the same experimental set up. The features of materials depending on their metallic, semiconductor or dielectric nature results in different excitation mechanisms after ultrafast laser irradiation. Although there are previous studies devoted to these processes, they are centered on a certain group of materials and have been performed under different experimental configurations. The second objective aimed in this dissertation studied whether there exist temporal differences in the surface dynamics of materials within a fluence range depending on their metallic or dielectric nature.

Surface excitation and melting of samples can be monitored with femtosecond pump-probe microscopy technique, but it can be remarked the observation of transient fringe pattern which evolves with time, or dynamic Newton's rings. It consists in an interference pattern which has been reported in a wide range of materials. It is associated to the formation of an optical multilayer system, composed by air, a solid-liquid layer at the air-sample interface of irradiated material, vaporized material which expands and pushes the liquid layer, and bulk or non-molten material.

This Doctoral Thesis then pursued the following objective. Study the influence of a fluence range in the observation of temporal differences of surface dynamics and the formation of dynamic Newton's rings.

It has been proven that the applied fluence from laser pulses is related to the amount of ablated mass due to the energy transferred to the sample. Under ultrashort laser irradiation, the power of light is increased due to the pulse duration and this implies that fluence can be related to the evolution of the surface dynamics.

Dynamic Newton's rings show an evolving pattern in the number of rings and width as the solid-liquid dome in the surface is being pushed outwards by the gas-liquid mixture of ablated material which is encapsulating before plasma formation. The amount of this mixture and the energy transferred by the laser pulse determines the deformation of the dome and, therefore, the evolution of the Newton's rings. Hence, the radial velocity of the expansion of these rings and their relationship with the applied fluence can be studied.

The effect of laser wavelength in laser ablation has been exhaustively studied by many authors, and it has reported that results can be improved depending on the applications. Most of these works have been performed with longer laser pulses, and there is little information reported with respect to ultrashort laser pulses. Materials have a different

response of their optical properties under different photon energies and, consequently, the ablation process is affected by this parameter. It was then established as an objective, using pump-probe microscopy, to observe the transient modifications during ablation, using different pump and probe wavelengths to determine their impact on the formation of Newton's rings.

One of the most popular applications of lasers is laser-induced breakdown spectroscopy (LIBS), as it is a technique which provides qualitative and quantitative information in real time and presents several advantages compared to other analytical techniques.

A great challenge in the study of LIBS and their applications is to understand when emission lines start their onset after the laser pulse. There are many studies which establish a deep and detailed description of ablation dynamics and their timescales. This comprehension is relevant in determining the optimal acquisition conditions for analysis in spectroscopic techniques as LIBS. On the other hand, there are still questions concerning to molecular spectra, as they can follow several ways due to recombination processes or fragmentation.

The final objective of this Doctoral Thesis is to determine a temporal relation between the surface dynamics presented during ablation processes with the onset and formation of spectral emission lines combining pump-probe microscopy and time-resolved LIBS. In addition, the temporal difference in CN molecular emission of polymers depending on the presence of nitrogen in their composition.

INTRODUCTION

1. FUNDAMENTALS OF LASER-MATTER INTERACTION: THEORETICAL BACKGROUND

1.1. Main processes in laser-matter interaction

Laser ablation is a process in which a high-power laser pulse is focused onto a sample with enough energy to remove a small amount of mass of the sample. This mass is instantaneously converted from solid state to molten or vapor gas particles.

The interaction of a focused laser onto a solid material is a complex combination of physical and chemical variables, but an understanding the implied mechanisms is fundamental for more efficient results in applications where laser-matter interaction is a key process. However, a general description of the interaction of light and matter can be overviewed, and the main processes can be then introduced and understood.

The fundamental process which origins any laser-matter interaction, is absorption of energy from the laser pulse for excitation of the matter by electron heating. During irradiation, the pulse interacts with a solid target and originates a dense electron plasma. Then, the nature of the sample plays a crucial role due to its atomic structure. In metals, absorption will frequently be dominated by free-carrier absorption. Electrons in the conduction band absorb photons and gain energy. In semiconductors, electrons from the valence band will be promoted to empty vacancies in the conduction band when the energy of the photons surpasses the band gap. On the other hand, dielectrics are characterized by a wide band gap, larger than the photon energy, so promotion of electrons to the conduction band must be driven by multiphoton transitions [1].

Laser pulses are electromagnetic waves, so their interaction with matter are ultimately defined by electromagnetic and optical physics. To introduce this interaction, let us consider the laser beam a polarized plane wave, with normal incidence on a medium. The wave propagates along the x-axis, normal to the surface, from vacuum at the x<0 space region, while material fills the x>0 region. In general terms, a non-magnetic medium $\mu_r=1$ can be described by a complex dielectric function ε and conductivity σ [2]. The electron mean-free path, and the distance traveled by electrons during a period wave v_e/ω (where v_e is the electron velocity) are usually shorter than the skin depth l_{abs} (typically in the order of several ten nanometers). This justifies that the normal skin approximation can be applied under these approximations [2-4]. This means that the laser energy is absorbed in the skin layer, which is mainly in the order of several ten nanometers, and most of light will be absorbed by a thin layer of the surface of the sample.

$$E = E_0 exp\left(i\frac{\omega\sqrt{\varepsilon}}{c}\right) = E_0 exp\left(i\frac{\omega nx}{c} - \frac{x}{l_{abs}}\right) \qquad (1)$$

$$\varepsilon = \varepsilon' + i\varepsilon'' \qquad (2)$$

$$\varepsilon' = n^2 - k^2 \qquad (3)$$

$$\varepsilon'' = 2nk \qquad (4)$$

The skin depth is obtained as the inverse of the imaginary part of the refractive index

$$\hat{n} = n + ik \Rightarrow l_{abs} = \frac{c}{\omega k} \qquad (5)$$

After absorption of light, different mechanisms in laser-matter interaction become dominant according to the characteristics of the laser beam (see details in section 1.3). They can be mainly grouped as a general approach in two ablation models. A first model is based on a classical frame of laser-matter interaction, which assumes that the energy of the laser pulse results in the vaporization of the material, and the ablation rate can be then estimated. The energy of the laser pulse is deposited on the irradiated surface, and heat conduction develops a temperature gradient. The material is heated up to the evaporation temperature by the energy of the laser pulse, and latent heats of melting and vaporization are overcome. The material ablated is then in vapor state when a certain threshold is overcome by the laser pulse fluence

$$F_{th} = \rho L_v a^{1/2} t_e^{1/2} \qquad (6)$$

The fluence threshold depends on the sample density ρ, L_v, which is the latent heat of vaporization, the laser pulse width t_e, and the thermal diffusivity a, which is defined as

$$a = \frac{K}{\rho C_p} \qquad (7)$$

where K is the thermal conductivity and C_p is the specific heat. The ablated mass can be then estimated by the following expression [5, 6].

$$m = \frac{N E_{pulse}}{c_p(T_v - T_0) + \Delta H_m + \Delta H_v} \qquad (8)$$

In this expression, N is the number of pulses, E is the energy of the pulse, c_p is the heat capacity, T_v is the vapor temperature, T_o is the room temperature, and H_m and H_v are enthalpies of melting and vaporization respectively.

However, this model loses its validity when a material is irradiated with the denominated ultrashort laser pulses (sub-nanosecond pulses). A non-classical approach of ultrafast laser-matter interaction must be then assumed, and the ablated mass is derived from a different expression [6, 7].

$$m = N\rho A \alpha^{-1} ln\left(\frac{F_a}{F_{th}}\right) \qquad (9)$$

In opposition to nanosecond laser ablation, the ablated mass with femtosecond laser pulses has a logarithmic dependence on the applied fluence, the focal spot of the area, and the optical penetration depth of the sample at the laser wavelength.

When a laser pulse is focused onto a surface, the ablated mass results in the formation of plasma with high temperature and electron density if the energy of the laser pulse is enough to overcome the fluence threshold. Different phenomena contribute to plasma formation, as multiphoton ionization, cascade ionization, thermal ablation, Coulomb explosion, among others, according to the nature of the target or the properties of the laser [8-10]. After the formation of the plasma, its evolution is leaded by the expansion of the plasma in the surrounding environment and is produced a decrease in gas and electron temperatures.

The fast expansion of plasmas involves a fast decrease of the number density of ablated species, as well as a decrease of the temperature. During the initial stage of expansion, plasmas are characterized by continuum emission, which it is generally attributed to a dominant combination of two mechanisms: free-free transitions (bremsstrahlung), and free-bond transitions (radiative recombination processes) are the dominant mechanisms [11-13].

As plasma expands, electron number density decreases, and emission lines emerge from continuum emission. But at this stage of plasma evolution, electron number density is still high enough that the observed lines correspond to ions or atomic transitions with low energy excited level, and after a certain time, more atomic lines are visible as plasmas down. In opposition to the continuum emission, a transition from an upper level i to a lower level j, leads to a emission line at a wavelength corresponding to the difference of energy between
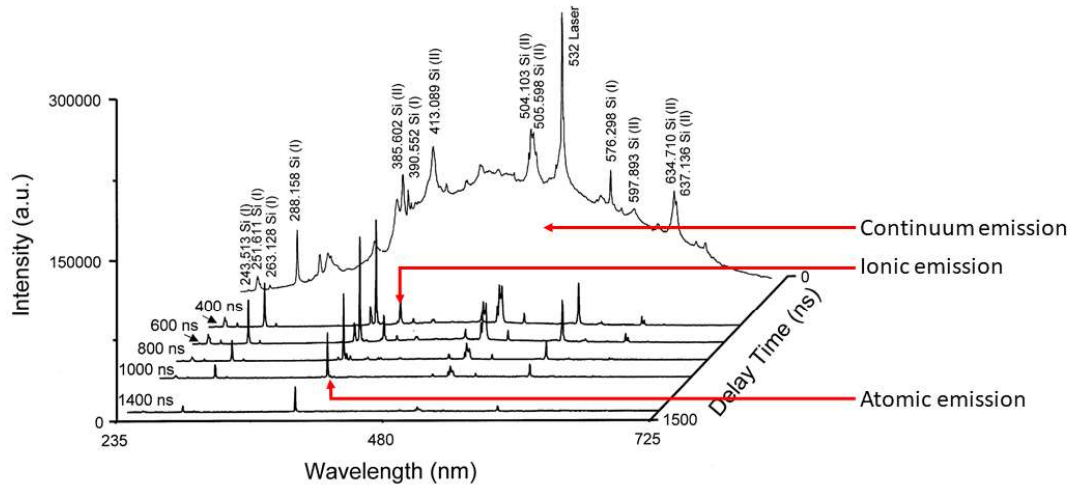
Figure 1: *Temporal evolution of silicon plasmas induced by a Nd:YAG laser at a wavelength of 532 nm and FWHM of 5 ns. Integration time 1 μs. Adapted from [15]*

these two levels [13, 14], as it is reflected in figure 1, and the intensity of this transition is given by

$$I_{ij} = \frac{1}{4\pi} A_{ij} h\nu_{ij} N_j \qquad (10)$$

In this expression, A_{ij} is the Einstein's coefficient corresponding to that transition, ν_{ij} is the frequency at that photon energy and N_j is the electron number density at level energy j

The evolution and expansion of plasmas with time produces cooling of its temperature, and the interaction of ablated atoms and molecules with the surrounding atmosphere can also drive into molecular emission at longer times than the characteristic for atomic and ionic emissions, as represented in figure 2. Emission of molecules have attracted the interest of the LIBS community in a wide variety of applications from polymer recycling to planetary exploration [16-19]. Numerous studies and theoretical models can be found [20-22] which have driven into some interesting conclusions. On one hand, there are three conditions to observe molecular band emission; an appropriate temperature which favours the molecular formation, enough atomic reactants in the surrounding ambient must be present, and the upper level of the molecular transition is low enough, so the transition is observable [12]. On the other hand, there are different pathways which can be followed by the atoms and molecular bonds and initiate molecular emission; single displacement reactions, double displacement reactions, decomposition reactions, and atomic recombination [23, 24].

40
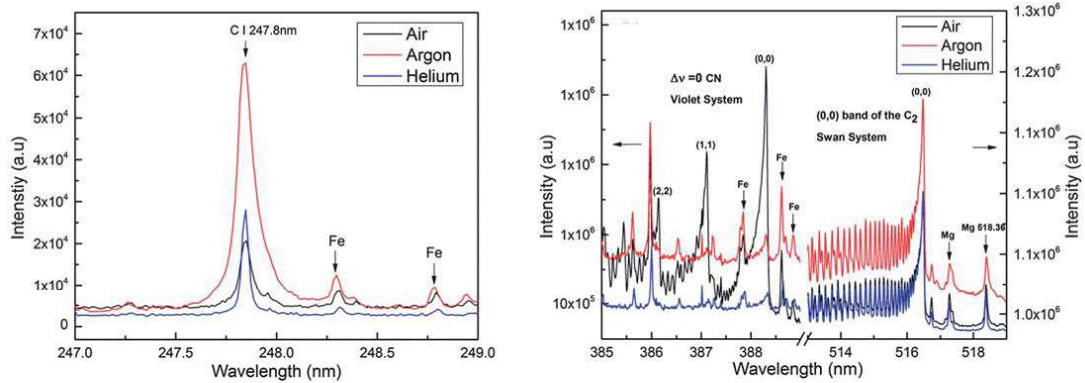
Figure 2: *Emission spectra of atomic carbon (left), and molecular emission from CN and C_2 bands (right) at different background atmospheres. Plasmas were induced by a Nd:YAG laser at 266 nm, with FWHM of 4 ns. Spectra were acquired at a delay of 400 ns using an integration time of 300 ns. Adapted from [25].*

1.2. Parameters for plasma characterization

The obtained plasma is constituted by a mixture of free electrons, ions and atoms in different excited states, and radiation. The resulting light is defined by the characteristics and physical-chemical processes of these components. In the previous section the fundamental processes that are relevant during laser-matter interaction, and plasma formation and emission have been introduced. They have been based on the experimental results observed and the theoretical models which explains those results. It should be remarked that electron number density and plasma temperature, play a relevant role in these processes. Nevertheless, either electron number density or plasma temperature can be determined independently on the LTE approximation.

Local thermodynamic equilibrium

Local thermodynamic equilibrium (LTE) is a very particular condition which is not satisfied in most of the plasmas. One of the conditions for LTE considers that electron energy distribution function (EEDF) is a Maxwell-Boltzmann distribution. This condition is valid when electron density is sufficient to ensure a high collision rate, which is satisfied for most of LIBS plasmas [26, 27].

In this sense, the McWirther criterion establishes [8, 14] the minimum electron density necessary for ensuring local or complete thermodynamic equilibrium, which is related to the electron temperature T_e and the energy transition ΔE between levels i and j.

$$N_e > 1.6 \cdot 10^{12} \sqrt{T_e} \cdot \Delta E_{ij}^3 \qquad (11)$$

Despite this criterion is the most used in the literature, and often considered as a sufficient condition, it should be considered for LTE. Exhaustive studies on the local thermodynamic equilibrium can be found in the literature which describe the circumstances of this criterion is fulfilled [27-29].

Plasma temperature

There exist several methods for an estimation of the plasma temperature depending on the experimental conditions which require to be satisfied the assumptions of being optically thin plasmas and local thermodynamic equilibrium. When the LTE condition is fulfilled, the different distribution functions which describe the plasma state are determined by the plasma temperature. This means that the plasma temperature can be estimated from the intensity ratio of a pair of spectral lines which can be compared, which are originated in different energy levels and the same ionization stage from the same chemical element [8]. The measured line intensity is proportional to the RHS of the relation

$$I_{ij} = n_i^s A_{ij} = \frac{A_{ij} g_i}{U^s(T)} n^s e^{-E_i/kT} \qquad (12)$$

In this expression, A_{ij} is the transition probability between the upper level i, and the lower level j, and g_i is the statistical weight of the upper level. The parameters related to the population of levels are n_i^s, which corresponds to the population density of the level i, and n_s corresponds to the total number density of excited particles in the plasma. The character k represents Boltmann's constant, E_i is the excitation energy of the level, and $U^s(T)$ is the internal partition function of the species at the temperature T [8].

If we consider two emission lines, at transition wavelength λ_{ij} and λ_{mn} of the same excited species, with different values of the upper level energy ($E_m \neq E_i$), the plasma temperature can be estimated as the ratio of the intensity of the two lines.

$$T = \frac{E_i - E_m}{kln\left(\frac{I_{mn} g_i A_{ji}}{I_{ij} g_m A_{mn}}\right)} \qquad (13)$$

Electron number density

Electron density can be estimated by optical emission spectroscopy. At early stages of plasma emission, it can be observed a line broadening and shift as a consequence of the still high density of free electrons and ions, which is known as Stark effect. This effect is produced by the electric field generated by the electrons in the plasma, and consequently energy levels of individual ions are perturbed and a broadening of the emission lines at these excited levels is observed. As the plasma evolves, electron number density decreases due to recombination. This effect in non-hydrogenic ions, is observed as a broadened line which tends to acquire a Lorentzian profile in the absence of other broadening factors as electron density decreases, as shown in figure 3. Other contribution in most typical LIBS plasmas can be neglected, and the full-width-at-half-maximum (FWHM) of emission lines can be deduced from the following simplified expression. Determination of the electron number density with this method is independent of any assumption regarding LTE [8].

$$\Delta\lambda_{1/2} \cong \Delta\lambda_{Stark} = 2W \left(\frac{n_e}{10^{16}}\right) nm \qquad (14)$$

Where W is the electron impact parameter and n_e is the electron density (cm^{-3}).

Another method for electron density estimation consist in the application of the Saha-Boltzmann equation. If plasma is under LTE conditions, the electron density can be derived from the intensity ratio of two lines from different ionization states of the same element. As the Saha-Boltzmann equation can be used to estimate the total density number of two ionization stages, a similar expression can be derived for two levels of different ionization stages and their intensity ratio [8].

$$n_e = \frac{2(2\pi m_e\, kT)^{3/2}}{h^3} \frac{n_m^I g_i^{II}}{n_i^{II} g_m^I} e^{-\frac{E_{ion}+E_i^{II}-E_m^I}{kT}} \qquad (15)$$
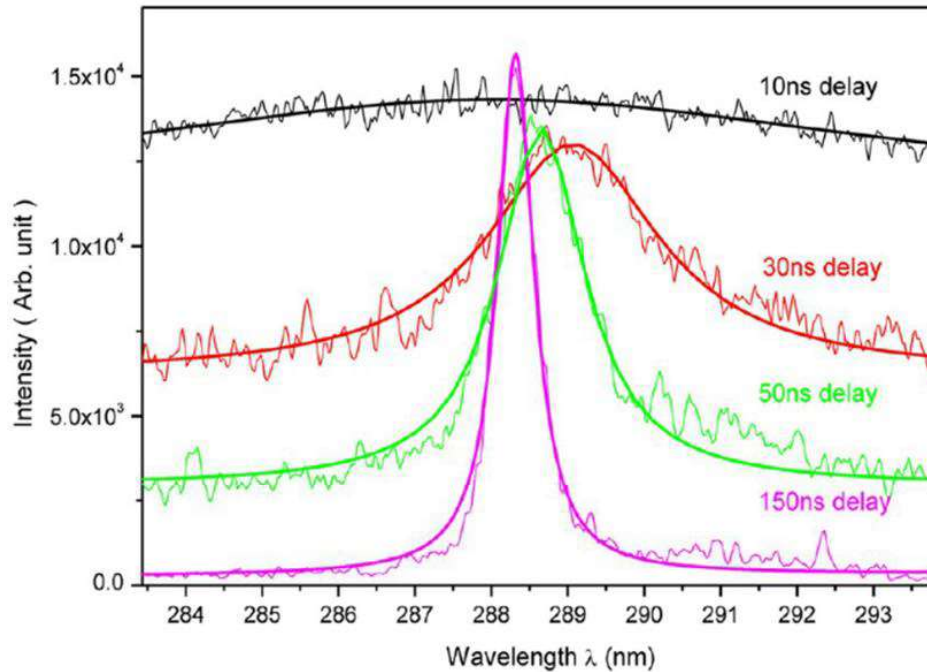
Figure 3: *Emission intensity measured from a silicon plasma, where it is displayed the evolution of continuum emission background, the spectral shift and broadening of the line Si(I) at 288.16 nm. Adapted from [10]. No data from the laser source and detection system were available in the reference.*

1.3. Influence of operational parameters on laser-induced plasmas

Operational parameters of laser sources play a relevant role in the physical properties of a performing plasma, as well as its emission of atoms, and particles or molecules. Many studies have been focused on unveiling the influence of laser parameters as wavelength, pulse duration, fluence, or surrounding atmosphere. As they will condition the final properties of the laser-induced plasma, they must be characterized, in order to obtain the best results for the goals of experiments. The following sections discuss briefly the effects of these parameters.

1.3.1 Laser pulse width

Laser pulse width is characterized by its FWHM, or the time interval where the pulse power is at least half the maximum power. According to the pulse width, different laser-matter interaction processes become dominant. For laser pulses widths set in the range of micro- and nanoseconds, the ablation process is dominated by heat conduction, melting, evaporation and plasma formation [6]. On the other hand, ultrashort laser pulses, between pico- and femtosecond widths, end before any material transformation can be induced, and laser-plasma interactions do not occur, as it can be seen in figure 4. As a high amount of energy is deposited in the target in a shorter time, they acquire higher intensity values, and makes necessary different physical descriptions, where the nature of the ablated material must also be considered.

In this sense, it is widely accepted the classification of these regimes attending to the parameters of electron cooling time (τ_e), the lattice heating time (τ_i) and the pulse duration (τ_L), according to the so-called two-temperature model (TTM) [7]. The nanosecond regime is characterized by a classical laser-matter interaction, where melting, evaporation and plasma formation are present [6]. Nanosecond ablation fulfills the condition $\tau_{L>>}\tau_e$, which implies that the lattices and electron temperatures are in equilibrium. The absorbed laser energy first heats the target surface to the melting point, and then the matter is vaporized from its liquid state [7]. Laser ablation in the picosecond range is accompanied by the electron heat conduction and formation of a melted zone inside the target [7]. Femtosecond
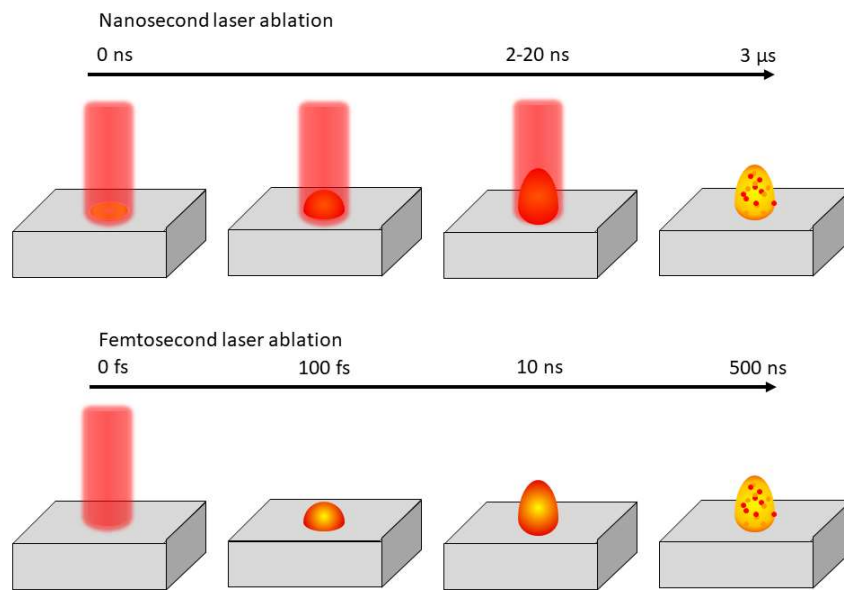
Figure 4: *Comparison of approximate time scales of nanosecond and femtosecond laser ablation*

laser ablation is characterized by a laser pulse much shorter than the electron cooling time, so the electron-lattice coupling can be neglected, and the heat transfer from electrons to lattice takes times on the order of few picoseconds.

Studies that compares LIBS measurements between nanosecond and femtosecond lasers showed that continuum emission were drastically reduced in early stages of plasma formation with femtosecond excitation (see figure 5 a) [12, 30-32] although these results were obtained applying different laser wavelengths, according to the characteristics of the laser systems used in the studies. Nevertheless, a direct comparison between nanosecond and femtosecond ablation using the same wavelength and fluence, remarked that background emission is much higher when single-shot nanosecond pulse irradiation was used [33]. This strong continuum emission would be explained by the laser-plasma interaction with nanosecond pulses, and the confinement of free electrons in the plume. For fluences above the plasma formation threshold, a higher signal-to-background ratio is also observed with nanosecond LIBS, due to the shape of the continuum spectrum [33, 34]. On the other hand, most species observed with ultrashort laser irradiation are neutral, while ns-LIBS provides more ionic lines, as the interaction of the laser source with expanding plasma and the core plasma free-free and free-bound transitions. Representative spectra showing these features are shown in figure 5 a. This also influences on the plasma temperature and electron density obtained with femtosecond laser sources, which are lower,

as the induced plasma expands without any other process. Both fs and ns plasmas present an exponential decay on temporal evolution of electron density, but the trend is much faster for fs plasmas, which results in a shorter plasma lifetime [35-37].
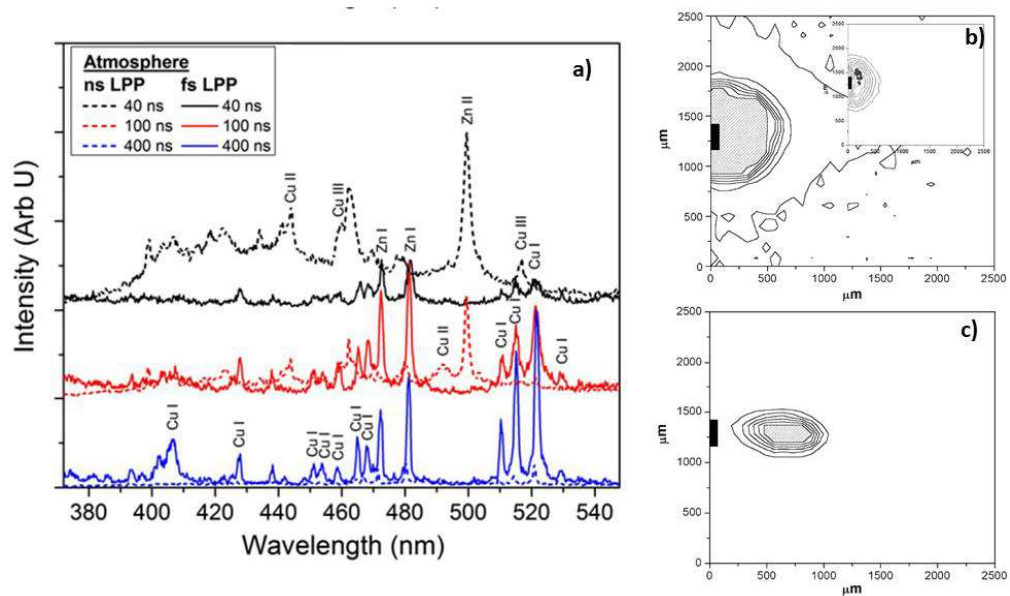
***Figure 5**: a) Temporal evolution from spectral emission for ns and fs LIBS plasmas of brass, collected 1 mm from the target and 2 ns gate width (adapted from [40]). Spectra have been normalized to the maximum peak intensity of each laser plasmas. The ns LPP were produced by a Nd:YAG laser with FWHM of 8 ns operating at 1064 nm, and fs LPP with a Ti:Sa with FWHM of 40 fs at 800 nm. b) and c) Plasma images of a titanium sample at a delay of 1300 ns and gate width of 300 ns, using a Nd:YAG laser of 7 ns at 532 nm for b), and a Nd:Glass laser of 250 fs at 527 nm for c). The black bars are plotted for showing the dimensions of laser spot size. Inset in b) represent the same emission at lower CCD gain to distinguish the inner core shell without saturation. Adapted from [38].*
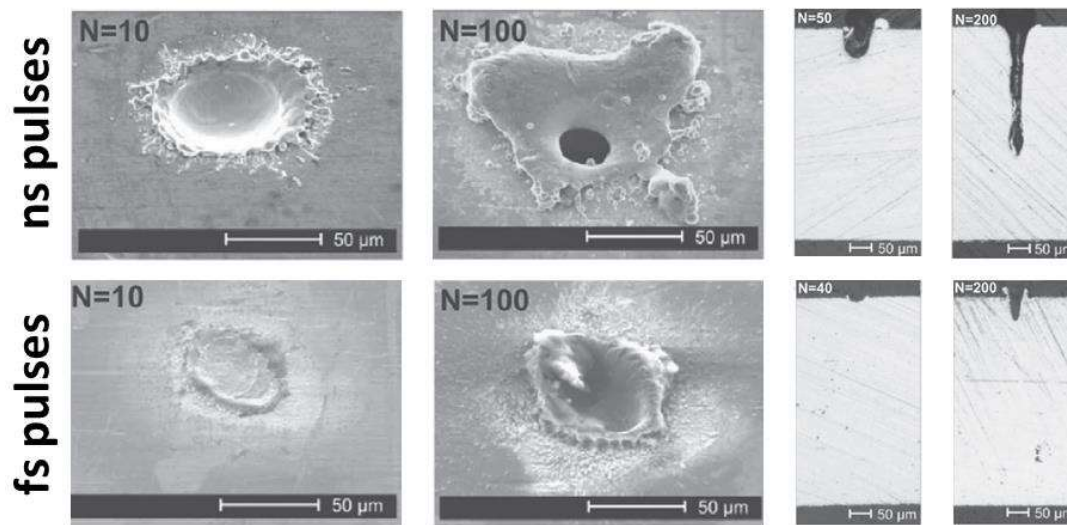
Figure 6: *Ablation of a steel sample with different laser pulse widths, at front and side views. N is the number of shots applied onto de the target. Ablation was carried using a ns laser of 60 ns FWHM operating at 532 nm, while ablation with fs pulses was performed with a laser of 170 fs at 800 nm. Figure adapted from [6].*

Plasma expansion also presents notable spatial and temporal differences according to the pulse width. The distribution of fs plasma plumes presents a narrower angular distribution of charged species compared to ns plumes due to the kinetic energy provided by the laser pulse. The differences in distribution are explained by the high-pressure confinement caused by the strong overheating on the irradiated area by the laser irradiation. This results in a spherical expansion of the plasmas generated by ns laser pulses, while plasmas generated with fs lasers expand firstly perpendicular to the target surface and show a cylindrical shape, as shown in (figure 5 b and c), and after several nanoseconds, start a slower lateral propagation [35-40].

In addition, the pulse width also produces differences in the final crater morphology. Many works have studied the efficiency of laser ablation according to the pulse width [3, 6, 7, 12, 42, 43] comparing mainly ns and fs ablation and their advantages applied to different applications. Ablation with nanosecond pulses implies that material is molten, and then vaporized for plasma formation. This results in a considerable molten layer and material removal. The diameter of the crater is increased when multishot ablation is applied, but as the material is then removed both at liquid and vapor phases, the vaporization process creates a recoil pressure which ejects molten material and creates a rim around the crater (figure 6) [6, 7]. On the other hand, the short duration of femtosecond pulses, only the irradiated volume is ablated, and the rapid creation of vapor and plasma obtained produces a negligible heat conduction. These rapid transitions allow a better control in drilling

application, and good reproducibility during experiments is achieved, with a smaller heat-affected zone and lower ablation threshold [7, 3, 44]. Although the ablation rate is higher with ns laser ablation, as it can be observed from figure 6, fs laser ablation offers higher efficiency and precision of material ablation, and results in minimal damage of the target [32, 35].

1.3.2. Laser pulse wavelength

The relevance of wavelength is widely known in common processes of our surrounding environment, so, it is intuitive that wavelength also plays a fundamental role during laser-matter interaction. Long wavelengths on the infrared electromagnetic spectrum are related to thermal effects as target heating, vaporization and thermal diffusion. These processes occur easier as photons have low energy, and are only able to excite electrons, and thus these wavelengths are appropriate for ablation of metals and semiconductors. In opposition, the photons associated to short wavelengths have higher energies and are the main responsible of processes such molecular dissociation and chemical reactions. These wavelengths are more suitable for ablating organic compounds and dielectrics due to their stronger binding energy and wide band gap [45, 46]. In addition, stoichiometry of the ablated mass must be representative (no fractionation of the sample) and the same amount of mass should be ablated independent of the sample properties to obtain an accurate chemical analysis. higher ablation mass rate and lower fractionation have been reported when irradiation with shorter wavelengths. As a result, reduced as before, and an enhanced laser-target coupling is obtained due to higher critical density of the plasma [8, 47].

These phenomena can be explained by the following description. When the photon energy is lower than the binding energy, the prevalent ablation mechanism in metals was associated to photothermal initiated by free electron energy dissipation with phonons vibrations. But in semiconductors and dielectrics ablation will be strongly dependent on the band gap energy of the material. On the other hand, if the photon energy is higher than the binding energy, the most relevant ablation mechanism is related to photochemical processes, with release of atoms, molecules and clusters as a consequence of chemical bond breaking [46]. The dependence of some processes as inverse bremsstrahlung, photoionization and absorption with wavelength have been appointed by several authors [48, 49], as well as a dependence of the ablation threshold [5, 46]. Higher ion kinetic energy

and plasma temperature are also reported when ablation with longer wavelengths are applied [50].

The main processes observed due to the laser wavelength also depends on the pulse width. It is then commented some significant results obtained under ultrashort laser irradiation as a function of the wavelength.

After irradiation, material is strongly ionized by the generation of an electron-hole plasma. In this sense besides the optical properties of materials, it was reported that the ablation threshold is influenced by the wavelength and the electron number density generated during excitation of the target. In the case of metals, the minimum energy required for an electron to escape from the atom must be equal to the work function, but electrons need an additional energy from the photon to drag an ion out the lattice of the sample. In dielectrics, in contrast, electrons must be promoted from the valence to the conduction band, and photons must provide an energy at least equal to the ionization potential [3]. It has also been found at further stages of ablation, an earlier melting of material and faster evolution of ablation processes with shorter wavelength under irradiation with fs laser pulses, as it is described in detail in Publication 3 of this dissertation.

Experiments with femtosecond lasers applied in LA-ICP-MS also reported that shorter wavelengths showed a lower ablation threshold, and higher particle counts [47]. Differences in detection limits as a function of energy, and higher signal with less energy was obtained when irradiation at 400 nm was used. Moreover, the important differences observed with shorter wavelengths in longer pulses ablation, have been improved with femtosecond laser irradiation as nanoetching, nanomachining or LIPSS [51-54].

1.3.3. Laser pulse energy

Fluence represents the deposited energy on the sample per unit area, while irradiance refers to the deposited power on the sample. According to these parameters, it has been studied its relevance in literature related to femtosecond laser ablation, as the energy is fully deposited onto the target. This involves a drastically different explanation of the ablation processes, since higher irradiance and fluence values are reached when femtosecond laser irradiation is applied.

One of the featuring characteristics related to fluence with ultrashort laser pulses is the lower ablation threshold of materials compared to ablation with longer laser pulses by theoretical approaches and experimental evidences, as reported in subsection 1.3.2 [3, 42, 43, 56]. Additionally, it was reported a dependence of the crater radius with the fluence of the laser beam when it has a Gaussian profile [54, 57], which results in an increase of the crater on the target proportional to the fluence, as seen in figure 7. The variation of the spot size with fluence provides a method for the estimation of the fluence threshold for ablation, besides the theoretical description proposed by Gamaly et al. [3]. Furthermore, two different ablation regimes can be found as a function of the laser fluence. At lower laser fluences, ablation will be determined by the optical skin-depth, while at higher fluences ablation will be governed by the electron thermal diffusion length [42, 58]. According to the purposes of material application, the fluence is adjusted to range from gentle ablation, with generation of jets or ripples [12, 59, 60], to drilling [61].

The general gaussian profile of femtosecond laser pulses involves that the energy of the pulse follows this distribution through the spatial profile of the pulse, and most of the energy is delivered by the centre of the pulse. This energy distribution has allowed fluence-resolved studies where the related ablation processes can be observed simultaneously during a single shot event [62-64]. These studies revealed that fluence is a key parameter during ablation of materials, and the evolution of an irradiated material can follow different processes during ablation and an earlier evaporation of material with increasing fluence, as it will be described in Publications 1 and 2.
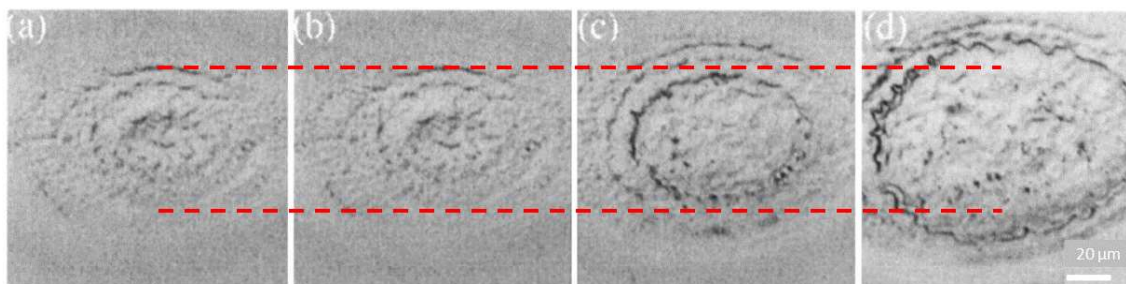
Figure 7: *Images of craters on a silicon sample produced after irradiation with a laser pulse of FWHM of 83 fs, operating at 800 nm, at different flueces. a) F = 0.5, b) F = 0.8, c) F= 1.0, d) F = 1.5 J/cm². Adapted from [55].*

As the processes involved during ablation are fluence dependent, it is derivable that plasma properties are also characterized by the applied fluence. Sirven et al. [33] carried out measurements comparing both the pulse width and fluence, keeping fixed all the external parameters. They observed that continuum emission increased proportional to the fluence of the laser pulse, both for ns and fs irradiation, and reported that both the atomic and ionic emission lines decreased by the same proportion of fluence decrease. It could be concluded that, both temporal dynamics of the emission and decay of the line intensity are determined by the laser fluence.

1.3.4. Other parameters

Among the parameters which have mentioned above, there are several external parameters. They are not related to the characteristics of the laser source but have a significant influence during ablation and plasma emission. A proper knowledge of the relevance of these parameters, set the complete frame of adequate laser ablation conditions for a particular purpose.

Most of industrial and spectroscopic applications are effectuated in ambient atmosphere conditions, but there are techniques that must be implemented under different atmospheric conditions as time-of-flight or mass spectroscopy. In this sense, the surrounding atmosphere is an external parameter which needs to be considered for a better understanding of plasma plume dynamics. Femtosecond laser-produced plasmas have been studied under different background atmospheres, and it was corroborated the one-dimensional expansion of the plume was compared in atmosphere and vacuum conditions [41].

The confinement produced because of atmosphere, a narrower angular distribution of species was observed, as it can be seen in figure 8 a and b and has been mentioned in
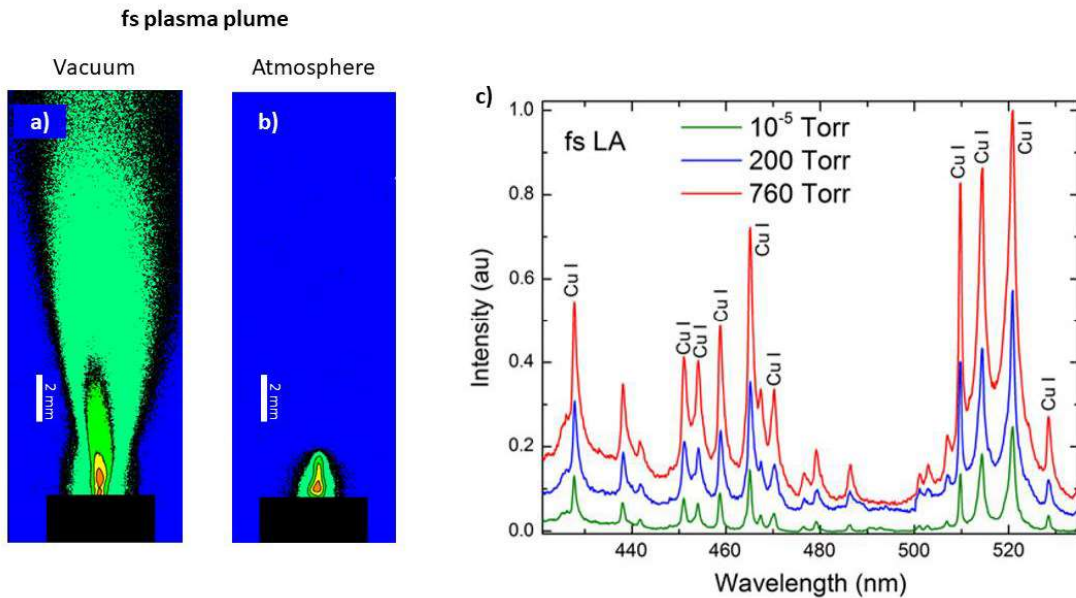
Figure 8: *ICCD of fs laser-produced plasmas in vacuum ≈10⁻⁵ Torr a) and atmosphere b). Intensities were displayed in logarithmic scale and normalized to the maximum intensity observed (adapted from [47]). c) Brass sample emission spectra from fs laser-produced plasma at different ambient pressures with a gate delay of 100 ns and a gate width of 1 µs (adapted from [40]). Laser parameters for a), b) and c) were a Ti:Sa laser with 40 fs FWHM, operating at 800 nm*

subsection 1.3.1. A decrease of the background signal with lower pressure during spectra acquisition regardless the laser pulse width was also reported. In opposition, the intensity of emission lines is decreased at lower pressures, due to the increase of the mean free path and the free expansion of the plume. Intensity then increases with ambient pressure and reaches its maximum for pressures near the ambient atmosphere [40] (figure 8 c).

In addition to contribution of the atmospheric pressure, it has to be considered also the composition of the surrounding environment. Remarkable differences in the intensity of emission lines according to the composition of the surrounding gas with ns laser irradiation have been reported. It was observed that emission intensity is increased when the buffer gas is helium, but a considerable enhancement of emission lines is obtained under argon atmosphere, as it is presented in figure 9 a. It was also studied the decay trends in atomic carbon and carbon molecular bands under these atmospheric conditions. While atomic carbon decreased faster under air conditions than under helium gas, it was found the opposite scenario in molecular emission, as carbon atoms interact with the oxygen and nitrogen from atmosphere [25]. It was also shown that argon atmosphere also involves higher broadening of emission lines when UV fs laser-produced plasmas were induced in those surrounding atmospheres figure 9 b. The fundamental contribution to line broadening is produced by the Stark broadening, introduced in Section 1.2, and is dominated by electron impact. The broadening observed at different buffer gases can be
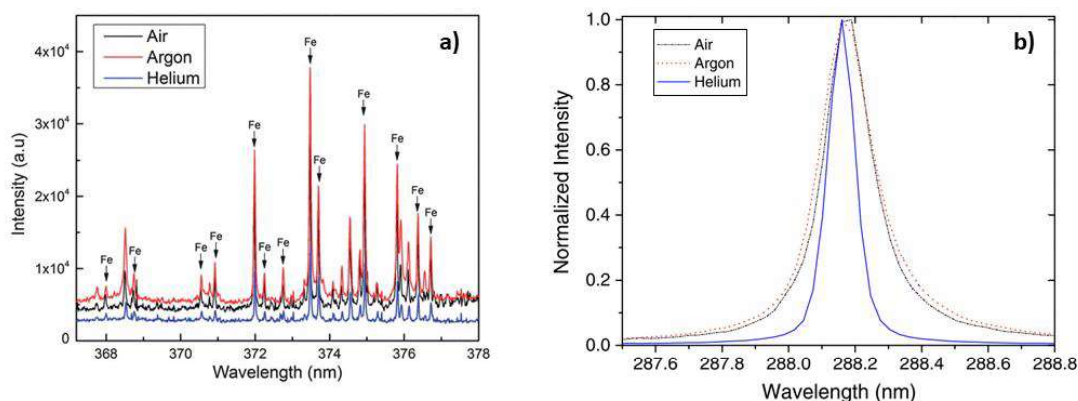
Figure 9: a) Spectra emission from a coal sample of fs laser-produced plasma acquired with different surrounding gas. Spectral window is centred between 367-378 nm for monitoring iron emission from ns laser-produced plasma (4 ns FWHM, Nd:YAG laser at 266 nm). Acquisition were developed with gate delay of 300 ns and gate width of 225 ns (adapted from [25]). b) Effect on the broadening of Si (I) emission line at 288.16 nm under different surrounding gases at atmospheric pressure. Intensity has been normalized to observe a better comparison of broadening. Plasma produced with a KrF laser at 248 nm and 450 fs FWHM. Delay time was 100 ns and gate width 1 μs (adapted from [65]).

explained considering that ionization potentials from air and argon are lower than the potential of helium, and consequently, they can be easier ionized and contribute to the Stark broadening [65].

The characteristics of materials are also relevant factors for laser ablation. The optical and thermodynamic properties intrinsic in any material and their response under irradiation determined by these physical properties, which are strongly related to the wavelength. The previous discussion has evidenced that fs laser ablation follows different physical processes, and also the nature of the target is an essential feature which must be considered when ablation experiments are carried out. The nature of the target is involved in ablation processes since the laser excites the electron system, and this will be further explained in Section 2 of this dissertation. In addition, the higher precision and accuracy, and the smaller heat affected zone during ablation with femtosecond laser pulses are advantageous in thin films laser ablation. Differences in craters produced by ns and ps laser irradiation have been reported when the effective penetration depth is larger than the film thickness [66]. This means that there is a dependence of the ablation threshold fluence and emission line intensity on the film thickness [67]. Nevertheless, these characteristic present advantages in applications as micromachining where thin films are involved, as fs laser ablation allows selective removal of thin films [68].

2. FUNDAMENTALS OF FEMTOSECOND LASER-MATTER INTERACTION

2.1 Temporal description of ablation processes

Laser-matter interaction is a multidisciplinary field which has ended in a wide variety of applications, but all of them have in common that matter is excited and influenced by the electromagnetic fields of a laser pulse. Ionization, heat and energy transport, hydrodynamic expansion, and plasma formation are some of the processes affected by the characteristics of the laser pulse, as it has been described in the previous section. Development and improvement of laser sources has offered the challenge of shortening laser pulse width, achieving femtosecond timescales. Femtosecond lasers, due to its short duration, allows studying the morphological processes induced on a sample separately in time.

In this section, the main processes reported during femtosecond laser ablation are explained, for a comprehension of this complex phenomenon. Briefly, excitation of the sample will take place during the first hundred femtoseconds, followed by melting, in a picosecond timescale. Morphological processes related to ablation and plasma formation will appear much later and remain for longer times compared to the laser pulse duration. Despite this evolution is presented in chronological order, it should be remarked that under certain circumstances as high intensity irradiation, some of these processes can coexist or follow different pathways.

2.1.1 Carriers excitation

It was mentioned previously that the laser energy is absorbed mostly in the skin layer, which usually has a depth of several ten nanometers. This parameter is much smaller compared to the size of the focal spot, so in most cases one-dimensional treatment of laser-matter interaction can be applied [2]. Plasma frequency, the effective electron collision frequency, absorption coefficient and the skin-depth, would vary as a response of the electron number density of the sample. Consequently, these parameters are functions of the laser intensity and time. But such scenario would turn complicated the treatment of these processes [3, 68] and is out of the focus of this work. As relaxation processes of the sample starts once the laser pulse has finished, it can be considered as a good approximation that matter remains at initial solid conditions. These considerations justify the time-independence

assumption of optical properties, and allow comparison with experimental data, as shown in [2].

The absorbed energy density can be also derived without any specific mechanism of light absorption. When time is averaged over many laser periods, it can be related to the initial laser intensity, and the absorption coefficient obtained from the Fresnel formula [2-4, 70]. The absorbed energy density rate can be then expressed by a reduced expression

$$Q_{abs} = \frac{2A}{l_{abs}} I(r, x, t) \qquad (16)$$

Absorption of light triggers the electron movement due to the electric field of the laser pulse, with frequency ω_L. The perturbation of electrons produces the excitation of the material and can be described by the Drude's model for a free-electron gas, associated to the following dielectric function

$$\varepsilon(\omega_L) = \varepsilon_r - \left(\frac{\omega_P}{\omega_L}\right)^2 \frac{1}{1 - i\,\nu_D/\omega_L} \qquad (17)$$

In this expression, the term ε_r corresponds to the dielectric constant of the unperturbed material, ν_D is the damping constant, and ω_P is the plasma frequency, which depends on the free electron number density n_e and electron effective mass m_e.

$$\omega_P^2 = \frac{n_e e^2}{m_e \varepsilon_0} \qquad (18)$$

This approach has been applied for electron excitation and establishing a comparison, regardless the nature of the material, with experimental results in dielectrics [63, 64], and applied in the description of excitation of metals [71]. This treatment remarks that electron excitation corresponds to a general response, which consists on an increase of the electron density on the surface where the material has been irradiated by the laser pulse, according
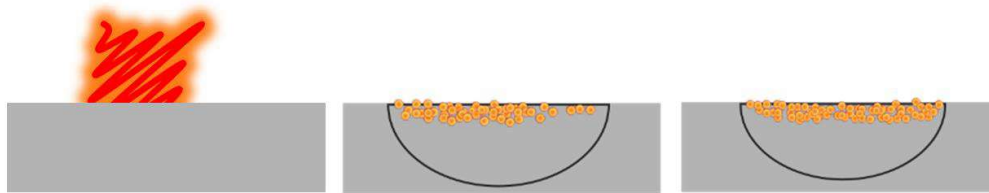
Figure 10: *Schematic view of excitation process under ultrashort laser. On the left it is depicted the arrival and penetration of the laser pulse. The pictures on the centre and right show a gradual increase of the electron density on the surface. The time lapse of this picture is less than 5 ps, depending on the energy of the laser pulse and the nature of the sample.*

to figure 10. But according to the material structure, different excitation mechanisms would be followed. An explanation of the processes involved after absorption of the laser energy is given afterwards, depending on the nature and physical properties of materials.

Metals

The presence of electrons in the conduction band in metals favors direct absorption of laser energy by electrons, undergoing collisions with nuclei or inverse bremsstrahlung [72]. Electrons below the Fermi edge can absorb photons ending at energies above the Fermi edge. The average energy increase of electrons in this sense will also be influenced by reflectivity and the free carrier absorption coefficient [71]. This results in an increase of electron number density on the surface of metals during laser pulse irradiation at hundreds of femtoseconds later.

The electron dynamics followed after laser excitation has been discussed under different scenarios. The discussion carried out in [73] suggested that the temperature of the electron gas would follow the laser pulse shape in time, due to the low mass and specific heat of degenerate electrons compared to the ions of the lattice. In case of ultra-short irradiation, the energy is instantaneously accumulated on the electron subsystem, and thermal equilibrium is reached after relaxation of electrons with the lattice system at longer times [12, 42]. The study of interactions among electron-electron and electron-phonon collisions was carried out in [74, 75], considering processes as inverse bremsstrahlung, and the generation of secondary electrons during dynamics after laser irradiation.

The combination of the laser energy deposition with a high thermal conductivity of metals can influence the interaction of electrons and results in sharp temperature gradient (72). While the temperature of electrons increases during laser irradiation, lattice temperature remains low due to the difference in heat capacities [2, 7].

Semiconductors

In semiconductors, electrons must be excited over the band gap, before the direct absorption of photons. Fortunately, the band gap in semiconductors, often lies in the range of visible photons, which increases considerably the probability of transition of electrons from the valence band to the conduction band. This transition favors the generation of an electron-hole plasma [71, 76]. Even in semiconductors with indirect bandgap, as silicon, it

is possible single-photon excitation [77]. This electron-hole plasma increases the density of free electrons in the conduction band, which can be estimated by the Drude's model, as commented in the beginning of the section (Eq 17) [12, 64, 71, 76].

Free carrier absorption is increased due to the generation of this electron-hole plasma, and, when some of the carriers are excited well above the bandgap, additional excited carriers can be generated by impact ionization and Auger recombination [77, 78]. However, single or multiphoton absorption processes would be attached to attenuation due to screening by the high density of electron-hole plasma [76, 78, 79]. It has been reported that, under strong excitation of semiconductors, a strong lattice instability is induced by carrier-carrier and carrier-phonon scattering in few hundred femtoseconds [71, 76, 77], which can be observed in a variation of the optical constants of semiconductors [80-82]. These instabilities are attributed to an ultrafast or non-thermal phase transition. They are provoked by direct stimulation of the laser pulse, in a sub-picosecond time scale, and involve neither lattice heating nor electron-phonon interactions [72].

Dielectrics

Excitation and absorption of visible light in wide band gap dielectrics, can only be carried out at high intensities, leaded by nonlinear processes. The most accepted description of excitation in dielectrics assumes that electron density increases until the real part of the dielectric function described previously may vanish, to acquire a negative value. A negative dielectric function results in a complex refractive index, which implies a strong absorption like the observed in metals. This description can be carried out when a critical electron density, n_{ec}, is reached under the following condition obtained from the Drude's model, described above in this section [71].

$$\frac{\omega_L}{\nu_D} \gg 1 \Rightarrow n_{ec} = \varepsilon_0 \varepsilon_r \frac{m_e \omega_L^2}{e^2} \qquad (19)$$

The generation of free electron density in the conduction band of a dielectric requires multiphoton ionization. Nevertheless, when high intensities are reached, a transition from this process to tunnel ionization takes place [12, 71, 83]. This transition is typically governed by the Keldysh parameter

$$\gamma_K = \omega_L \frac{\sqrt{m_e^* \varepsilon_{gap}}}{e E_L} \qquad\qquad (20)$$

This parameter is basically the ratio of the band gap energy to the pondermotive energy of the electron oscillating in the electric laser field. In this expression, m_e represents the reduced electrons and holes masses, ε_{gap} is the band gap of the material and E_L is the laser field electric field amplitude. A wide band gap and a small ponderomotive energy, imply that many photons should be absorbed, and correspond to a Keldysh parameter $\gamma_K \gg 1$. On the other hand, if the ponderomotive energy surpasses by far the band gap, electron can appear in the conduction band by tunneling ionization [71]. Approximate expressions, studies according to different parameters and experimental cross-sections related to these processes can be found in the literature [84-87].

Once electrons are in the conduction band of the dielectric, they empower more electrons to overcome the band gap. This situation takes place when free electrons have a high energy, above a certain critical value in the order of the band gap energy. The rate of electrons excited by impact ionization and photoionization will depend on the free electron density. The probability for these processes to occur can be calculated by the multi rate equation (MRE), which gives the rate of increase of the total free electron density, avoiding a complex approximation [88, 71].

2.1.2. Sample melting

In the previous section it has been discussed that excitation of materials ends up in a high increase of the electron density in the conduction band. During melting of material, recombination processes should be considered, as well as nonlinear propagation of light or relaxation processes [12, 71, 85, 88-90]. This implies that the evolution of melting stage can last from few to several hundred picoseconds. Several stages can be identified, according to the energy of the laser pulse or the route followed during excitation, although they can coexist.

Once the electronic system of the irradiated material has been heated, electrons and phonons are out of thermodynamic equilibrium. This situation fits with a Fermi distribution of a high temperature by thermalization of electrons, and the electron-phonon system finally thermalizes by electron relaxation [71]. Thermalization can be considered a two-event process. On one hand, electron-electron collisions happen in a timescale of several
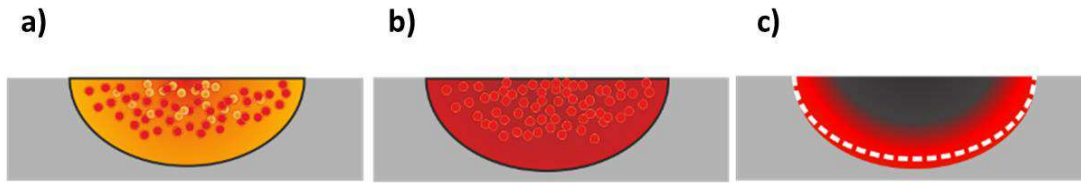
Figure 11: *Representation of the main processes described during melting of materials under ultrashort laser irradiation. a) Electron thermal gradient and onset of thermal wave. b) Electron-phonon interaction and start of ablation. c) Propagation of ablation or rarefaction wave through the molten volume.*

hundred femtoseconds [71]. On the other hand, electrons transfer their energy by collisions with the phonons in the lattice, and induce atomic vibrations, which are usually described as electron-phonon coupling [7, 73, 91] and set the commencement of melting processes. This non-thermal response of the material is fast, but takes place in a picosecond timescale as a result of the electron/ion mass ratio, much longer than the characteristic time of electron-electron collisions.

The electron-lattice energy exchange induced by electron-phonon collisions, is responsible of the transient optical and transport properties of excited materials, while the energy exchange rate controls relaxation to equilibrium once electron and lattice have reached a common temperature [92]. In this sense, prediction and interpretation of these processes, requires a confluence of different experimental techniques as, time-resolved optical, x-ray, and electron diffraction probing of short pulse laser melting [64, 93, 94], with theoretical analysis [71, 82], molecular dynamics (MD) simulations [95, 96], and the so-called two-temperature model (TTM), which has been widely applied in order to reveal mechanisms of melting in materials with ultrashort laser irradiation [7, 79, 97].

The scenario that could summarize melting of materials by the excitation of atomic motion under these experiments is presented as follows: During fast excitation of electrons, phonons remain at room temperature, and preserve their vibrations as in the unperturbed solid. When electrons reach their maximum temperature, at the end of the laser pulse, creates an electron temperature gradient in the skin layer, proportional to the absorbed energy density. The temperature gradient acts on atoms as an electron thermal wave, inducing atomic motion and a fast displacement (figure 11 a). By this time, the force responsible for the atomic vibrations in the unperturbed solid is still larger than the electronic gradient. Then, phonons vibrations last during the energy transfer from the electrons to the lattice, until the lattice acquires temperature close to the melting point, and

harmonic vibrations from "cold" phonons gradually lose their character. Interaction of different phonons modes becomes nonlinear and transforms a solid into a different phase or a disordered state, and ablation of the target is initiated (figure 11 b). An ablation wave (or rarefaction wave) starts its propagation behind the thermal wave. As electron-ions collisions involve energy-losses, the front of the thermal wave is slowed, and finally overtaken by the ablation wave (figure 11 c) [1, 2, 61, 92].

According to this description, it can be deduced that melting usually starts at the surface of the material, where the energy barrier for heterogeneous nucleation of a liquid layer at the solid-vapor interface is zero. The melting front propagates from the surface of the material limited by the characteristic speed of sound of that material. It should be considered that the time limit for melting then would be estimated by taking the thickness of the heated layer, divided by the melting front velocity [1, 98, 99]. But the physical properties of the materials, and the energy of the irradiated light, condition the heating of the lattice. Depending on the range of heating, melting can be described by several processes at different timescales.

Under conditions of high energy of the laser pulses, there are additional processes than the described during melting. It was suggested by Rethfeld et al. [98] the possibility of melting of crystals by homogeneous nucleation. This study proposed that bulk crystal could be molten in less than 1 ps under sufficiently superheated conditions. Despite melting time cannot be calculated exactly due to the dependence on many parameters, melting times in sub-picosecond timescales can be easily reached [71]. When conditions are sufficient for initiating ablation, the total time for lattice melting is limited by electron-lattice heating, and homogeneous melting is limited by lattice heating. Experimental melting times on metals agree with this assumption in a range from few to tens picoseconds [1, 93]. Nevertheless, heterogeneous melting, in addition to homogeneous melting have been observed by molecular dynamics simulations during femtosecond laser irradiation in metals and semiconductor films [71].

In semiconductors when the forces experienced by ions are strong enough, their effective potential is altered by the significant number of electron-hole pairs created [12, 77, 100, 101]. Eventually, a quasi-instantaneous disorder could be induced, even earlier than electron-phonon coupling emergence. This phenomenon has been studied both theoretical and experimentally, occurs at room temperature and is commonly called ultrafast melting [71]. However, these conditions can only be achieved under very high laser fluences, well

above the applied energy range applied on the presented study, and most of studies of this phenomenon are based on *ab initio* computational models [71].

Another ultrafast transition that has been proposed in literature is the so-called Coulomb's explosion. This process has been observed in large clusters or molecules, when highly excited electrons leave the structure, and the cluster is destroyed by the resulting repulsive force generated [71]. However, the assumption that Coulomb's explosion is present in materials under ultrashort laser irradiation has been formulated by computational methods. In this sense, it could be mentioned the study carried out by Bulgakova et al. [102], which suggest that only dielectrics could present the possibility of developing Coulomb's explosion process, but no consistent enough experimental evidences have been reported of this effect.

2.1.3 Surface deformation

Melting drives the material into a non-equilibrium state of high pressure and high temperature. The rarefaction wave from the surface of material, across the heated volume, is considered as the initial stage of expansion and ablation. But the expansion and ablation process are much slower compared to the times spent during excitation and melting [1].

Solid matter is now in a highly excited state due to the phase transitions experienced during melting. However, the density of the material can be still approximated to solid density, as ultrafast (or isochorical) heating and phase transitions produce negligible density variations. Expansion, on the other hand, is connected to atomic movement and spends much longer time than heating [71]. In this sense, we can assume a simple expansion model [71] to explain several experimental observations [103], in which a dome encapsulates the ablated material, and forms an ablation front with remarking properties, which has been supported by further analytical and numerical considerations [71].

The expansion model assumes that the material remains at a solid-state density, but, when the critical temperature of the material is reached, its expansion is modeled as a uniformly heated, semi-infinite layer which can be described by equations of gas dynamics. When these conditions are applied, a direct dependence of pressure on density is found as a result of the excitation of the pulse within the material, which initiates expansion. Expansion of matter sets the coexistence of a two-phase region (liquid and vapor) and can be described by a density profile. On the other hand, sound velocity is a function of density. The sound

velocity has a constant value before the start of the two-phase regime. The solution yields an exponential expansion profile of the surface of the material and can be considered as the head of the ablation front. However, the velocity of sound is drastically decreased when the material enters in the two-phase region, which means the existence of a density steep gradient, which acts as an optically sharp interface [71].

This model can be further understood as follows. In subsection 2.1.2 it was mentioned that the melting front of material is followed by a rarefaction wave and propagates with a speed close to the velocity of sound of that material (figure 12 a). However, when the rarefaction wave reaches the interface of unmolten material, and is reflected, the molten material is left in a liquid-gas mixture as it propagates backwards. The velocity of sound is then drastically decreased, due to the expansion of the ablated material, which is decreasing its density (figure 12 b). As a result, the expansion of the gas-liquid mixture is faster than the velocity of sound of the rarefaction wave. The ablated surface area cannot be reached by the rarefaction wave, remaining in condensed state (figure 12 c). Increasing the fluence increases the gas-liquid mixture, but the thickness of condensed shell decreases. The Gaussian beam distribution of ultrashort laser pulses, as they present a fluence gradient, is then related to the shape of the expanding material and presents a dome shape which could be compared to the structure of a gas bubble (figure 12 d) [71, 104, 105].
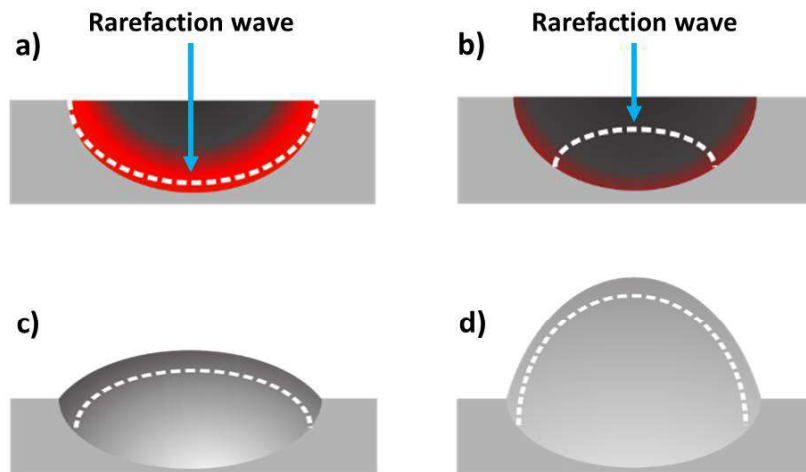
Figure 12: *Schematic plot of the expansion model of materials irradiated with ultrashort laser pulses. a) Arrival of the rarefaction wave to molten-unmolten material interface. b) Reflection of the rarefaction wave. c) Expansion of gas-liquid mixture of material. Rarefaction wave propagates behind slower. d) A gradient density in the ablated material is created due to expansion. The surface is in a solid-liquid state and creates a dome, while gas-liquid mixture is encapsulated*

The thickness and optical properties of this system makes possible that a laser beam can pass through the dome, and even through the gas-liquid mixture. Under these circumstances, the use of probe techniques with laser beams showed that the probe beam interacts with the system and develops an interference pattern [106] of Newton's rings due to the symmetry of ablated volume [107]. The optical properties of ablated material require that probe light must be reflected in order to produce interferences. One of the reflecting surfaces is the bulk (or non-ablated surface), and the second surface is the dome with liquid density, with thickness in the order of tens nanometers. Probe light is partially transmitted through the dome, since the ablated material would act as a transparent medium, and then, the light would be reflected by the non-ablated interface, creating the interference pattern.
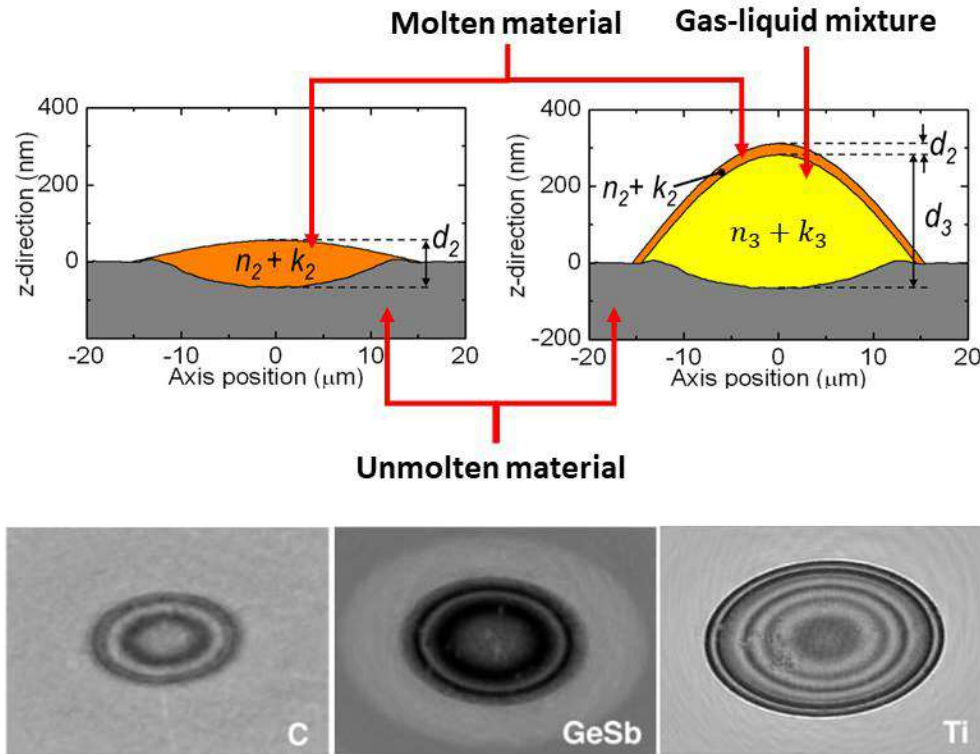
Figure 13: *Up. Example of expansion model based on experimental results on LiNbO$_3$ and computational models. In the figure, n is the refractive index and k the absorption coefficient, and d is the depth of the layer in the system. The sub index 2 refers to the optical constants of molten material and the sub index 3 refers to the liquid-gas mixture. Adapted from [105]. Down. Examples of Newton's Rings pattern in different materials. Adapted from [106].*

However, some requisites must be accomplished by the optical properties of ablated material in order to perform this ring pattern [105, 106]:

I.   The system of ablated material must consist in two optically smooth interfaces with a change of the optical properties over characteristic distances which are much shorter than the optical wavelength.

II. The layer possesses a high refractive index (n>2) and rather low absorption ($\alpha < 10^{-3}$ cm^{-1}).

This means that metallic materials, under ablation conditions would be in a state with optical properties of a highly refractive insulator [106, 108].

As it can be observed in the upper representations of Figure 13, when the melting front is propagating through the irradiated volume, the molten material has as optical constants n_2 (refractive index) and k_2 (absorption coefficient). On the other hand, during expansion of material, the gas-liquid mixture has n_3 and k_3 as optical constants, while the solid-liquid

65

layer remains with n_2 and k_2. Then, the optical constants and optical thickness $h_i = d_i n_i$ could be determined considering different approximations, including numerical, and optical ray tracing [105, 109-111]. Some results of these optical constants were determined by numerical and experimental approximation in [105]. The optical constants for the solid-liquid layer were n_2 = 1.5±0.1 and k_2 = 0.50±0.05, and n_3 = 1.3±0.1 and k_2 = 0 for the gas-liquid mixture at a delay of 315 ps on a $LiNbO_3$ sample. These studies have shown that the formation of Newton's rings pattern is a process of general nature (figure 13), which can be observed in any material if they have a surface smooth enough to avoid dispersion of the probe beam (Publication 2).

The influence and evolution of Newton's rings with fluence is shown in Publications 1 and 2. It was observed that increasing the fluence, resulted in a faster development of Newton's rings, as well as a high number of rings spaced narrower, which confirms that an increase of the energy of the pump pulse produces a faster expansion of the dome which encapsulates the liquid-vapor mixture of ablated material. Nevertheless, for a complete vision of the processes occurring during expansion stage, complementary experimental techniques have also used in the study of these processes. Imaging techniques as shadowgraphy, have reported that expansion of material is evidenced after irradiation with femtosecond laser pulses, which agrees with the observation of Newton's rings when front view imaging techniques were applied [35, 55, 110]. As material is expanding with time, at a certain time after irradiation, the liquid-state dome will break, and vaporized material will be ejected as a plasma plume which evolves with time.

2.2. Expansion of the plasma plume

Once the dome formed by molten material during expansion breaks, the vaporized material which was encapsulated is ejected as high temperature plasma. These particles expand then perpendicularly to the sample surface. Due to interaction of ultrashort laser pulses with matter, a completely different scenario is created compared to plasmas induced with longer laser pulses, as is has been explained in Sections 1.1 and 1.3. The vaporized material during femtosecond laser ablation is ejected perpendicularly normal to the sample surface during the earliest stages of plume ejection [40], and later will also expand laterally due to collisions of the front plume with the ambient gas [35, 41]. This biased expansion is explained due to a pressure confinement in the irradiated volume by the strong overheating of the material in the laser impact zone. The negligible thermal effects during ultrashort
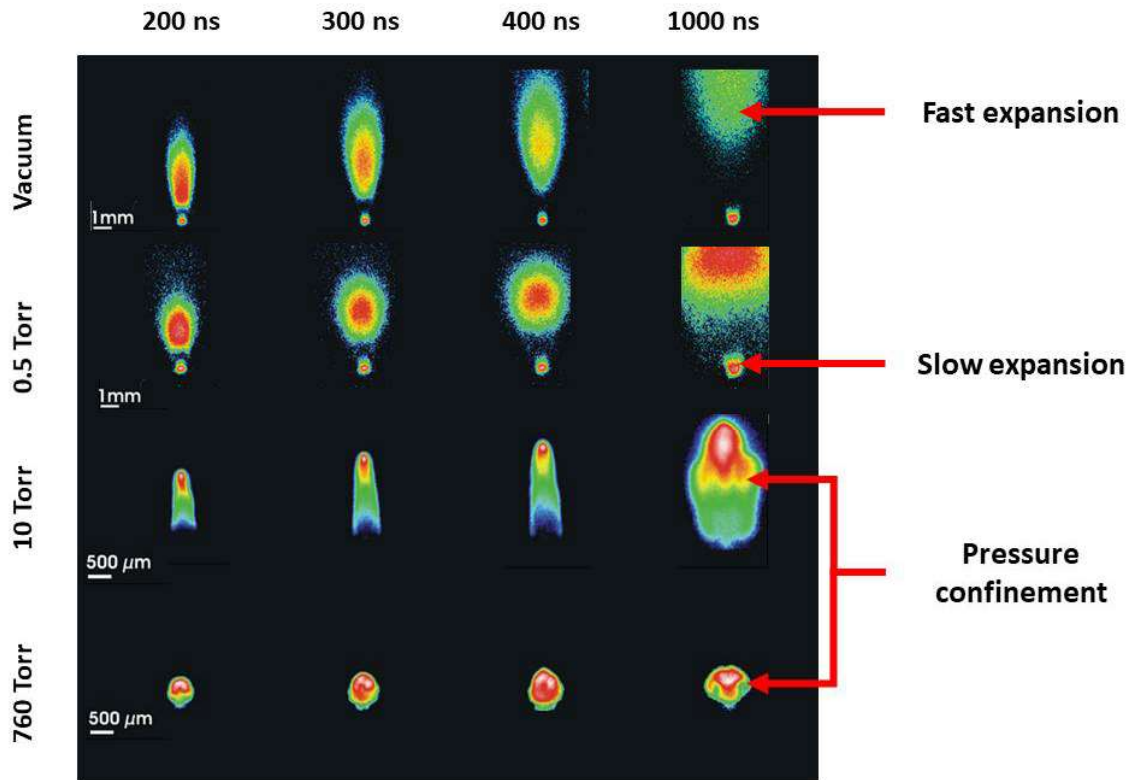
Figure 14: *Temporal evolution of brass plume under different Ar pressures, where it can be identified two expansion components and the confinement due to atmosphere. Images were normalized to their maximum intensity and the exposure time were a 10% of the delay respect to the laser irradiation. Plasma plume were produced by a Ti:Sa laser at 800 nm with 40 FWHM. Adapted from [114, 115]*

laser ablation and the absence of laser-plasma coupling result in a narrower angular distribution of the kinetic energy of the ejected particles [40, 41].

Plume shows then a cylindrical expansion and particles can be observed at larger distances from the target compared to plasmas induced with longer pulses. This characteristic cylindrical propagation is kept and can be seen enhanced with decreasing ambient pressure, as it is shown in figure 14. Furthermore, it has been reported that under low ambient pressure conditions, two components in plasma plumes with different expansion dynamics and intensity evolution are produced by femtosecond lasers. A fast component is observed propagating and occupying a great volume, with a strong decrease of intensity with time, and it is mainly composed by neutral and ions. On the other hand, a slower component which remains closer to the surface of the sample is observed which has a stronger intensity emission, and it is associated to nanoparticles generation [112-114]. However, this effect is not observed under ambient pressure due to collisions of the plume with the air increase and stops the expansion of the plume, as it can be seen in figure 14.

As many applications of laser ablation are developed in a background gas at atmospheric pressure, the effect of collisions among the plasma plume during its expansion and the surrounding atmosphere should be considered. In this sense, it is widely accepted the description provided by the Sedov´s model, which proposes that expansion of the plasma is generated by the energy deposited by the laser pulse, on the irradiated area of the target during the initial instant (116).

When the plasma plume is ejected away from the target, pushes and compresses the surrounding air and generates shockwaves. Depending on the laser pulse width, irradiance, laser wavelength or the background gas conditions, different kinds of mechanisms will take place [55, 116, 117].

According to Sedov's model, a relation between the deposited energy on the target, E, and the expansion distance between the target surface and the position of the shockwave, R, as function of the time of propagation, t.

$$R = \lambda \left(\frac{E}{\rho} \right)^{1/(2+\beta)} t^{2/(2+\beta)} \qquad (21)$$

In this expression, λ is a constant approximately equal to 1, ρ is the density of unperturbed air, and β represents the dimensionality of propagation; $\beta = 1$ for planar propagation, $\beta = 2$ for cylindrical propagation, and $\beta = 3$ for spherical propagation. This expression is valid until the counter-pressure of the ambient gas can be neglected. [35].
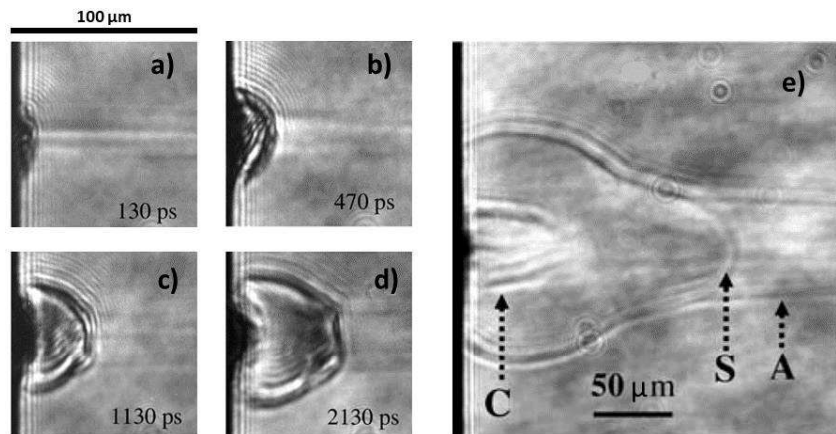
Figure 15: *(a-d) Temporal evolution of shockwave produced after fs laser irradiation on a Si sample. e) Plasma image after 10 ns after fs laser irradiation, (A) points air breakdown of surrounding air, (S) is the shock front, and (C) is the contact front. Images were obtained by laser shadowgraphy. Irradiation was induced by a Ti:Sa laser of 100 fs FWHM working at its third harmonic (266 nm). Adapted from [35]*

The structure of the shockwaves generated after femtosecond laser irradiation can be evidenced by shadowgraphic images, as shown in figure 15. A thin layer of shocked air can be distinguished which is the shock front, followed by a region of shocked and ionized air, surrounding the contact front, which limits the plasma plume. It can be also noticed the air breakdown along the femtosecond laser path due to the much larger irradiance of the laser pulse compared to nanosecond irradiation. The evolution of the shock wave generated by femtosecond laser ablation shows one dimensional propagation at times shorter than 1 ns after irradiation. Measurements of the propagation of the shockwave at this interval were fitted with $\beta = 1$ using Sedov's model and presented strong agreement, while several nanoseconds later, the shockwave propagates both in perpendicular and lateral directions [35].

2.3. Emission and decay of the plasma

The distinctive processes induced on materials after femtosecond laser irradiation has been described previously. Excitation, melting and expansion culminate with the ejection of highly temperature plasma. By the time that this material expands and interacts with the surrounding atmosphere, the excited atoms and ions decay and are excited again independently on the recombination process. Ablated material, once it was excited by a femtosecond laser pulse, has no additional source of heating, in opposition to plasmas

induced with longer pulses and results in remarkable differences concerning to experimental results.

Continuum emission produced during material recombination and interaction with atmosphere is much lower in ultrashort laser produced plasmas. The characteristic emission time is also shorter and allows the visualization of emission lines earlier than plasmas produced with longer laser pulses [38]. The main responsible of these characteristics in background emission are plasma temperature and electron number density. Plasma temperature and electron number density are lower compared to plasmas produced with longer pulses at initial stages of emission, and show a faster decay, again due to the absence of laser heating [30, 33, 35]. Furthermore, the lower temperature of plasma and the recombination processes occurring at different times explain the reduced population of ionic species observed in fs-LIBS measurements [38].

These characteristics can be considered an advantage instead of a drawback according to the goals of a study. The lower plasma temperature favors molecular band emission, and
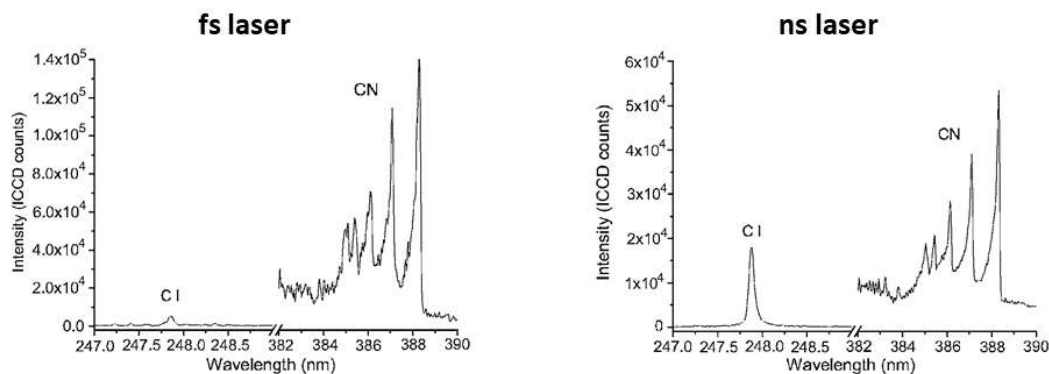
Figure 16: *Comparison of spectra from E. Coli bacteria showing C(I) line at 247.86 nm and CN molecular band with its fundamental mode at 388.30 nm. Femtosecond plasmas were produced with a Ti:Sa laser working at 810 nm with 120 fs FWHM. Nanosecond plasmas were produced with a Nd:YAG laser working at 1064 nm with 5 ns FWHM. Adapted from [118].*
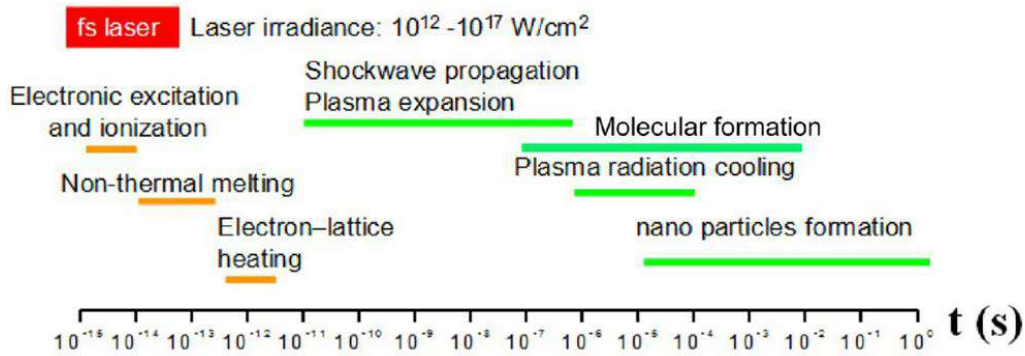
Figure 17: *Schematic representation of the temporal evolution in femtosecond laser-matter interaction. Adapted from [10].*

the lower and shorter continuum, in addition to a lower line broadening [41, 119] allows the observation of emission lines earlier than studies with longer laser pulses. This results in a higher ratio between molecular and atomic emissions (see figure 16) and observing temporal differences on emission according to their formation route of molecules [45, 118]. This has been attributed to the forward-bias expansion of the plasma plume, which has been commented previously and would present a lower plasma-atmosphere interaction [23, 119].

In summary, the description of femtosecond laser-matter interaction and evolution of the induced plasmas present distinctive features which are briefly depicted in figure 17.

3. INSTRUMENTATION USED IN THIS THESIS

In this section, the principles of femtosecond lasers are introduced, as well as the main optical components used in the progress of these experiments. Fundamental information of the description of these instruments were provided from the User's manuals.

3.1. Ultrafast laser system

3.1.1. Mai Tai laser system

The Spectra Physics Mai Tai ultrafast laser is a short pulse oscillator which seeds ultrafast amplifiers. This system comprises two lasers; a CW laser diode-pumped laser and a mode-locked Ti:sapphire pulsed laser, which are enclosure in two chambers. In figure 18 can be observed both lasers of the system running.

The CW chamber contains a high-power, fiber-coupled diode laser module, and its output power is used to end-pump a Nd:YVO4 (vanadate) lasing medium which provides laser light at 1064 nm, and produces more than 15 W of IR power with a conversion efficiency higher than 50%. This output wavelength is converted into 532 nm using a lithium triborate (LBO) crystal, as a frequency doubling medium. Despite this crystal has a lower nonlinear coefficient than other materials, provides several advantages. The output light delivered from the LBO crystal is then driven to a dichroic mirror, which allows the 532 nm light exiting from the pump chamber to the output chamber, while the 1064 nm light is reflected into the cavity.

The output chamber contains as main components a Ti:sapphire rod, rod focusing mirrors, cavity fold and end mirrors, an acousto-optic modulator for regenerative mode-locking, prism dispersion control elements and a tuning element. The frequency-double light from the Vanadate laser at 532 nm is used to pump in the output chamber the Ti:sapphire rod, which is the responsible of producing the pulsed laser output of the Mai Tai system. The absorption transitions of the rod occur in a range from 400 to 600 nm of the electromagnetic spectrum. On the other hand, the fluorescence band of the rod covers a range from 600 to more than 1000 nm, so, lasing is only possible at wavelengths greater than 670 nm, where there is no overlapping of absorption and fluorescence spectra of the rod.
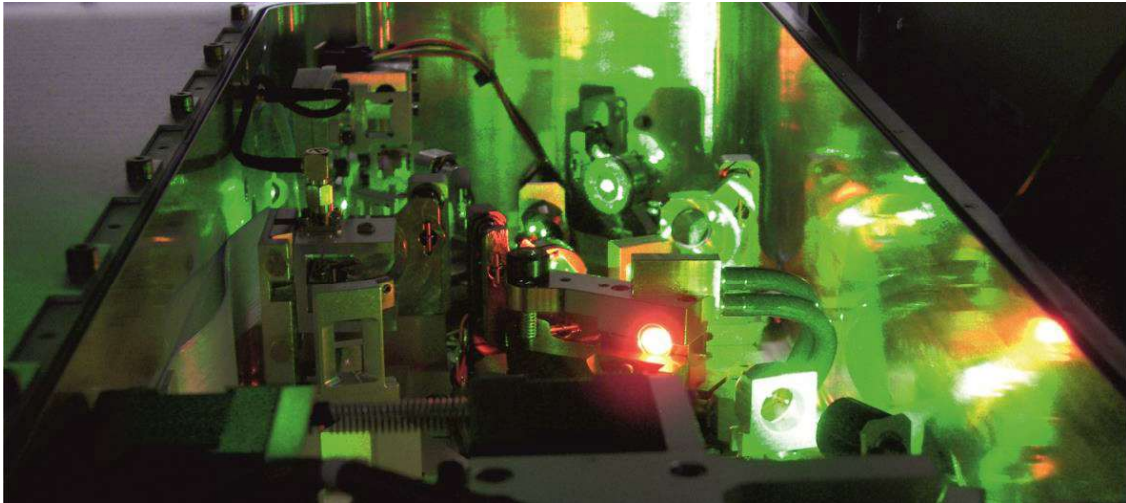
Figure 18: *Mai Tai laser system open during operation. Both lasers were running when the image was acquired. The Vanadate laser located in the CW laser chamber delivers green light at 532 nm after frequency doubling. The mode-locked Ti:sapphire laser is set on the output chamber, supplying red light.*

The output chamber is then the second stage of the Mai Tai, and works as a mode-locked laser. The cavity is longer than the found in the CW laser, with the aim to let the Mai Tai to run at an optimized repetition frequency near to 84 MHz. The mode-locked operation is ensured by the support of an acousto-optic modulator (AOM). When the laser starts its emission it also provides smooth wavelength tuning once the laser is running. Afterwards, the pulse laser uses the Ti:sapphire rod, which is oriented in such way that uninterrupted tuning is achieved within the cavity, and produces a wavelength tuning range from 780 to 820 nm. The drivers and controls for wavelength selection are in the laser head.

The femtosecond laser pulse is wavelength tuned by means of a sequence of prisms and a slit. Figure 19 shows the sequence of prisms depicted. In this system, Pr2 and Pr3 creates a region in the cavity where the wavelength components of the pulse are spatially dispersed, and the slit is placed in this dispersed beam. When the position of the slit is changed, the output wavelength is tuned.

The characteristics of the pulse width of a Ti:sapphire laser are influenced by three factors: The intrinsic characteristics in Ti:sapphire as a material itself, the cavity parameters and the selected wavelength. In this sense, as the Ti:sapphire material cannot be changed, the most adequate technique consists in modifying the net group velocity dispersion (GVD) of the cavity.
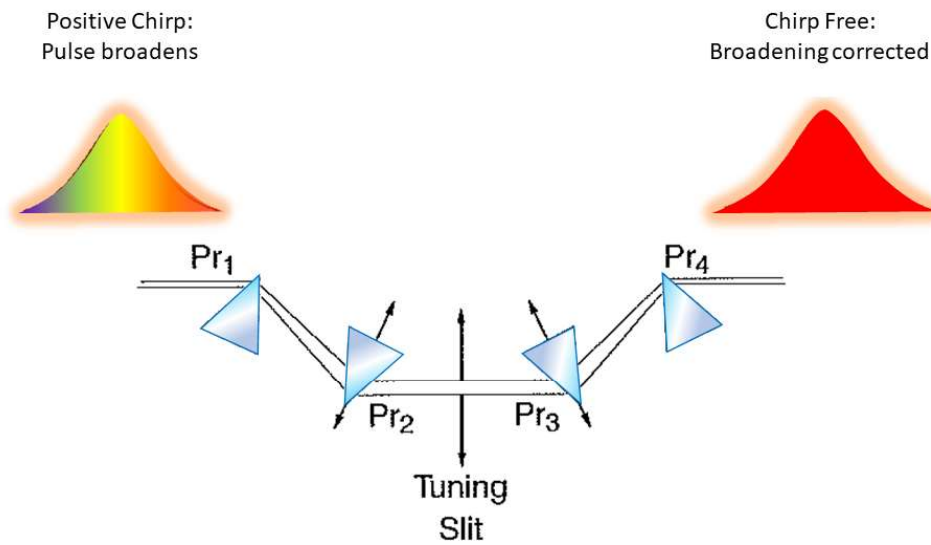
Figure 19: *Schematic representation of the prism system for intracavity GVD broadening compensation in the Mai Tai laser system. Adapted from Mai Tai SP user's Manual (Spectra Physics, Inc.)*

group velocity dispersion is said to be positive when the longer or redder wavelengths head the shorter wavelengths. In case that longer wavelengths are delayed respect to the shorter, it is said that GVD is negative. The optical components in the laser cavity produce positive GVD and the pulse is also spread due to nonlinear effects of the Ti:sapphire refractive index. These effects must be compensated in order to obtain stable and short output pulses with negative GVD. As GVD is dependent of the wavelength, it can be efficiently compensated using prism pairs. Prism pair are generally used in GVD compensation for ultrashort laser pulses, as losses can be minimized if the prisms are oriented to their Brewster's angles and the negative compensation of the GVD has a linear response over a bandwidth. In the Mai Tai laser system, two prism pairs are used to generate stable ultrashort laser pulses as shown in figure 19.

3.1.2. Ti:sapphire regenerative amplifier

The system used for regenerative amplification for carrying out the presented experiments in this work is the model Spitfire Pro XP (Spectra Physics, Inc). Basically, amplifies individual laser pulses selected from a stream of pulses which are produced by a separate, mode-locked Ti:sapphire laser (Mai Tai SP). This model was optimized by the manufacturer for delivering amplified pulses with 35 fs FWHM and a mean energy of 3.5 mJ, with a maximum frequency rate of 1 KHz.

The amplification in the Spitfire Pro system is supplied by a Ti:sapphire crystal. Nevertheless, this material is linked to damage or fracture when is optically pumped at high average powers. The responsible mechanism of this hazards in the crystal is an effect called self-focus which can be produced when a laser beam is travelling through a Ti:sapphire laser. Self-focusing is a nonlinear optical effect where an intense beam modifies the refractive index of the material as it is passing through, causing the beam to focus and intensify even further, and permanent damage can be produced in the crystal.

To overcome this situation, it is applied a technique called Chirped Pulse Amplification (CPA) [120-123]. CPA is accomplished in three fundamental steps. In summary, laser pulses are stretched to amplification and then recompressed. The implementation of this technique in the regenerative amplifier system enables amplification of laser pulses above their peak power, while the power density in the amplifier is maintained below the damage threshold of the Ti:sapphire crystal. Figure 20 shows schematically where are located the involved components in the Spitfire Pro system to ensure the correct development of this technique. It can also be seen the location in the system of the key components to implement this technique in figure 21.

The first step is increasing the width the ultra-short seed pulse which is provided by the femtosecond laser or seed laser (Mai Tai SP). This reduces the peak power of the pulse and
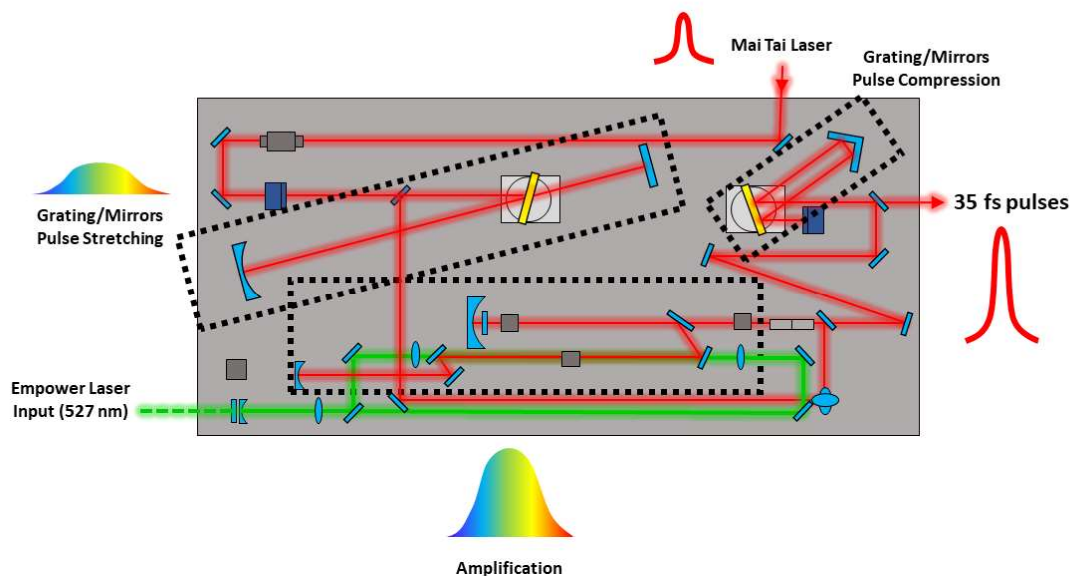
Figure 20: *Representation of the Ti:Sa regenerative amplifier, where it has been plot the optical path beam of seed laser (Mai Tai) and pump laser (Empower). Stages of CPA technique and its place in the amplifier have been remarked in dotted squares. Adapted from Spitfire User's Manual*

73

the probability of damage of the Ti:sapphire crystal. This broadening is achieved by passing the laser pulse through a dispersive medium and inducing a positive (GVD). In this sense, a diffraction grating can also be used for inducing GVD, as wavelengths from a pulse are spatially separated and can be directed to longer or shorter optical paths while the dispersion induced by other optical elements in the system are compensated.

In this laser system, it is introduced a combination of a retroreflector mirror mounted on a translational stage or stretcher. The bluer frequency components of the laser pulses travel a longer path than the redder components. This beam is multipassed through these optical elements combination, and achieves a high spectral broadening, while complexity of the system and addition of optical elements are avoided.

Once the laser pulses leave the stretcher, they are leaded to the Pockels cells to control their polarization and make pulse selection in the regenerative amplifier. The material in a Pockels cell has a certain voltage applied and can rotate the polarization of incoming light. In this system, vertically polarized light is trapped in the regenerative amplifier cavity. When the Pockels cells are on, the polarization of the pulses is controlled until they have reached their maximum amplification and they are allow leaving the cavity.

The second step in CPA consists in amplifying the stretched pulse. The selected broadened pulses which were amplified in the cavity, as they leave it, are driven to the Ti:sapphire crystal. Inmediately before the arrival of these seed pulses, the synchronous addition of a
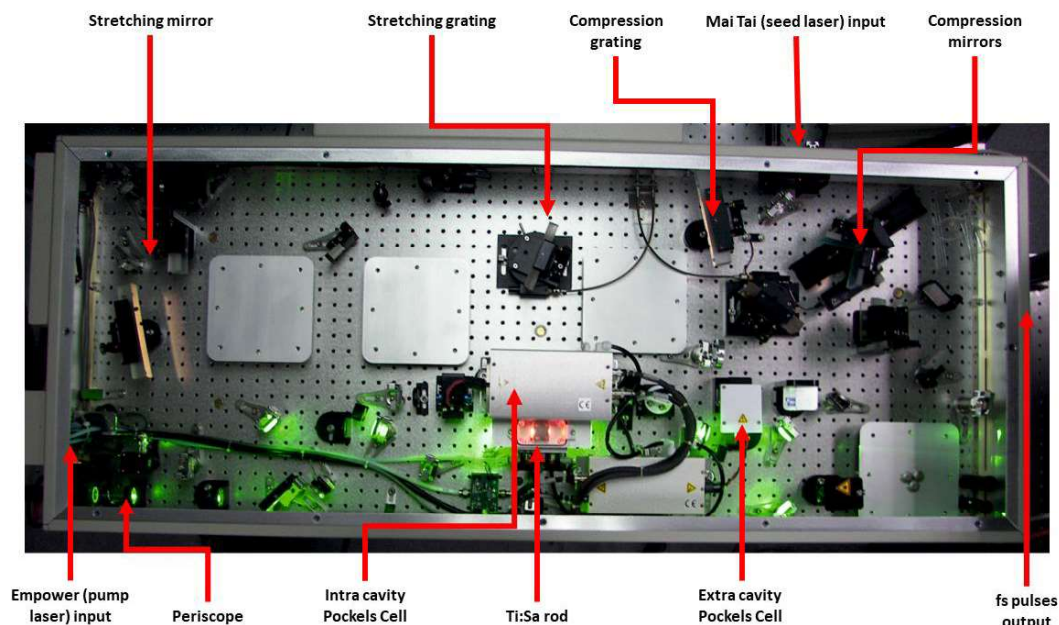
Figure 21: *Spitfire regenerative amplifier open during Empower laser alignment. The main components involved in CPA technique have been labelled.*

high-energy pulse from a pump laser (Empower, Spectra Physics Inc.) excites the crystal to achieve the condition of population inversion. Most of the energy from the pump pulse is retained by the Ti:sapphire crystal and transferred to the seed pulses. The stretched seed pulses pass several times (10 or even more) and with every pass acquire more energy from the pump pulses, until the pulse energy level saturates the population inversion in the amplifier rod, and then is ejected to the compressor.

The third step recompresses the amplified and stretched pulse as close as possible to its original width. This compression is implemented in the amplified pulse by a reverse optical combination (a diffraction grating with a retroreflector in a translational stage) than the applied during pulse stretching, which induces negative GVD and compensates all the higher-order dispersion effects resulted two previous steps of CPA technique. Finally, a 35 fs FWHM laser pulses with a mean energy of 3.5 mJ per pulse is delivered by the laser system, with a frequency from 4 Hz to 1 kHz.

3.1.3. Autocorrelator

The autocorrelator used in the development of this work (PulseScout, Spectra Physics Inc.) consisted of two modules: an optics module and the electronic control, which was controlled by an external control panel, which could be triggered to the laser amplifier.

The fundamental function of the autocorrelator is to control the shape and temporal FWHM of the laser pulse. This device can help in preventing the formation of pre- or post-pulses which could affect the measurements. Once the laser beam is out of the regenerative amplifier, is split by a beam sampler, and a 1% of the output laser energy is driven to the input aperture of the autocorrelator, and its optical path beam.

The optical path beam is represented in figure 22 and is split into two branches by a beam splitter. Each branch is sent to a Michelson-interferometer arm, with two mirrors in retroreflector configuration. One of the retroreflectors has a fixed length, while the length of the other retroreflector can be varied as is mounted on a linear translation stage. The two beams are then directed and recombined to the beam splitter, and they are focused by a mirror, and overlapped in a non-linear crystal. The light generated in the crystal is ultimately detected by a photodiode, then is mixed, and second-harmonic light is delivered, and driven to the detector. To ensure a good signal, an angular driver in the control panel of the autocorrelator can vary the orientation of the angle of the crystal. Once the detector
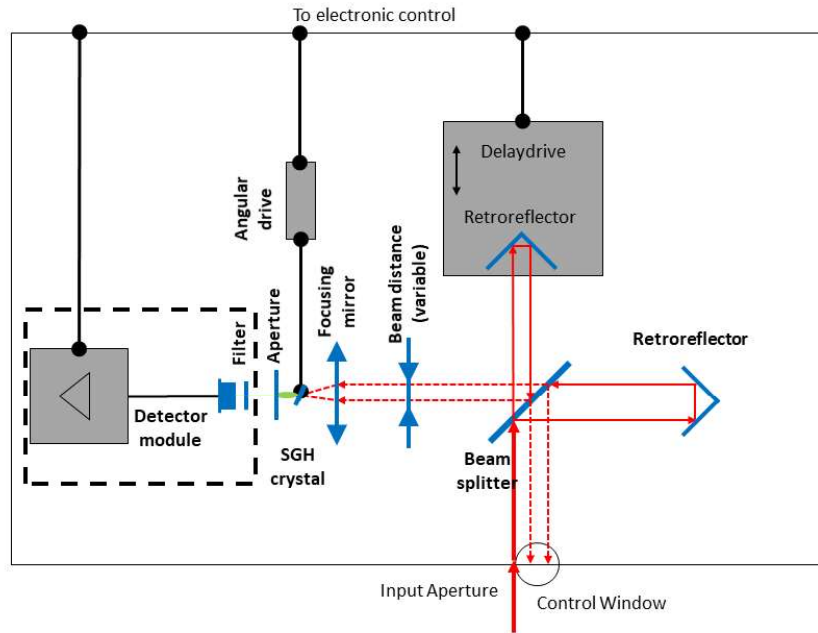
Figure 22: *Optical path beam of the laser inside the Autocorrelator for measuring the FWHM of pulses. Adapted from Pulse Scout User's manual.*

receives enough light, the detector finally converts this light into an electrical signal which is sent by a BNC connector to the rear panel of the electronic module. Finally, the FWHM of delivered pulses is shown in the screen of the electronic module.

3.1.4. Optical components

The experimental set up that has been implemented for developing the results presented in this dissertation required optical components with specific characteristics, according to the intensity which can be provided by ultrashort laser pulses. Details of the location of all optical components and their purposes in experiments can be found in Publications 1 to 4 of this dissertation.

The mirrors, plano-convex lenses and beam splitters used for leading the optical path beam consisted in a fused silica substrate with a dielectric coating, which avoided undesirable effects as group delay dispersion or energy losses, which would affect to the pulse width and the deposited energy per pulse. Parameters related to the reflected wavelengths as polarization, angle of incidence and the reflection bandwidth were carefully considered, in order to keep the most accurate results.

Additional components set in the optical path beam were optical attenuators. They were constituted by a system of three polarizers. When laser pulses input into this device, the passed firstly through a half waveplate mounted in a rotatory stage, and the laser beam could be divided into p and s-polarized beams and then, two thin film polarizers reflected s-polarized light and transmitted p-polarized light. This device provided two output beams which could be energy controlled by the rotatory stage. Optical attenuators were adequate to the incident wavelength. Indeed, an optical attenuator centred at 400 nm was the responsible of splitting second harmonic light when pump-probe experiments using a configuration of 400/400 nm were carried out.

There is a considerable number of studies which have used time-resolved microscopy using fundamental and second harmonic lights from a laser system to record transient processes during laser ablation. Despite they have used a nonlinear crystal in their experimental set up, the presented results used a harmonic generator (Spectra Physics Inc.). This device has the advantage of supplying fundamental, second and third harmonics wavelengths. This system ensures these processes by setting in fixed mounts mirrors, and nonlinear crystals mounted on rotatory stages which control the angle of crystals to the incident beam and consequently, the power.

It must be also described the optical components used during image acquisition, as they play a primary role in the effectiveness of these experiments. Craters obtained during ultrashort laser irradiation, should be magnified to record with enough resolution theis transient processes involved in materials during fs laser ablation. With this purpose, it was set in the experimental set up a microscope objective. The objective selected was a 20X (Mitutoyo Plan Apo Infinity Corrected Long WD Objective). The objective had a working distance of 20 mm, a resolving power of 0.7 μm and a numerical aperture (NA) of 0.42. The apochromatic plane objective lens avoided chromatic aberrations. Its correction for working with long or infinity distances required the support of a tube lens for focusing the light and recording images. Additionally, as a complement to this microscope objective, was located a tube lens (Mitutoyo, f = 200 mm). Its role is focusing the light and creating an image onto the sensor when infinity corrected objectives are used.

Two different optical sensors were used during measurement acquisitions. For image acquisition it was used a CMOS camera. The CMOS camera (DCC1240M, Thorlabs) recorded images acquired from pump-probe experiments. It consisted in a monochrome 8-bit sensor, with an sensitive area of 6.78 mm x 5.43 mm, and a square pixel size of 5.3 μm², which provided a resolution of 1280 x 1024 pixels. During acquisition, it was tried to

maintain the CMOS gain at its minimum level, and keeping all settings constant, in order to results among different materials could be compared. It was also ensured an exposure time shorter than two pump pulses interval.

On the other hand, LIBS measurements were acquired using an optical fibre with 1 mm diameter with fused silica core, which sent the light from laser-produced plasmas to a 0.5 focal length Czerny-Turner imaging spectrograph (Shamrock 500, Andor). The spectrograph had in its optical path beam three diffraction gratings of 1200, 1800 and 2400 lines per mm, which could be selected by the user in the software supplied by the manufacturer. The spectrograph had coupled an iCCD (iStar, Andor) on one of its outputs. The iCCD had a pixel size of 13 μm^2 and provided matrix files of 1024 x 1024 pixels.

3.2. Time-resolved optical microscopy

3.2.1. Imaging techniques. State of the art

The study of laser ablation and laser-produced plasmas requires the application of techniques which explain the complex phenomena involved [12]. Imaging techniques support theoretical approaches and experimental evidences which have been reported by other experimental procedures. They have in common an optical sensor as detector, and a specific configuration of optical elements such as filters or polarizers are the tools for providing powerful information, which allow combining them for complementary information of an experiment. In this section, some of the most frequently used imaging techniques and the information they can provided are described.

Shadowgraphy

Shadowgraphy uses a plane collimated beam and transmitted through a plasma, as it is shown in figure 23. A shadow pattern is obtained due to this interaction which can be recorded by a camera. The recorded images show differences in the image intensity as a result of the shadow pattern, and this can be related to the refractive index properties and density of the plasma. Although not very sensitive to small variations in plasma density, it is capable of showing large density gradients [124].

Shadowgraphy provides both spatial and time-resolved measurements. One of the most remarkable results achieved with this technique is the observation of shock waves during
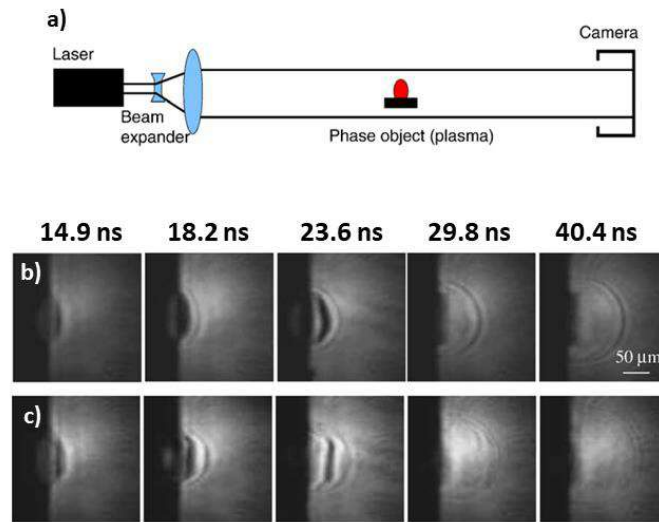
Figure 23: *a) Schematic representation of a shadowgraphy experimental set up. Adapted from [124]. Temporal evolution of shockwave propagation after fs laser irradiation (80 fs FWHM at 800 nm) on silicon b) single pump pulse irradiation, and c) double pulse irradiation (delay of 1 ps between both pump pulses). Adapted from [125].*

laser produced plasmas. Studying the dynamics of plasma and expansion velocities, and differences between single and double shot ablation, a more detailed comparison of plasmas evolution according to their pulse width [110, 117, 125-127].

Schlieren

Schlieren technique follows a similar experimental set up than shadowgraphy, but it has a lens with a knife edge on its focal point of the lens, and light is partially obstructed. The deflected light is proportional to the refractive index and can be more sensitive than shadowgraphy, although shadowgraphy is more suitable for large phase-shifts [124].

Some highlighted works which applied this technique studied temporal and spatial resolution of the electron density plasma at low ambient pressure or characterization processes in ablation of biological tissues [129-132].

Interferometry

Interferometry can be considered the most sensitive compared to the ones previously mentioned. This technique detects small phase-shifts and allows obtaining some quantitative results. A schematic interferometry experimental set up is represented in figure 24. Basically, a laser beam is divided by two, and further in the optical path beam the two
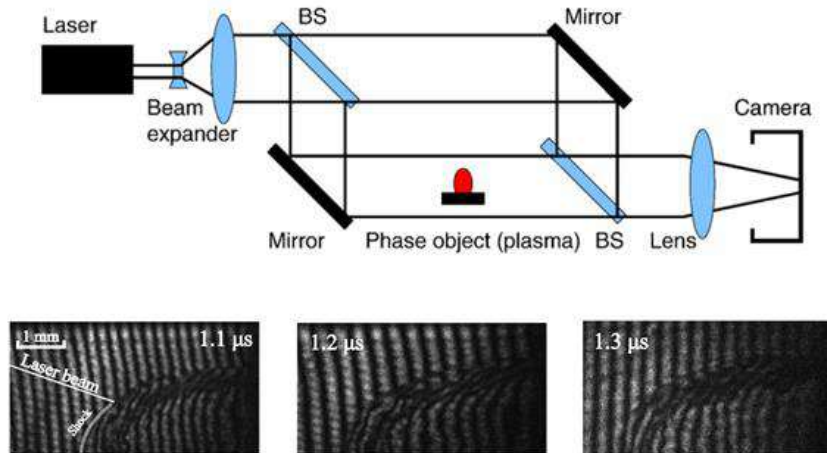
Figure 24: *Up. Schematic experimental set up for interferometry experiments. Adapted from [124]. Down. Interferograms for studying the temporal evolution of shockwaves induced with a CO_2 laser (120 ns FWHM) and probing light from a Nd:YAG laser at 532 nm. Adapted from [128].*

arms are recombined, to obtain an interference pattern. If a plasma is located in one of the arms of the two beams, the light transmitted through the plasma induces a phase shift when it is recombined with the unperturbed beam. This technique supplies measurements of electron densities where the fringe pattern appears, but, on the other hand, its accuracy is limited to the number of fringes and their deformation, while the two previous techniques information can be obtained from every pixel of an image [124].

Experiments using the Mach-Zehnder configuration for measuring the electron density in laser-induced plasmas and their correlation with the laser irradiance have been performed in the past. Another interesting study used the Michelson interferometer to investigate the behaviour of the refractive index in plasmas, observing that a strong decrease of the refractive index is developed behind the shock front [128, 133-135].

Integrated iCCD imaging

This technique is used for recording the intensity of plasmas by an intensified charge coupled device (iCCD). This is a versatile instrument which can be used in different experiments as the determination of plasma plume dynamics with temporal and spatial resolution [38, 40], laser-induced fluorescence [136] or absorption spectroscopy [137]. Another application of this imaging technique is hyperspectral imaging, which can reveal

the dynamics of different components of plasmas setting filters between the plasma and the iCCD centred at emission wavelength of the species of interest [116].

3.2.2. Pump-probe microscopy

Pump-probe microscopy is the selected imaging technique to carry out the results which are presented in this dissertation. This technique uses image acquisition in front view configuration to observe the sample where laser has been focused on to produce a plasma and allows studying the morphological processes which have been induced after irradiation. As these processes arise in very short timescales, image acquisition requires a meticulous procedure.

One of the main drawbacks which was found while developing the experimental set up of this dissertation was the following. The mechanical limitations of cameras to record these fast phenomena is associated to the opening and closure times of their shutter and therefore the exposure time. To overcome this issue, a suitable solution can be found in the principles of stroboscope photography. A flashlight is generated to illuminate the sample, and the image is acquired once the camera shutter is open. This implies that the temporal resolution will be ultimately defined by the duration of the flashlight. If the flashlight is a femtosecond laser pulse, the camera is then capable to record dynamic processes as its exposure time would be the width of the laser pulse.

The basis of this experimental procedure was introduced by Downer et al. [138] in their study of the excitation of a silicon sample using a 80 fs FWHM laser system. An improvement in acquisition image and longer times in the temporal delays of measurement revealed a detailed sequence of events during femtosecond laser irradiation [106] in different materials, which started a large number of studies, and some of them are presented in this dissertation.

Experimental set up

A scheme of the set up used in the experiments presented in this work is shown in figure 25. The optical path beam followed the procedures described in [62-64, 103-107]. It followed a customized design proposed by the author of this Doctoral Thesis adapted to the laboratory facilities and approved by the directors. The basis of this technique consists in using a laser pulse to induce ablation on the target, or pump pulse, and another pulse which is used to
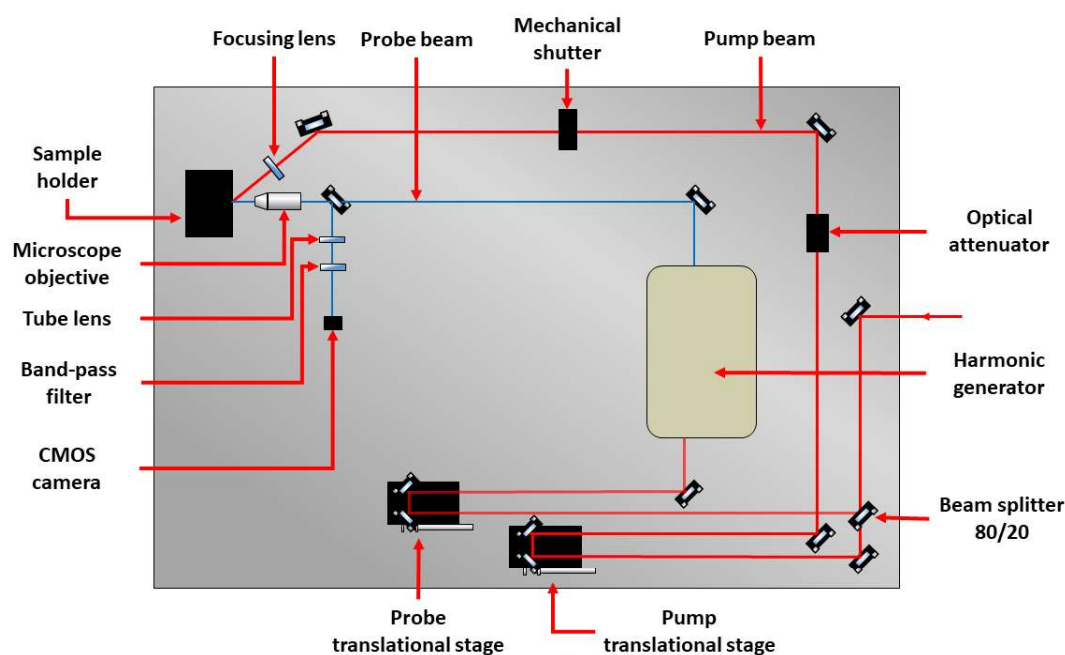
Figure 25: *Representation of the pump-probe experimental set up used in the presented studies in this Thesis. The configuration used in this figure used pump beam at 800 nm and probe beam at 400 nm.*

illuminate the target. As it has been mentioned, the temporal width of the pulse is a crucial parameter which influences in the temporal resolution for recording the morphological processes induced by the pump pulse. A high temporal resolution can then be achieved by splitting a femtosecond laser pulse into two branches, each of them run across a different optical path beam and encounter at the sample.

Once the optical lay out was completed, one of the most sensitive steps before acquiring the micrographs was the coincidence of both laser beams onto the same area of the target. A carefully alignment of the optical components was followed, otherwise the probe beam would not illuminate the area of interest of the sample. This step was accomplished when the CMOS camera could record an image of a crater generated by the pump pulse illuminated by the probe pulse and optical aberrations or diffraction effects were compensated.

To success in this experiment it is crucial to achieve a precise synchronization between the two pulses. A rough approximation of the length of the branches was obtained by measuring both optical path beams. But at a femtosecond timescale, it required a highly precise measure of the distances run by the pulses. This critic step was overcome using the linear stages with micrometric resolution. The distances run by the both beams were measured,

and their differences were compensated by the adjustment of the linear stages. A photodiode was located in the sample holder, connected to an oscilloscope, and an approximate synchronization between pump and probe beams could be measured. A more detailed description can be found in the Publication 1 of this dissertation. When any ablation process was observed, time zero between both beams was obtained, and image acquisition procedure was carried out as part of the experimental results.

Image acquisition

The procedure followed during image acquisition with time-resolved pump-probe microscopy, consisted in a collection of measurements at each time delay of interest. Each measurement performed three image acquisition series, as figure 26 shows. The first image recorded the sample light before the incidence of the pump pulse. During this step, the pump beam was blocked by a mechanical shutter, so, the sample was only illuminated by the probe beam (figure 26 a). The second image recorded the process induced after the arrival of the pump pulse when the shutter was open, with the delay which was set between the pump and probe beams (figure 26 b). The third image recorded the permanent damage of the target several seconds after the irradiation. The pump beam was blocked again in this acquisition step, and it could be then ensured that the permanent damage on the target was produced by the irradiation of one single shot (figure 26 c). The mechanical shutter and the CMOS camera were controlled by a pulse delay generator (DG535, Stanford Research Systems), which used as external trigger source a TTL signal from the Spitfire Pro system amplifier. The camera used a delay output as it could be selected its exposure time in the software settings, while the mechanical shutter was connected to the pulse output attached to the camera output to ensure a global synchronization of the experimental set up.

Images obtained during acquisition had a size of 960 x 760 pixels, when the optimal acquisition settings of the CMOS camera were selected. The combination of the pixel size of the camera, and the amplification of the microscope objective, provided a conversion factor of 0.34 μm per pixel. This equivalence was checked using white light microscope measurements of the craters obtained during pump-probe experiment, and the comparison of both images.

This experimental set up was able to record the ablation dynamics of laser irradiated samples. The images shown in figure 26 were acquired on a silicon sample with a high degree of polish, which allowed the record of the evolution of Newton's rings. Once satisfactory results were obtained, different materials were studied, attending to their degree of polish, nature of sample (dielectrics, metals, or semiconductors), and bulk samples or deposited on a glass. Despite some processes as the electron-hole plasma could be observed in a wide variety of samples, the evolution of Newton's rings required highly polished samples, as silicon or metals deposited by electronic deposition on silica glass. Otherwise, fluctuations of the reflectivity of the sample would be observed, but not the formation of the Newton's rings, as it is explained in Publication 2.

Every pump-probe measurement was taken in a wide clean area. This avoided the interaction of previous craters generated on the sample, or contribution of artefacts which could produce optical aberrations. The heat affected area of the crater was small compared to the images, but the surrounding was checked prior any acquisition of images.

Image processing
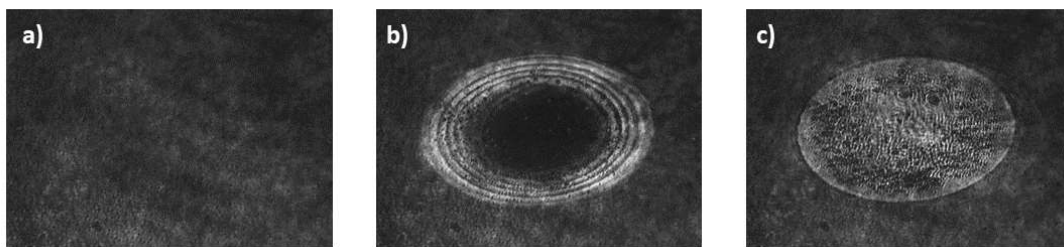
Figure 26: *Example of measurement series in pump-probe experiments. The figure shows raw images of a silicon sample before image processing. a) represents the sample with before irradiation, b) image of irradiated sample at a delay of 300 ps between pump and probe pulses, and c) permanent damage on the sample several seconds after irradiation . Pump pulses operated at fundamental wavelength at 800 nm at an energy of 200 μJ while probe pulses were frequency-doubled*

Some of the most relevant results presented in this dissertation were obtained by processing the acquired images with pump-probe microscopy technique. The acquired images were analysed and compared by a home-made script written in MATLAB®. The first image
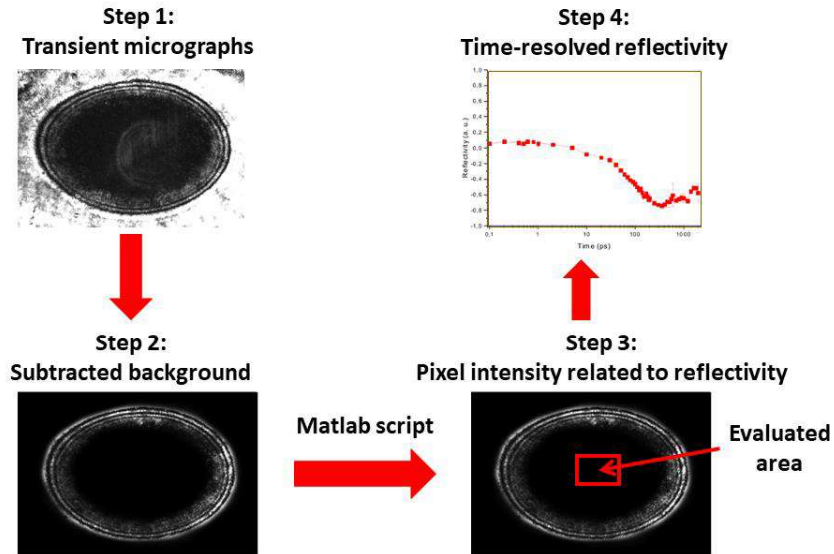
Figure 27: *Representation of the steps followed during image processing. Steps 1-3 corresponds to fs irradiation on a gold film of 200 nm thick deposited on fused silica bulk. Irradiation with a 35 fs FWHM laser pulse at 800 nm with an energy of 200 µJ. Results from reflectivity measurements as a function of time are represented for the same sample and laser system at an energy of 20 µJ*

acquired in each measurement was taken as a reference by the script, and the second image was compared to the first image. The main steps taken by the script are described in this section.

The script read the first and second images from a measurement series (figure 26 a and b), and stored them as matrices, Then, these images were converted from RGB coordinates to 255 grey level images. Despite the CMOS camera used in these experiments operated in monochrome configuration, images were saved by the camera software in RGB system. After this conversion, each pixel of the images had assigned an intensity value from 0 to 255 assigned, where 0 means black and 255 means white.

The next pre-analysis step was normalization of the grey levels. Each image is divided by 256, so their pixel intensities are now evaluated from 0 (black) to 1 (white). With this transformation, all images would be stretched to have 0 as minimum value and 1 as maximum, and results from different samples could be compared accurately

The following step consisted in subtracting the first image (figure 26 b) from the second image (figure 26 a). The result is divided by the first image and shows in the resulting image

the normalized reflectivity of the sample at a certain delay can be studied. This workflow is represented in Steps 1-3 of figure 27.

Once the images were subtracted and divided, the script required an entry parameter for evaluating the normalized reflectivity of the target during that event or experiment. The user selected an area of interest from the image and entered the x and y coordinates of the pixel where the user wanted to start the evaluation of the image.

Once the coordinates of the pixel were typed into the script, a matrix of 20 x 20 pixels had their normalized reflectivity evaluated, and the script output the mean value of these results. Estimations with a higher number of pixels were tested and presented no significant differences in results. It was then decided to keep this size of matrix in order to avoid outliers in our measurements due to the presence of hidden defects in the sample prior ablation or influence of the Newton's rings pattern. This procedure was repeated at least in five measurements at each delay time, and the obtained reflectivity was stored in an output matrix, where the mean and standard deviation of the measurements could be represented as a function of time, as seen in Step 4 of figure 27.

Other results extracted from images were image profiles, which could be obtained using both MATLAB or OriginLab. A procedure similar to the one described for the estimation of normalized reflectivity was followed. The second image of each set had its background corrected by subtracting the first image. In this way, most of possible defects from the images were removed. Then, it can be requested the intensity profiles of the images: Lower values of profiles correspond to dark values, while high values to light colours, as it was associated during image acquisition. Image profiles at different time provided the velocity of lateral expansion of Newton's rings, as it will be shown in Publication 2. Other studies have attempted to estimate the optical properties of the material during the ablation process using a multilayer system and iterative algorithms [105, 110].

3.2. Time-resolved optical spectroscopy

3.2.1. Spectroscopy techniques. State of the art

There are many spectroscopic techniques which requires a laser source, or which can be used to study laser-induced plasmas, according to their species distribution, composition and plume dynamics [12]. In the last decades laser-induced breakdown spectroscopy (LIBS) has become a very popular tool due to its distinctive features. It has been demonstrated its applicability in any sample without requiring sample preparation, as well as its capacity of fast response and versatility to adapt this technique to any requirement of a wide variety of problems. It presents the additional advantage that it can be combined to complement the limitations which other spectroscopic techniques or support experimental results. Furthermore, imaging techniques, as described in Section 4, are powerful allies to spectroscopic techniques to understand the physicochemical processes in laser-produced plasmas. In this section are introduced some of the most commonly used spectroscopy techniques in combination with LIBS as a representation of the wide range of techniques and applications.

Laser-induced fluorescence uses a probe laser beam to promote atoms or molecules to a higher level of excitation and followed by spontaneous emission of light from excited species. This technique provides temporal, spatial and spectral resolution with high sensitivity. It can be used to obtain information about densities of ablated species, energy transfer processes, or energy-level population distribution [139]. It was also applied to study the expansion of fs laser induced plasmas on copper and compare plume expansion and blast waves with theoretical studies [140].

Absorption spectroscopy was applied in the study of ozone and nitrogen oxides production in multiple laser breakdown oxygen-nitrogen mixtures [141]. This technique has also been
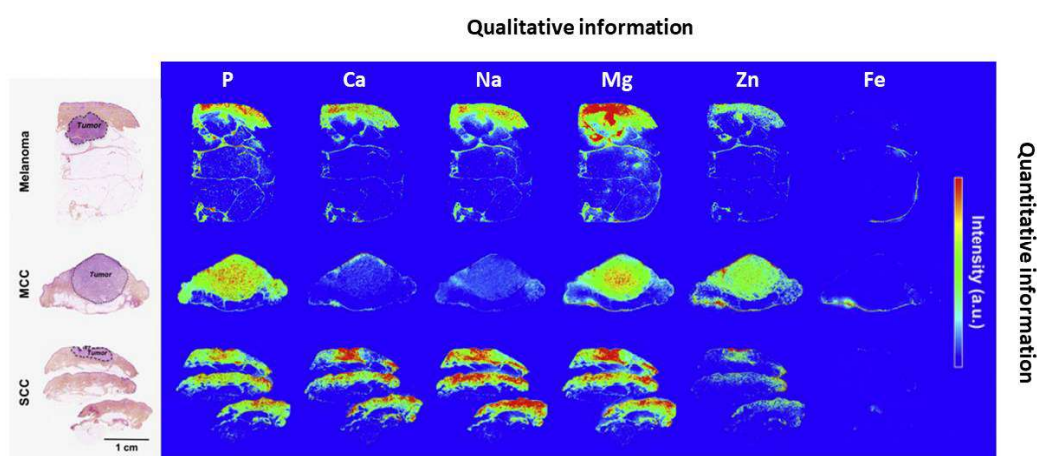
Figure 28: *Mapping of different skin cancer types compared to their histological picture. The figure shows the distribution and concentration of P, Ca, Na, Mg, Zn and Fe in the studied tissues. Spectra obtained from plasmas produced with a Nd:YAG laser at 1064 nm with 5 ns FWHM. Adapted from [147].*

performed for studying the temporal evolution of ablation plumes and determining experimental conditions for isotope analysis in uranium [142].

Raman spectroscopy uses a laser source to stimulate molecules from a sample and determine their vibrational and rotational modes, and it has demonstrated its application in a wide range of research areas as analysis of minerals [143], explosives [144] or planetary exploration [145, 146]. Other spectroscopic techniques use electric or magnetic fields for analytical purposes [47, 148-150].

It should also be considered the combination of spectroscopic and imaging techniques. It has been introduced in section 4 that iCCD imaging technique, can provide also information about the composition of the plasma plume. However, elemental mapping is a technique which combines imaging and spectroscopic data from a sample and provides valuable quantitative and qualitative information (see figure 28) in different areas of study [147, 151, 152].

3.2.2. Laser-induced breakdown spectroscopy (LIBS)

It has been possible to visualize the dynamic evolution of the morphological transformations induced in the sample, using a highly accurate temporal resolution with pump-probe technique. However, this technique is limited to front view perspective, and cannot provide information about the evolution of plasma plume and its emission. This motivated the association of pump-probe technique with LIBS, so that, it could be drawn a more detailed record of the temporal events from laser irradiation to plasma emission, taking the advantage of pump-probe temporal resolution. In this section is afterwards described the features implemented on LIBS experiments.

Experimental set up

This experiment followed the fundamental purpose of monitoring the onset of plasma emission and its evolution, to relate them to the results obtained with pump-probe microscopy. Furthermore, there is a high interest in the detection of molecular species and their possible mechanisms of formation. Using this procedure, it could be studied whether CN emission of samples would present temporal differences between their formation routes.

The study combined LIBS measurements with pump-probe microscopy, the experimental set up described in Section 4 was used. It was added an optical fibre of 1 mm core diameter

at 45° degrees respect to the sample surface and it was connected to the spectrograph with an iCCD presented in Section 3. No additional optical components were set in the optical path between the laser system and the sample.

To accomplish this experiment and results presented in Publication 4, issues which appeared during the experimental procedure had to be overcome. The first step was the synchronization of the iCCD device to the laser and then to the pump-probe measurements. The iCCD shutter was used in external trigger configuration. It was connected to the same delay pulse generator as the shutter and the CMOS camera were connected. For a precise synchronization of the complete experiment, pump and probe beams were set at time zero delay, following the procedure described in Section 4 and Publication 1. LIBS measurements usually use a time delay (gate delay) with respect to the sample irradiation to start the acquisition of the spectra with a given exposure time (gate width). However, as the purpose of this experiment was monitoring the onset of emission lines after laser irradiation, it was decided to open the iCCD shutter before the laser arrival with a fixed gate width, and then increase the delay of the iCCD shutter. This means that as the delay of the iCCD detector increased, light acquisition would be determined by the arrival of the pump-probe pulses and the falling edge of the detector. Then, the interest was to estimate the closure time of the shutter in order to have LIBS spectra with the complete signal as acquisition criteria. If the shutter would not be completely open, it could affect the results on giving wrong estimations in the onset of events of interest.

To estimate the closure time and establish a time-zero as reference, after pump and probe beams synchronization, pump beam was blocked with the mechanical shutter to avoid ablation and plasma formation. The sample was only irradiated by the probe beam, then no damage could be induced on the sample due to its minimal energy. The laser amplifier sends a trigger signal and a laser pulse is delivered from the regenerative amplifier. This trigger pulse is used to delay the iCCD and the CMOS connected to the PDG. This means that their shutters were open when the next probe pulse is delivered. This delay was then adjusted in the channel of the iCCD to obtain a curve of light which showed when the shutter was completely open, and the time-reference could be established.

Data acquisition

The experimental procedure which has been detailed in the previous subsection and in Publication 4 purposed to acquire emission spectra from continuum emission, onset of emission lines and their decay. This temporal evolution could then be related to the morphological alterations shown by pump-probe microscopy technique.

The acquisition of spectra from a material which showed a good contrast of its temporal evolution was a mandatory requirement for the calibration of the experiment. Despite the processes described in Section 2 are observed in a wide range of materials, the materials studied in this work revealed that silicon would be an excellent candidate for LIBS measurements. Silicon presented a high contrasted Newton's rings pattern at earliest times than other materials. It also showed a high increase of its reflectivity on the irradiated area during the first hundred femtoseconds after irradiation, so synchronization between of pump and probe beams could be accurately achieved.
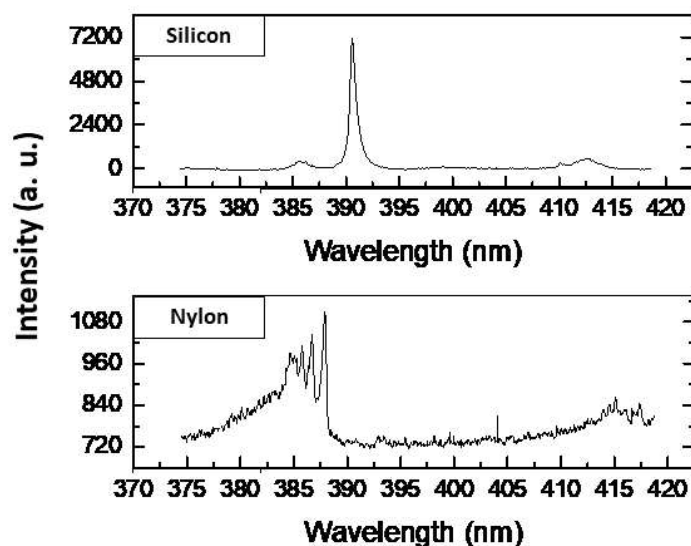
Figure 30: *Spectra acquired during time-resolved femtosecond LIBS experiments on Silicon and Nylon. Parameters for both spectra were identical: gate width of 50 fs, Energy of the laser pulse of 2 mJ at 800 nm with 35 fs FWHM. The delay between laser irradiation and falling edge of the iCCD shutter was 70 ns*

The spectral window of the spectrograph recorded the region of the electromagnetic spectrum between 375-415 nm. This spectral window was selected for the following reasons. First, probe beam was centred at 400 nm. Second, silicon has both neutral (390.55 nm) and ionic lines (385.60 nm) in this range, and third, the 0-0 mode of CN molecular band emission is centred at 388.30 nm. It was not necessary to change the spectral window during all the experiments as it can be seen in figure 30.

Acquisition were recorded increasing the delay in gradual steps between the arrival of the pump-probe pulses and the detector. During silicon and CN emission records, the probe beam was blocked to avoid a fainted emission signal. Measurements were taken in steps of 100 ps up to 3 ns after laser irradiation. Afterwards, delay was increased in steps of 500 ps between 3 to 15 ns after laser irradiation and increased in steps of 1 ns between 15 and 25 ns. For further delays steps of 5 ns, 10 ns and 50 ns were taken. At every measurement, calibration and delay where measurements were performed, a sample of 50 individual spectra was taken to compensate possible fluctuations induced by jitter in the delay generator.

Data processing

Spectral processing was carried out in several steps to provide a narrow temporal resolution of the temporal evolution of plasma emission. First at all, measurements corresponding to a same time delay were grouped and were averaged. Then, the baseline of each averaged spectrum was subtracted according to the shape of emission background.

The following stage in processing consisted in measuring the intensity lines of spectra by measuring the peak to background ratio in atomic and ionic lines and fundamental mode of CN molecular band. Despite measurements were acquired with a fixed gate width of 50 ns, a narrow temporal resolution could be achieved by applying a time-bracketing of measurements. This means that "n-measurement" would have subtracted "n-1 measurement", obtaining an estimated data with temporal resolution which could reach 100 ps.

REFERENCES

REFERENCES

[1] B. Rethfeld, K. Sokolowski-Tinten, D. von der Linde, S. I. Anisimov, Timescales in the response of materials to femtosecond laser excitation, Appl. Phys. A. 79 (2004) 767. https://doi.org/10.1007/s00339-004-2805-9

[2] E. G. Gamaly, The physics of ultra-short laser interaction with solids at non-relativistic intensities. Physics Reports. 508 (2011) 91–243. https://doi.org/10.1016/j.physrep.2011.07.002

[3] E. G. Gamaly, A. V. Rode, B. Luther-Davies, V. T. Tikhonchuk, Ablation of solids by femtosecond lasers: Ablation mechanism and ablation thresholds for metals and dielectrics, Physics of Plasmas. 9 (2002) 949. http://dx.doi.org/10.1063/1.1447555

[4] L. D. Landau, E. M. Lifshitz, L.P. Pitaevskii, Electrodynamics of Continuous Media. Vol. 8 (2nd ed.). Butterworth-Heinemann (1984). ISBN 978-0-7506-2634-7.

[5] L. M. Cabalín, J. J. Laserna, Experimental determination of laser induced breakdown thresholds of metals under nanosecond Q-switched laser operation, Spectrochim. Acta B. 53 (1998) 723-730 https://doi.org/10.1016/S0584-8547(98)00107-4

[6] K. H. Leitz, B. Redlingshöfer, Y. Reg, A. Otto, M. Schmidt, Metal Ablation with Short and Ultrashort Laser Pulses, Physics Procedia. 12 (2011) 230–238. https://doi.org/10.1016/j.phpro.2011.03.128

[7] B. N. Chichkov, C. Momma, S. Nolte, F. von Alvensleben, A. Tünnermann, Femtosecond, picosecond and nanosecond laser ablation of solids, Appl. Phys. A 63 (1996) 109-115. https://doi.org/10.1007/BF01567637.

[8] A. W. Miziolek, V. Palleschi, and I. Schechter, Laser-Induced Breakdown Spectroscopy (LIBS), Fundamentals and Applications, Cambridge University Press, Cambridge, UK (2006)

[9] R.E. Russo, X. Mao, S.S. Mao, The physics of laser ablation in microchemical analysis, Anal. Chem. 74 (2002) 70A–77A. https://doi.org/10.1021/ac0219445

[10] R. E. Russo, X. Mao, J. J. Gonzalez, V. Zorba, J. Yoo. Laser ablation in analytical chemistry, Anal. Chem. 85(13) (2013) 6162-6177, https://dx.doi.org/10.1021/ac4005327

[11] A. De Giacomo, R. Gaudiuso, M. Dell'Aglio, A. Santagata, The role of continuum radiation in laser induced plasma spectroscopy, Spectrochim. Acta B 65 (2010) 385–394. https://doi.org/10.1016/j.sab.2010.03.016

[12] D. Bäuerle, Laser Processing and Chemistry, Springer-Verlag Berlin Heidelberg (2011). https://doi.org/10.1007/978-3-642-17613-5

[13] A. De Giacomo, and J. Hermann, Laser-induced plasma emission: from atomic to molecular spectra, J. Phys. D: Appl. Phys. 50 (2017) 183002. https://doi.org/10.1088/1361-6463/aa6585

[14] A. De Giacomo, M. Dell'Aglio, O. De Pascale, R. Gaudiuso, V. Palleschi, C. Parigger and A. Woods, Plasma processes and emission spectra in laser induced plasmas: A point of view, Spectrochim. Acta B. 100 (2014) 180–188. https://doi.org/10.1016/j.sab.2014.08.013

[15] M. Milan, J.J. Laserna, Diagnostics of silicon plasmas produced by visible nanosecond laser ablation, Spectrochim. Acta B. 56 (2001) 275-288. https://doi.org/10.1016/S0584-8547(01)00158-6

[16] C. Lopez-Moreno, S. Palanco, J. J. Laserna, F. DeLucia Jr, A. W. Miziolek, J. Rose, R. A. Walters and A. I. Whitehouse, Test of a stand-off laser-induced breakdown spectroscopy sensor for the detection of explosive residues on solid surfaces, J. Anal. At. Spectrom. 21 (2006) 55-60 https://doi.org/10.1039/B508055J

[17] P. Lucena, A. Doña, L.M. Tobaria, and J.J. Laserna, New challenges and insights in the detection and spectral identification of organic explosives by laser induced breakdown spectroscopy, Spectrochimica Acta part B. 66 (2011) 12–20. https://doi.org/10.1016/j.sab.2010.11.012

[18] S. Grégoire, V. Motto-Ros, Q. L. Ma, W. Q. Lei, X. C. Wang, F. Pelascini, F. Surma, V. Detalle, J. Yu, Correlation between native bonds in a polymeric material and molecular emissions from the laser-induced plasma observed with space and time resolved imaging, Spectrochim. Acta B 74–75 (2012) 31–37. https://doi.org/10.1016/j.sab.2012.07.020

[19] D. E. Anderson, B. L. Ehlmann, O. Forni, S. M. Clegg, A. Cousin, N. H. Thomas, J. Lasue, D. M. Delapp, R. E. McInroy, O. Gasnault, M. D. Dyar, S. Schröder, S. Maurice, and R. C. Wiens, Characterization of LIBS emission lines for the identification of chlorides, carbonates, and sulfates in salt/basalt mixtures for the application to MSL ChemCam data, J. Geophys. Res. Planets 122 (2017) 744–770. https://doi.org/10.1002/2016JE005164

[20] T. E. Itina, V. N. Tokarev, W. Marine and M. Autric, Monte Carlo simulation study of the effects of nonequilibrium chemical reactions during pulsed laser desorption, J. Chem. Phys. 106 (21) (1997) 8905-8912. https://doi.org/10.1063/1.473948

[21] T. E. Itina, J. Hermann, P. Delaporte, and M. Sentis, Laser-generated plasma plume expansion: Combined continuous-microscopic modelling, Phys. Rev. E 66 (2002) 066406. https://doi.org/10.1103/PhysRevE.66.066406

[22] S. V. Shabanov, I. B. Gornushkin, Modeling chemical reactions in laser-induced plasmas, Appl. Phys. A. 121 (2015) 1087–1107. https://doi.org/10.1007/s00339-015-9445-0.

[23] J. Serrano, J. Moros and J. J. Laserna, Molecular signatures in femtosecond laser-induced organic plasmas: comparison with nanosecond laser ablation, Phys. Chem. Chem. Phys. 18 (2016) 2398. https://doi.org/10.1039/c5cp06456b

[24] A. Fernández-Bravo, T. Delgado, P. Lucena, J. J. Laserna, Vibrational emission analysis of the CN molecules in laser-induced breakdown spectroscopy of organic compounds, Spectrochim. Acta B 89 (2013) 77–83. http://dx.doi.org/10.1016/j.sab.2013.08.004

[25] M. Dong, X. Mao, J. J. Gonzalez, J. Lu and R. E. Russo, Time-resolved LIBS of atomic and molecular carbon from coal in air, argon and helium, J. Anal. At. Spectrom. 27 (2012) 2066, http://dx.doi.org/10.1039/c2ja30222e

[26] C. Aragón, J.A. Aguilera, Characterization of laser induced plasmas by optical emission spectroscopy: A review of experiments and methods, Spectrochim. Acta B 63 (2008) 893–916. http://dx.doi.org/10.1016/j.sab.2008.05.010

[27] D. W. Hahn, N. Omenetto, Laser-Induced Breakdown Spectroscopy (LIBS), Part I: Review of Basic Diagnostics and Plasma—Particle Interactions: Still-Challenging Issues within the Analytical Plasma Community, Appl. Spec. 64(12) (2010) 335A-336A. http://dx.doi.org/10.1366/000370210793561691.

[28] G. Cristoforetti, E. Tognoni, L.A. Gizzi, Thermodynamic equilibrium states in laser-induced plasmas: From the general case to laser-induced breakdown spectroscopy plasmas, Spectrochim. Acta B 90 (2013) 1–22. http://dx.doi.org/10.1016/j.sab.2013.09.004

[29] G. Cristoforetti, A. De Giacomo, M. Dell'Aglio, S. Legnaioli, E. Tognoni, V. Palleschi, N. Omenetto, Local Thermodynamic Equilibrium in Laser-Induced Breakdown Spectroscopy: Beyond the McWhirter criterion, Spectrochim. Acta B. 65 (2010) 86-95. http://dx.doi.org/10.1016/j.sab.2009.11.005

[30] B. Le Drogoff, J. Margot, M. Chaker, M. Sabsabi, O. Barthelemy, T.W. Johnston, S. Laville, F. Vidal, Y. von Kaenel, Temporal characterization of femtosecond laser pulses induced plasma for spectrochemical analysis of aluminum alloys, Spectrochim. Acta B. 56 (2001) 987-1002. https://doi.org/10.1016/S0584-8547(01)00187-2

[31] K. L. Eland, D. N. Stratis, D. M. Gold, S. R. Goode, S. M. Angel, Energy Dependence of Emission Intensity and Temperature in a LIBS Plasma Using Femtosecond Excitation, Applied Spectroscopy, 55 (3) (2001) 286–291. https://doi.org/10.1366/0003702011951902

[32] K. L. Eland, D. N. Stratis, T. Lai, M. A. Berg, S. R. Goode, S. Michael Angel, Some Comparisons of LIBS Measurements using Nanosecond and Picosecond Laser Pulses, Appl. Spectrosc. 55 (2001) 279-285.

[33] J. B. Sirven, B. Bousquet, L. Canioni, L. Sarger, Time-resolved and time-integrated single-shot laser-induced plasma experiments using nanosecond and femtosecond laser pulses, Spectrochim. Acta B. 59 (2004) 1033–1039. https://doi.org/10.1016/j.sab.2004.05.009

[34] G.W. Rieger, M. Taschuk, Y.Y. Tsui, R. Fedosejevs, Comparative study of laser-induced plasma emission from microjoule picosecond and nanosecond KrF-laser pulses, Spectrochim. Acta B 58 (2003) 497–510, https://doi.org/10.1016/S0584-8547(03)00014-4

[35] X. Zeng, X.L. Mao, R. Greif, R.E. Russo, Experimental investigation of ablation efficiency and plasma expansion during femtosecond and nanosecond laser ablation of silicon, Appl. Phys. A 80 (2005) 237–241. https://doi.org/10.1007/s00339-004-2963-9

[36] B. Verhoff, S. S. Harilal, J. R. Freeman, P. K. Diwakar, and A. Hassanein, Dynamics of femto- and nanosecond laser ablation plumes investigated using optical emission spectroscopy, J. Appl. Phys. 112 (2012) 093303. http://dx.doi.org/10.1063/1.4764060

[37] T. A. Labutin, V. N. Lednev, A. A. Ilyin, and A. M. Popov, Femtosecond laser-induced breakdown spectroscopy, J. Anal. At. Spectrom, 31 (2016) 90. http://dx.doi.org/10.1039/c5ja00301f

[38] A. De Giacomo, M. Dell'Aglio, A. Santagata, R. Teghil, Early stage emission spectroscopy study of metallic titanium plasma induced in air by femtosecond- and nanosecond-laser pulses, Spectrochim. Acta B 60 (2005) 935–947.

http://dx.doi.org/10.1016/j.sab.2005.05.026

[39] B. Verhoff, S. S. Harilal, and A. Hassanein, Angular emission of ions and mass deposition from femtosecond and nanosecond laser-produced plasmas, J. of Appl. Phys. 111 (2012) 123304. https://doi.org/10.1063/1.4730444

[40] S. S. Harilal, N. Farid, J. R. Freeman, P. K. Diwakar, N. L. LaHaye, A. Hassanein, Background gas collisional effects on expanding fs and ns laser ablation plumes, Appl. Phys. A 117 (2014) 319. https://doi.org/10.1007/s00339-014-8268-8

[41] J. R. Freeman, S. S. Harilal, P. K. Diwakar, B. Verhoff, A. Hassanein, Comparison of optical emission from nanosecond and femtosecond laser produced plasma in atmosphere and vacuum conditions, Spectrochim. Acta B 87 (2013) 43–50, http://dx.doi.org/10.1016/j.sab.2013.05.011

[42] K. Furusawa, K. Takahashi, H. Kumagai, K. Midorikawa, M. Obara, Ablation characteristics of Au, Ag, and Cu metals using a femtosecond Ti:sapphire laser, Appl. Phys. A 69 [Suppl.] (1999) S359–S366. https://doi.org/10.1007/s003390051417

[43] M. Hashida, A. F. Semerok, O. Gobert, G. Petite, Y. Izawa, J. F. Wagner, Ablation threshold dependence on pulse duration for copper, Appl. Sur. Sci 197 (2002) 862 https://doi.org/10.1016/S0169-4332(02)00463-4

[44] F. J. Fortes, J. Moros, P. Lucena, L. M. Cabalín, J. J. Laserna, Laser-Induced Breakdown Spectroscopy, Anal. Chem. 85(2) (2013) 640-669. https://doi.org//10.1021/ac303220r

[45] M. Baudelet, L. Guyon, J. Yu, J. P. Wolf, T. Amodeo, E. Fréjafon, P. Laloi, Spectral signature of native CN bonds for bacterium detection and identification using femtosecond laser-induced breakdown spectroscopy, Appl. Phys. Lett. 88 (2006) 063901. https://doi.org/10.1063/1.2170437

[46] L. Torrisi, A. Borrielli, D. Margarone, Study on the ablation threshold induced by pulsed lasers at different wavelengths, Nucl. Instrum Meth. B. 255(2) (2007) 373-379. https://doi.org/10.1016/j.nimb.2006.12.144

[47] N. L. LaHaye, S. S. Harilal, P. K. Diwakar, A. Hassanein, and P. Kulkarni, The effect of ultrafast laser wavelength on ablation properties and implications on sample introduction

in inductively coupled plasma mass spectrometry, J. Appl. Phys. 114 (2013) 023103. http://doi.org/10.1063/1.4812491

[48] A. Bogaerts, Z. Chen, Effect of laser parameters on laser ablation and laser-induced plasma formation: A numerical modelling investigation, Spectrochim. Acta B 60 (2005) 1280–1307, http://doi.org/10.1016/j.sab.2005.06.009

[49] L. Fornarini, V. Spizzichino, F. Colao, R. Fantoni, V. Lazic, Influence of laser wavelength on LIBS diagnostics applied to the analysis of ancient bronzes, Anal Bioanal. Chem. 385 (2006) 272–280. http://doi.org/10.1007/s00216-006-0300-1

[50] L. Torrisi, S. Gammino, L. Andò, V. Nassisi, D. Doria, A. Pedone, Comparison of nanosecond laser ablation at 1064 and 308 nm wavelength, Appl. Surf. Sci. 210(3) (2003) 262-273. https://doi.org/10.1016/S0169-4332(02)01467-8

[51] I. Zergioti, S. Mailis, N. A. Vainos, A. Ikiades, C. P. Grigoropoulos, C. Fotakis, Microprinting and microetching of diffractive structures using ultrashort laser pulses, Appl. Surf. Sci. 138–139 (1999) 82–86,

[52] V. Zorba, X. Mao, R. E. Russo, Laser Wavelength effects in ultrafast near-field laser nanostructuring of Si, Appl. Phys. Lett. 95 (2009) 041110, https://doi.org/10.1063/1.3193537

[53] L. Gallais, D. B. Douti, M. Commandré, G. Batavičiūtė, E. Pupka, M. Ščiuka, L. Smalakys, V. Sirutkaitis, and A. Melninkaitis, Wavelength dependence of femtosecond laser-induced damage threshold of optical materials, J. of Appl. Phys. 117 (2015) 223103. https://doi.org/10.1063/1.4922353

[54] J. J. J. Nivas, K. K. Anoop, R. Bruzzese, R. Philip, and S. Amoruso, Direct femtosecond laser surface structuring of crystalline silicon at 400 nm, Appl. Phys. Lett. 112 (2018) 121601. https://doi.org/10.1063/1.5011134

[55] T. Y. Choi, C. P. Grigoropoulos, Plasma and ablation dynamics in ultrafast laser processing of crystalline silicon, J. Appl. Phys. 92 (2002) 4918. https://doi.org/10.1063/1.1510565

[56] V. Margetic, A. Pakulev, A. Stockhaus, M. Bolshov, K. Niemax, R. Hergenröder, A comparison of nanosecond and femtosecond laser-induced plasma spectroscopy of brass

samples, Spectrochim. Acta B 55 (2000) 1771-1785. https://doi.org/10.1016/S0584-8547(00)00275-5

[57] J. M. Liu, Simple technique for measurements of pulsed Gaussian-beam spot sizes, Opt. Lett. 7 (5) (1982) 196-198. https://doi.org/10.1364/OL.7.000196

[58] M. Ye, and C. P. Grigoropoulos, Time-of-flight and emission spectroscopy study of femtosecond laser ablation of titanium, J. Appl. Phys. 89 (2001) 5183. https://doi.org/10.1063/1.1360696

[59] C. Unger, J. Koch, L. Overmeyer, and B. N. Chichkov, Time-resolved studies of femtosecond-laser induced melt dynamics, Optics Express 20(22) (2012) 24864-24872. https://doi.org/10.1364/OE.20.024864

[60] S. Rapp, J. Rosenberger, M. Domke, G. Heise, H. P. Huber, M. Schmidt, Ultrafast pump-probe microscopy reveals the mechanism of selective fs laser structuring of transparent thin films for maskless micropatterning, Appl. Surf. Sci. 290 (2014) 30 368-372. https://doi.org/10.1016/j.apsusc.2013.11.086

[61] C. Momma, B. N. Chichkov, S. Nolte, F. von Alvensleben, A. Tiinnermann, H. Welling, B. Wellegehausen, Short-pulse laser ablation of solid targets, Optics Comm. 129 (1996) 134-142. https://doi.org/10.1016/0030-4018(96)00250-7

[62] J. Bonse, S. Baudach, J. Krüger, W. Kautek, M. Lenzner, Femtosecond laser ablation of silicon–modification thresholds and morphology, Appl. Phys. A 74 (2002) 19–25. https://doi.org/10.1007/s003390100893.

[63] D. Puerto, W. Gawelda, J. Siegel, J. Bonse, G. Bachelier, J. Solis, Transient reflectivity and transmission changes during plasma formation and ablation in fused silica induced by femtosecond laser pulses, Appl. Phys. A. 92 (2008) 803. https://doi.org/10.1007/s00339-008-4586-z

[64] D. Puerto, J. Siegel, W. Gawelda, M. Galvan-Sosa, L. Ehrentraut, J. Bonse, and J. Solis, Dynamics of plasma formation, relaxation, and topography modification induced by femtosecond laser pulses in crystalline and amorphous dielectrics, J. Opt. Soc. Am. B. 27 (2010) 1065-1076. https://doi.org/10.1364/JOSAB.27.001065

[65] M. P. Mateo, V. Piñon, D. Anglos, G. Nicolas, Effect of ambient conditions on ultraviolet femtosecond pulse laser induced breakdown spectra, Spectrochim. Acta B 74-75 (2012) 18–23, https://doi.org/10.1016/j.sab.2012.06.031

[66] M. Domke, L. Nobile, S. Rapp, S. Eiselen, J. Sotrop, H. P. Huber, M. Schmidt, Understanding thin film laser ablation: The role of the effective penetration depth and the film thickness, Physics Procedia 56 (2014) 1007–1014. https://doi.org/10.1016/j.phpro.2014.08.012.

[67] C. M. Ahamer, K. M. Riepl, N. Huber, J. D. Pedarnig, Femtosecond laser-induced breakdown spectroscopy: Elemental imaging of thin films with high spatial resolution, Spectrochim. Acta B 136 (2017) 56–65. http://dx.doi.org/10.1016/j.sab.2017.08.005

[68] J. Hermann, M. Benfarah, G. Coustillier, S. Bruneau, E. Axente, J. F. Guillemoles, M. Sentis, P. Alloncle, T. Itina, Selective ablation of thin films with short and ultrashort laser pulses, Appl. Surf. Sci. 252 (2006) 4814–4818. http://dx.doi.org/10.1016/j.apsusc.2005.06.057

[69] A. A. Ionin, S. I. Kudryashov, A. A. Samokhin, Material surface ablation produced by ultrashort laser pulses, Phys.-Usp. 60 (2017) 149-160. https://doi.org/10.3367/UFNe.2016.09.037974

[70] M. Born, E. Wolf, Principles of optics, Elsevier (1980) ISBN: 978-0-08-026482-0

[71] B. Rethfeld, D. S. Ivanov, M. E. Garcia and S. I. Anisimov, Modelling ultrafast laser ablation, J. Phys. D: Appl. Phys. 50 (2017) 193001. https://doi.org/10.1088/1361-6463/50/19/193001

[72] M. V. Shugaev, C. Wu, O. Armbruster, A. Naghilou, N. Brouwer, D. S. Ivanov, N. M. Bulgakova, W. Kautek, B. Rethfeld, and L.V. Zhigilei, Fundamentals of ultrafast laser–material interaction, MRS Bulletin. 41(12) (2016) 960-968. https://doi.org/10.1557/mrs.2016.274

[73] S. I. Anisimov, B. L. Kapeliovich, T. L. Perel'man, Electron emission from metal surfaces exposed to ultrashort laser pulses, Zh. Eksp. Teor. Fiz. 66 (1974) 776-781

[74] B. Rethfeld, A. Kaiser, M. Vicanek, G. Simon, Femtosecond laser-induced heating of electron gas in aluminium, Appl. Phys. A. 69 [Suppl.] (1999) S109–S112. https://doi.org/10.1007/s003399900228

[75] B. Rethfeld, A. Kaiser, M. Vicanek, and G. Simon, Ultrafast dynamics of nonequilibrium electrons in metals under femtosecond laser irradiation, Phys. Rev. B 65 (2002) 214303. https://doi.org/10.1103/PhysRevB.65.214303

[76] K. Sokolowski-Tinten, D. von der Linde, Generation of dense electron-hole plasmas in silicon, Phys. Rev. B. 61(4) (2000) 2643-2650. https://doi.org/10.1103/PhysRevB.61.2643

[77] S. K. Sundaram, E. Mazur, Inducing and probing non-thermal transitions in semiconductors using femtosecond laser pulses, Nature Materials. 1 (2002) 217–224. https://doi.org/10.1038/nmat767

[78] H. M. van Driel, Kinetics of high-density plasmas generated in Si by 1.06- and 0.53-μm picosecond laser pulses, Phys. Rev. B, 35(15) (1987) 8166. https://doi.org/10.1103/PhysRevB.35.8166

[79] A. Rämer, O. Osmani, B. Rethfeld, Laser damage in silicon: Energy absorption, relaxation, and transport, J. Appl. Phys. 116 (2014) 053508. https://doi.org/10.1063/1.4891633

[80] J. P. Callan, A. M. T. Kim, C. A. D. Roeser, and E. Mazur, Universal dynamics during and after ultrafast laser-induced semiconductor-to-metal transitions, Phys. Rev. B 64 (2001) 073201. https://doi.org/10.1103/PhysRevB.64.073201

[81] A. M. T. Kim, J. P. Callan, C. A. D. Roeser, and E. Mazur, Ultrafast dynamics and phase changes in crystalline and amorphous GaAs, Phys. Rev. B 66 (2002) 245203. https://doi.org/10.1103/PhysRevB.66.245203

[82] B. Rethfeld, K. Sokolowski-Tinten, D. von der Linde, S. I. Anisimov, Timescales in the response of materials to femtosecond laser excitation, Appl. Phys. A. 79 (2004) 767. https://doi.org/10.1007/s00339-004-2805-9

[83] L. V. Keldysh, Ionization in the Field of a Strong Electromagnetic Wave, JETP 20(5) (1965) 1307.

[84] P. Balling, and J. Schou, Femtosecond-laser ablation dynamics of dielectrics: basics and applications for thin films, Rep. Prog. Phys. 76 (2013) 036502. https://doi.org/10.1088/0034-4885/76/3/036502

[85] J. R. Gulley, T. E. Lanier, Model for ultrashort laser pulse-induced ionization dynamics in transparent solids, Phys. Rev. B 90 (2014) 155119. https://doi.org/10.1103/PhysRevB.90.155119

[86] V. E. Gruzdev, Photoionization rate in wide band-gap crystals, Phys. Rev. B 75 (2007) 205106. https://doi.org/10.1103/PhysRevB.75.205106

[87] V. V. Temnov, K. Sokolowski-Tinten, P. Zhou, A. El-Khamhawy, and D. von der Linde, Multiphoton Ionization in Dielectrics: Comparison of Circular and Linear Polarization, Phys. Rev. Lett. 97 (2006) 237403. https://doi.org/10.1103/PhysRevLett.97.237403

[88] B. Rethfeld, O. Brenk, N. Medvedev, H. Krutsch, D. H. H. Hoffmann, Interaction of dielectrics with femtosecond laser pulses: application of kinetic approach and multiple rate equation, Interaction of dielectrics with femtosecond laser pulses: application of kinetic approach and multiple rate equation, Appl. Phys. A 101 (2010) 19–25. https://doi.org/10.1007/s00339-010-5780-3

[89] N. Medvedev, and B. Rethfeld, A comprehensive model for the ultrashort visible light irradiation of semiconductors, J. Appl. Phys. 108 (2010) 103112. https://doi.org/10.1063/1.3511455

[90] B. H. Christensen, and P. Balling, Modelling ultrashort-pulse laser ablation of dielectric materials, Phys. Rev. B 79 (2009) 155424, https://doi.org/10.1103/PhysRevB.79.155424

[91] D. Fisher, M. Fraenkel, Z. Henis, E. Moshe, and S. Eliezer, Interband and intraband (Drude) contributions to femtosecond laser absorption in aluminium, Phys. Rev. E 65 (2001) 016409, https://doi.org/10.1103/PhysRevE.65.016409

[92] E. G. Gamaly, A. V. Rode, Physics of ultra-short laser interaction with matter: From phonon excitation to ultimate transformations, Progress in Quantum Electronics. 37 (2013) 215–323. http://dx.doi.org/10.1016/j.pquantelec.2013.05.001

[93] B. J. Siwick, J. R. Dwyer, R. E. Jordan, R. J. D. Miller, An Atomic-Level View of Melting Using Femtosecond Electron Diffraction, Science 302(5649) (2003) 1382-1385. http://dx.doi.org/10.1126/science.1090052

[94] K. Sokolowski-Tinten, C. Blome, J. Blums, A. Cavalleri, C. Dietrich, A. Tarasevitch, I. Uschmann, E. Förster, M. Kammler, M. Horn-von-Hoegen & D. von der Linde, Femtosecond X-ray measurement of coherent lattice vibrations near the Lindemann stability limit, Nature 422 (2003) 287–289. http://dx.doi.org/doi:10.1038/nature01490

[95] D. S. Ivanov and L. V. Zhigilei, Effect of Pressure Relaxation on the Mechanisms of Short-Pulse Laser Melting, Phys. Rev. Lett. 91 (2003) 105701. https://doi.org/10.1103/PhysRevLett.91.105701

[96] D. S. Ivanov and L. V. Zhigilei, Kinetic Limit of Heterogeneous Melting in Metals, Phys. Rev. Lett. 98 (2007) 195701. https://doi.org/10.1103/PhysRevLett.98.195701

[97] J. Hohlfeld, J. G. Müller, S. S. Wellershoff, E. Matthias, Time-resolved thermoreflectivity of thin gold films and its dependence on film thickness, Appl Phys 64 (1997) 387-390. https://doi.org/10.1007/s003400050189

[98] B. Rethfeld, K. Sokolowski-Tinten, D. von der Linde, and S. I. Anisimov, Ultrafast thermal melting of laser-excited solids by homogeneous nucleation, Phys. Rev. B 65 (2002) 092103. https://doi.org/10.1103/PhysRevB.65.092103

[99] K. Sokolowski-Tinten, J. Bialkowski, M. Boing, A. Cavalleri, and D. von der Linde, Thermal and nonthermal melting of gallium arsenide after femtosecond laser excitation, Phys. Rev. B 58 (1998) R11805(R). https://doi.org/10.1103/PhysRevB.58.R11805

[100] P. Stampfli and K. H. Bennemann, Theory for the instability of the diamond structure of Si, Ge, and C induced by a dense electron-hole plasma, Phys. Rev. B 42 (1990) 7163, https://doi.org/10.1103/PhysRevB.42.7163

[101] P. Stampfli, and K. H. Bennemann, Time dependence of the laser-induced femtosecond lattice instability of Si and GaAs: Role of longitudinal optical distortions, Phys. Rev. B 49 (1994) 7299. https://doi.org/10.1103/PhysRevB.49.7299

[102] N. M. Bulgakova, R. Stoian, A. Rosenfeld, I. V. Hertel, and E. E. B. Campbell, Electronic transport and consequences for material removal in ultrafast pulsed laser ablation of materials, Phys. Rev. B 69 (2004) 054102. https://doi.org/10.1103/PhysRevB.69.054102

[103] K. Sokolowski-Tinten, J. Bialkowski, A. Cavalleri, D. von der Linde, A. Oparin, J. Meyer-ter-Vehn, and S. I. Anisimov, Transient States of Matter during Short Pulse Laser Ablation, Phys. Rev. Lett. 81 (1998) 224. https://doi.org/10.1103/PhysRevLett.81.224

[104] D. von der Linde, K. Sokolowski-Tinten, The physical mechanisms of short-pulse laser ablation, Appl. Sur. Sci. 154–155 (2000) 1–10. https://doi.org/10.1016/S0169-4332(99)00440-7

[105] M. Garcia-Lechuga, J. Siegel, J. Hernandez-Rueda, and J. Solis, Femtosecond laser ablation of dielectric materials in the optical breakdown regime: Expansion of a transparent shell, Appl. Phys. Lett. 105 (2014) 112902. http://dx.doi.org/10.1063/1.4895926

[106] K. Sokolowski-Tinten, J. Bialkowski, A. Cavalleri, M. Boing, H. Schueler, D. von der Linde, Dynamics of femtosecond-laser-induced ablation from solid surfaces, Proc. SPIE 3343, High-Power Laser Ablation. (1998). https://doi.org/10.1117/12.321593

[107] A. A. Ionin, S. I. Kudryashov, L. V. Seleznev, and D. V. Sinitsyn, Dynamics of the Spallative Ablation of a GaAs Surface Irradiated by Femtosecond Laser Pulses, Jetp Lett. 94 (2012) 753. https://doi.org/10.1134/S002136401122005X

[108] T. E. Glover, G. D. Ackerman, A. Belkacem, P. A. Heimann, Z. Hussain, R. W. Lee, H. A. Padmore, C. Ray, R. W. Schoenlein, W. F. Steele, and D. A. Young, Metal-Insulator Transitions in an Expanding Metallic Fluid: Particle Formation Kinetics, Phys. Rev. Lett. 90 (2003) 236102. https://doi.org/10.1103/PhysRevLett.90.236102

[109] S. I. AnisimovV. V. ZhakhovskiïN. A. InogamovK. NishiharaYu. V. PetrovV. A. Khokhlov, Ablated Matter Expansion and Crater Formation under the Action of Ultrashort Laser Pulse, J. Exp. Theor. Phys. 103 (2006) 183. https://doi.org/10.1134/S1063776106080024

[110] J. P. McDonald, J. A. Nees, and S. M. Yalisove, Pump-probe imaging of femtosecond pulsed laser ablation of silicon with thermally grown oxide films, Journal of Applied Physics 102 (2007) 063109. http://dx.doi.org/10.1063/1.2778740

[111] N. E. Bykovskii, and Y. V. Senatskii, On the Formation Mechanism of Interference Rings in the Ablation Area on the Condensed Medium Surface under Irradiation with Femtosecond Laser Pulses, Phys. Solid State 60 (2018) 404−411. https://doi.org/10.1134/S1063783418020087

[112] D. Grojo, J. Hermann, and A. Perrone, Plasma analyses during femtosecond laser ablation of Ti, Zr, and Hf, J. Appl. Phys. 97 (2005) 063306. http://dx.doi.org/10.1063/1.1861519

[113] S. Nöel, J. Hermann, T. Itina, Investigation of nanoparticle generation during femtosecond laser ablation of metals, Appl. Sur. Sci. 253 (2007) 6310−6315. http://dx.doi.org/10.1016/j.apsusc.2007.01.081

[114] P. K. Diwakar, S. S. Harilal, M. C. Phillips, and A. Hassanein, Characterization of ultrafast laser-ablation plasma plumes at various Ar ambient pressures, J. Appl. Phys. 118 (2015) 043305. https://doi.org/10.1063/1.4927625

[115] P. K. Diwakar, S. S. Harilal, A. Hassanein, and M. C. Phillips, Expansion dynamics of ultrafast laser produced plasmas in the presence of ambient argon, J. Appl. Phys. 116 (2014) 133301. https://doi.org/10.1063/1.4896169

[116] J. Yu, Q. Ma, V. Motto-Ros, W. Lei, X. Wang & X. Bai, Generation and expansion of laser-induced plasma as a spectroscopic emission source, Front. Phys. 7 (2012) 649−669. https://doi.org/10.1007/s11467-012-0251-2

[117] C. Y. Liu, X. L. Mao, R. Greif, R. E. Russo, Time Resolved Shadowgraph Images of Silicon during Laser Ablation: Shockwaves and Particle Generation, J. Phys.: Conf. Ser. 59 (2007) 338-342. https://doi.org/10.1088/1742-6596/59/1/071

[118] M. Baudelet, L. Guyon, J. Yu, J. P. Wolf, T. Amodeo, E. Fréjafon, P. Laloi, Femtosecond time-resolved laser-induced breakdown spectroscopy for detection and identification of bacteria: A comparison to the nanosecond regime, J. Appl. Phys. 99 (2006) 084701 https://doi.org/10.1063/1.2187107

[119] H. Hou, X. Mao, V. Zorba, and R. E. Russo, Laser Ablation Molecular Isotopic Spectrometry for Molecules Formation Chemistry in Femtosecond-Laser Ablated Plasmas, Anal. Chem. 89(14) (2017) 7750-7757. https://doi.org/10.1021/acs.analchem.7b01750

[120] D. Strickland, G. Mourou, Compression of amplified chirped optical pulses, Optics Comm. 56(3) (1985) 219-221. https://doi.org/10.1016/0030-4018(85)90120-8

[121] P. Maine, D. Strickland, P. Bado, M. Pessot, G. Mourou, Generation of ultrahigh peak power pulses by chirped pulse amplification, IEEE J. Quantum Electron. 24(2) (1988) 398-403. https://doi.org/10.1109/3.137

[122] M. Pessot, J. Squier, G. Mourou, and D. J. Harter, Chirped-pulse amplification of 100-fsec pulses, Opt. Lett. 14(15) (1989) 797-799. https://doi.org/10.1364/OL.14.000797

[123] M. D. Shirk and P. A. Molian, A review of ultrashort pulsed laser ablation of materials, J. Laser Appl. 10 (1998) 18-28. http://dx.doi.org/10.2351/1.521827

[124] I. B. Gornushkin, U. Panne, Radiative models of laser-induced plasma and pump-probe diagnostics relevant to laser-induced breakdown spectroscopy, Spectrochim. Acta B 65 (2010) 345−359, http://dx.doi.org/10.1016/j.sab.2010.03.021

[125] T. Y. Choi, D. J. Hwang, C. P. Grigoropoulos, Femtosecond laser induced ablation of crystalline silicon upon double beam irradiation. Appl. Surf. Sci. 197−198 (2002) 720−725. https://doi.org/10.1016/S0169-4332(02)00400-2

[126] M. Hauer, D. J. Funk, T. Lippert, A. Wokaun, Time resolved study of the laser ablation induced shockwave, Thin Solid Films 453–454 (2004) 584–588. https://doi.org/10.1016/j.tsf.2003.11.139

[127] G. Cristoforetti, S. Legnaioli, L. Pardini, V. Palleschi, A. Salvetti, E. Tognoni, Spectroscopic and shadowgraphic analysis of laser induced plasmas in the orthogonal double pulse pre-ablation configuration, Spectrochim. Acta B 61 (2006) 340–350. https://doi.org/10.1016/j.sab.2006.03.004

[128] K. Shimamura, K. Hatai, K. Kawamura, A. Fukui, A. Fukuda, B. Wang, T. Yamaguchi, K. Komurasaki, and Y. Arakawa, Internal structure of laser supported detonation waves by two-wavelength Mach–Zehnder interferometer, J. Appl. Phys. 109 (2011) 084910. https://doi.org/10.1063/1.3574922

[129] P. L. G. Ventzek, R. M. Gilgenbach, J. A. Sell and D. M. Heffelfinger, Schlieren measurements of the hydrodynamics of excimer laser ablation of polymers in atmospheric pressure gas, J. Appl. Phys. 68 (1990) 965-968. https://doi.org/10.1063/1.346661

[130] O. Iwase, W. Süß, D. H. H. Hoffmann, M. Roth, C. Stöckl, M. Geissel, W. Seelig and R. Bock, Laser-Produced Plasma Diagnostics by a Combination of Schlieren Method and Mach-Zehnder Interferometry, Phys. Scr. 58 (1998) 634-635. https://doi.org/10.1088/0031-8949/58/6/017

[131] A. Vogel, and V. Venugopalan, Mechanisms of Pulsed Laser Ablation of Biological Tissues, Chem. Rev. 103 (2003) 577–644. https://doi.org/10.1021/cr010379n

[132] A. Vogel, I. Apitz, S. Freidank, and R. Dijkink, Sensitive high-resolution white-light Schlieren technique with a large dynamic range for the investigation of ablation dynamics, Opt. Lett. 31(12) (2006). https://doi.org/10.1364/OL.31.001812

[133] L. A. Doyle, G. W. Martin, A. Al-Khateeb, I. Weaver, D. Riley, M. J. Lamb, T. Morrow, C. L. S. Lewis, Electron number density measurements in magnesium laser produced plumes, Appl. Surf. Sci. 127–129 (1998) 716–720. https://doi.org/10.1016/S0169-4332(97)00731-9[134] H. Schittenhelm, G. Callies, P. Berger, H. Hugel, Time-resolved interferometric investigations of the KrF-laser-induced interaction zone. Appl. Surf. Sci. 109–110 (1997) 493-497. https://doi.org/10.1016/S0169-4332(96)00793-3

[135] E. Amer, P. Grena, F. H. Kaplan, M. Sjödahl, M. El Shaerb, Comparison of the laser ablation process on Zn and Ti using pulsed digital holographic interferometry Appl. Surf. Sci. 256 (2010) 4633–4641. https://doi.org/10.1016/j.apsusc.2010.02.063

[136] Y. Matsuo, T. Kobayashi, M. Kurata-Nishimura, T. Kato, T. Motobayashi, J. Kawai and Y. Hayashizaki, LIF observation of neutral atoms and ions produced by femtosecond laser ablation of Sm on a substrate, J. Phys.: Conf. Ser. 59 (2007) 555-558. https://doi.org/10.1088/1742-6596/59/1/118

[137] J. S. Hirsch, E. T. Kennedy, A. Neogi, J. T. Costello, P. Nicolosi and L. Poletto, Vacuum-ultraviolet photoabsorption imaging system for laser plasma plume diagnostics, Rev. Sci. Instrum. 74(6) (2003) 2992-2998. https://doi.org/10.1063/1.1571974

[138] M. C. Downer, R. L. Fork, and C. V. Shank, Femtosecond imaging of melting and evaporation at a photoexcited silicon surface, J. Opt. Soc. Am. B 2(4) (1985) 595-599. https://doi.org/10.1364/JOSAB.2.000595

[139] V. S. Burakov, N. V. Tarasenko, N. A. Savastenko, Plasma chemistry in laser ablation processes, Spectrochim. Acta B 56 (2001) 961-971. https://doi.org/10.1016/S0584-8547(01)00192-6

[140] V. Margetic, T. Ban, F. Leis, K. Niemax, R. Hergenröder, Hydrodynamic expansion of a femtosecond laser produced plasma, Spectrochim. Acta B 58 (2003) 415–425. https://doi.org/10.1016/S0584-8547(02)00273-2

[141] I. B. Gornushkin, C. L. Stevenson, G. Galbács, B. W. Smith, J. D. Winefordner, Measurement and Modeling of Ozone and Nitrogen Oxides Produced by Laser Breakdown in Oxygen—Nitrogen Atmospheres, Applied Spectroscopy 57(11) (2003) 1442–1450. https://doi.org/10.1366/000370203322554626

[142] M. Miyabe, M. Oba, H. Iimura, K. Akaoka, Y. Maruyama, H. Ohba, M. Tampo, I. Wakaida, Absorption spectroscopy of uranium plasma for remote isotope analysis of next-generation nuclear fuel, Appl Phys A 112 (2013) 87–92. https://doi.org/10.1007/s00339-012-7181-2

[143] A. Giakoumaki, I. Osticioli & D. Anglos, Spectroscopic analysis using a hybrid LIBS-Raman system, Appl. Phys. A 83 (2006) 537–541. https://doi.org/10.1007/s00339-006-3541-0

[144] J. Moros, J. A. Lorenzo, P. Lucena, L. M. Tobaria, and J. J. Laserna, Simultaneous Raman Spectroscopy-Laser-Induced Breakdown Spectroscopy for Instant Standoff Analysis of Explosives Using a Mobile Integrated Sensor Platform, Anal. Chem. 82 (2010) 1389–1400. https://doi.org/10.1021/ac902470v

[145] S. K. Sharma, P. G. Lucey, M. Ghosh, H. W. Hubble, K. A. Horton, Stand-off Raman spectroscopic detection of minerals on planetary surfaces, Spectrochim. Acta A 59 (2003) 2391-2407. https://doi.org/10.1016/S1386-1425(03)00080-5

[146] A. De Giacomo, M. Dell'Aglio, O. De Pascale, S. Longo, M. Capitelli, Laser induced breakdown spectroscopy on meteorites, Spectrochim. Acta B 62 (2007) 1606–1611. https://doi.org/10.1016/j.sab.2007.10.004

[147] S. Moncayo, F. Trichard, B. Busser, M. Sabatier-Vincent, F. Pelascini, N. Pinel, I. Templier, J. Charles, L. Sancey, V. Motto-Ros, Multi-elemental imaging of paraffin-embedded human samples by laser-induced breakdown spectroscopy, Spectrochim. Acta B 133 (2017) 40–44, http://dx.doi.org/10.1016/j.sab.2017.04.013

[148] K. Meissner, T. Lippert, A. Wokaun, D. Guenther, Analysis of trace metals in comparison of laser-induced breakdown spectroscopy with LA-ICP-MS, Thin Solid Films 453–454 (2004) 316–322. http://dx.doi.org/10.1016/j.tsf.2003.11.174

[149] R. Freydier, F. Candaudap, F. Poitrasson, A. Arbouet, B. Chatel and B. Dupré, Evaluation of infrared femtosecond laser ablation for the analysis of geomaterials by ICP-MS, J. Anal. At. Spectrom. 23 (2008) 702–710. http://dx.doi.org/10.1039/B709415A

[150] G. O. Williams, G. M. O'Connor, P. T. Mannion, T. J. Glynn, Langmuir probe investigation of surface contamination effects on metals during femtosecond laser ablation, Appl. Surf. Sci. 254 (2008) 5921–5926. https://doi.org/10.1016/j.apsusc.2008.03.192

[151] F. J. Fortes, J. Cuñat, L. M. Cabalín, J. J. Laserna, In Situ Analytical Assessment and Chemical Imaging of Historical Buildings Using a Man-Portable Laser System, Applied Spectroscopy, 61(5) (2007) 558–564. https://doi.org/10.1366/000370207780807722

[152] G. Nicolas, M. P. Mateo and V. Piñon, 3D chemical maps of non-flat surfaces by laser-induced breakdown spectroscopy, J. Anal. At. Spectrom. 22 (2007) 1244-1249. https://doi.org/10.1039/B704682K

PUBLICATIONS

TESIS DOCTORAL POR COMPENDIO DE PUBLICACIONES

En cumplimiento con los requisitos especificados en el Reglamento de Doctorado de la Universidad de Málaga, la presente Tesis Doctoral ha sido autorizada por los Directores de Tesis y el Órgano Responsable del Programa de Doctorado para ser presentada en el formato de "compendio de publicaciones".

Las referencias de los artículos en los que el doctorando figura como primer o segundo autor y que avalan la presente Tesis Doctoral se detallan a continuación de acuerdo con su orden cronológico de publicación:

A femtosecond time-resolved microscope (fs-TRM) based on pump–probe excitation has been used to follow the dynamic of the processes occurring during laser–matter interaction, from initial surface alterations to final solidification through transient melting. The time-resolved microscope described in the manuscript has been designed to allow a precise control of the excitation beam to cover ranges below and above the plasma formation energy, and a large temporal variation in the pump–probe delay to include the different timescales of the different processes occurring up to the plasma formation. The microscope has been demonstrated to be robust and allows the subpicosecond monitoring of laser ablation single-shot events, of importance in the analysis of ultra thin layers, or biological tissues. The fs-TRM excites (pump) the sample with 35-fs laser pulses at 800 nm and follows the processes by a second (probe) beam at 400 nm. The relative delay between both beams allows the acquisition of pictures with a temporal resolution of 200 fs up to 3 ns after the reaching of the pump pulse. In the ablative regime near the ablation threshold, transient surface reflectivity patterns (dynamic Newton fringes) are observed from a ps to ns timescale. The timescale and number of such rings are affected by the fluence value. Significant differences between metals (Al, Cu and Sn), semiconductors (Si) and polymers (polytetrafluoroethylene and polyurethane) have been also observed in the transformation patterns.

I. Carrasco-García, J. M. Vadillo, J. J. Laserna, Monitoring the dynamics of the surface deformation prior to the onset of plasma emission during femtosecond laser ablation of noble metals by time-resolved reflectivity microscopy, Spectrochim. Acta Part B 131 (2017) 1–7.

http://dx.doi.org/10.1016/j.sab.2017.02.014

The generation of an expanding plasma during laser ablation is preceded at early times by the formation and evolution of a subsurface melted front. The monitoring of such transient event can't be studied by conventional spectroscopic techniques. Pump-probe femtosecond microscopy allows the following of the surface changes during femtosecond laser ablation taking advantage of the formation of a number of dynamic Newton rings that evolve with time. Measurements at different times allow the quantification of the radial expansion velocity of the molten material. For Au and Ag, expansions in the range of 7000–12,000 m/s for Au and 3000–21,000 m/s have been calculated depending on the pump energies. Such values correspond to hypersonic velocities with Mach number between 3 and 6.

I. M. Carrasco-García, J. M. Vadillo, J. J. Laserna, Wavelength and energy dependence on ablation dynamics under femtosecond laser pulses observed by time-resolved pump–probe microscopy, Spectrochim. Acta Part B 158 (2019) 105634.

https://doi.org/10.1016/j.sab.2019.105634

Pump–probe femtosecond microscopy has been applied to reveal the time evolution of the ablation processes at sub-picosecond resolution with combined pulses of different photon energies. Experimental results revealed that differences in the photon energies of ablation pulses influenced the temporal response of the material. Significant differences in the excitation and melting of the material within 10 ps of irradiation were observed. The analysis of dynamic Newton's rings observed with the pump–probe technique confirmed and explained the faster expansion of ablated matter when using shorter irradiation wavelengths. The results also implied that optical properties of the material play a significant role.

Femtosecond time-resolved images acquired by using a two-color pump – probe microscope have been used in combination with optical emission spectroscopy to determine the time scales for the onset of atomic and molecular emission in laser-induced plasmas. A time-slicing acquisition scheme has been used to follow the build-up of emission lines in the spectra. Microscopy images suggest that the ejection of material from silicon starts several nanoseconds before photon emission is detected in our system. The time elapsed is material dependent and proceeds much slower in organics as demonstrated for nylon and Te fl on. This fi nding is of great interest for time-resolved measurements in laser-induced plasmas and should be used for extracting maximum information from spectral data following femtosecond laser ablation.

Visualization of surface transformations during laser ablation of solids by femtosecond pump–probe time-resolved microscopy

Irene Carrasco-García, José M. Vadillo, J. Javier Laserna *

Universidad de Málaga, Departamento de Química Analítica, 29071 Málaga, Spain

A B S T R A C T

A femtosecond time-resolved microscope (fs-TRM) based on pump–probe excitation has been used to follow the dynamic of the processes occurring during laser–matter interaction, from initial surface alterations to final solidification through transient melting. The time-resolved microscope described in the manuscript has been designed to allow a precise control of the excitation beam to cover ranges below and above the plasma formation energy, and a large temporal variation in the pump–probe delay to include the different timescales of the different processes occurring up to the plasma formation. The microscope has been demonstrated to be robust and allows the subpicosecond monitoring of laser ablation single-shot events, of importance in the analysis of ultra thin layers, or biological tissues.

The fs-TRM excites (pump) the sample with 35-fs laser pulses at 800 nm and follows the processes by a second (probe) beam at 400 nm. The relative delay between both beams allows the acquisition of pictures with a temporal resolution of 200 fs up to 3 ns after the reaching of the pump pulse. In the ablative regime near the ablation threshold, transient surface reflectivity patterns (dynamic Newton fringes) are observed from a ps to ns timescale. The timescale and number of such rings are affected by the fluence value. Significant differences between metals (Al, Cu and Sn), semiconductors (Si) and polymers (polytetrafluoroethylene and polyurethane) have been also observed in the transformation patterns.

© 2015 Elsevier B.V. All rights reserved.

1. Introduction

Laser ablation, in its stricter connotation, implies the removal of the very first atoms or molecules from a solid surface due to the effect of a laser pulse, although in broader terms is commonly used to describe any process of sample removal regardless how explosive may it be. Within such definition, laser ablation currently covers a variety of energetic regimes from gentle surface vaporization to laser drilling that involves many different technology and scientific areas. Despite the diversity of niches of application, a common aspect in laser ablation is the need of the affected surface to change its state of aggregation. This process is normally accompanied by changes in chemical or physical properties during the time that the transition is taking place [1].

Femtosecond laser ablation (fs-LA), due to its unique laser–matter interaction in comparison to that using nanosecond lasers, have become an advanced tool for industrial and scientific applications. While during short-pulse laser ablation (ns to few tens of ps) the electrons and the lattice remain in thermal equilibrium (favoring the heat to diffuse out of the irradiated area), in fs-LA the energy deposition occurs in timescale shorter than all the major relaxation processes [2].

The ultra-short time-scale makes fs lasers ideally suited for studying electron and lattice dynamics including the observation of the onset of melting, evaporation and ablation in materials [3] as under fs excitation the basic processes occurring during the laser–matter interaction are temporally separated, allowing an independent description of each of them [4]. Thus, excitation takes place on a timescale comparable with the duration of the laser pulse ($\ll 1$ ps), as a consequence of absorption of photons by the electronic subsystem of the material. This stage is then followed by melting, which roughly occurs in the picosecond regime, and by the removal of material (ablation), whose establishment may require up to several nanoseconds as has been clearly evidenced by means of a picosecond-resolved shadowgraphy set-up in both picosecond [5], and femtosecond [6] ablation. Although the information provided is powerful, shadowgraphies just show the expansion process or modifications in the sample from a lateral view. All the phase transformations occurring in the sample after laser irradiation and the time-scales associated to them must be studied following a different approach.

A whole picture from early photon absorption to the final material removal and plasma expansion may be obtained with the help of the right temporally-resolved tool. In this sense, the use of a laser pump–probe excitation scheme in combination with a magnified vision system turns into a time-resolved microscope capable of capturing the transformations in the sample surface with a temporal resolution provided by the time width of the laser source. Dynamic of ultrafast non-thermal

* Corresponding author.
  E-mail address: laserna@uma.es (J. Javier Laserna).

ELSEVIER

SPECTROCHIMICA ACTA

Wavelength and energy dependence on ablation dynamics under femtosecond laser pulses observed by time-resolved pump–probe microscopy☆

Check for updates

I.M. Carrasco-García, J.M. Vadillo, J.J. Laserna*

Departamento de Química Analítica, UMA LASERLAB, Universidad de Málaga, Jimenez Fraud 4, ES 29010, Spain

A B S T R A C T

Pump–probe femtosecond microscopy has been applied to reveal the time evolution of the ablation processes at sub-picosecond resolution with combined pulses of different photon energies. Experimental results revealed that differences in the photon energies of ablation pulses influenced the temporal response of the material. Significant differences in the excitation and melting of the material within 10 ps of irradiation were observed. The analysis of dynamic Newton's rings observed with the pump–probe technique confirmed and explained the faster expansion of ablated matter when using shorter irradiation wavelengths. The results also implied that optical properties of the material play a significant role.

1. Introduction

Laser-based techniques allow the modification of materials in the melting, spallation, and ablation regimes, which includes the gentle removal of just a few atoms or molecules to a high material mass removal rate. Several different analysis techniques have been used in an effort to visualize and understand the phenomena involved in the interaction of a femtosecond laser pulse with solid matter from surface emission up to permanent damage. Depending on the intended application of laser ablation, different characteristics of the laser pulse will be of more interest. Various studies over the last decades have investigated the influence of the pulse width [1–5]. Ablation with nanosecond lasers is dominated by laser–matter and laser–plasma processes, as the pulse duration is long enough that it persists as evaporation of material is taking place. These processes affect the total deposition of energy on the target, which influences the resulting crater and surface damage [6]. The key difference with femtosecond pulses is that the laser–matter interaction is shorter in time than all the processes induced by this interaction which, among other advantages, results in material being removed only from a confined region corresponding to the irradiated area [5,7,8].

The influence of the laser wavelength on the properties of the plasmas produced with short pulses [9–14], have been studied from the point of view of the acquisition of laser-induced breakdown spectroscopy (LIBS) spectra. In the case of ultrashort pulses, different experimental techniques including filamentation LIBS [15–17], inductively

coupled plasma mass-spectroscopy (ICP-MS) [18], and micromachining and drilling [12] have been used to investigate the effect of the laser wavelength. Techniques as shadowgraphy, or the use of streak cameras can help in revealing the dominat processes during ablation [19–21]. Although they help visualize the processes that induce ablation, they do not show what is happening in the structure of the material. Pump–probe microscopy has proved to be a useful and robust tool to monitor phase-change processes [22–28]. The use of femtosecond laser pulses for both ablating and probing the irradiated target offers a temporal resolution limited by the pulse width, providing deeper insight into the processes involved in ablation and plasma formation. Additionally, the absence of laser–plasma interaction when using femtosecond pulses, makes it possible to deposit more laser energy into the target compared to longer laser pulses [29,30]. The process occurring on dielectrics are complex and demand high energy densities to occur [31–33] while on metals, due to the absence of a band gap in their electronic configuration, the main mechanism of energy absorption is by free carriers, so less energy is required from the laser pulse to induce the ablation [29,34–36].

The present study applies time-resolved pump–probe microscopy to determine the effect of irradiation wavelength on the processes taking place prior to plasma formation during femtosecond laser ablation. Time-resolved pump–probe microscopy provides insight into the morphological dynamics of the material with high temporal resolution. Gold has been used as test sample due to its significant different reflectance behavior along the UV-VIS spectra and the easiness in the

---

PAPER

Check for updates
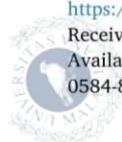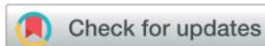
Onset of optical emission in femtosecond laser-induced plasmas and its correlation with surface dynamics monitored by pump–probe time-resolved microscopy

I. Carrasco-García, José M. Vadillo and J. Javier Laserna [ID] *

Femtosecond time-resolved images acquired by using a two-color pump–probe microscope have been used in combination with optical emission spectroscopy to determine the time scales for the onset of atomic and molecular emission in laser-induced plasmas. A time-slicing acquisition scheme has been used to follow the build-up of emission lines in the spectra. Microscopy images suggest that the ejection of material from silicon starts several nanoseconds before photon emission is detected in our system. The time elapsed is material dependent and proceeds much slower in organics as demonstrated for nylon and Teflon. This finding is of great interest for time-resolved measurements in laser-induced plasmas and should be used for extracting maximum information from spectral data following femtosecond laser ablation.

Introduction

The registration of the whole sequence of events occurring in a laser-induced plasma from the early photon arrival at the surface to the build-up of the plasma is typically performed with gated detectors synchronized with a laser source. The accurate measurement of such a sequence of events is limited by the tradeoff between the acquisition bandwidth, spectral coverage and temporal resolution of the detection system. The conventional set-up of an intensified matrix detector coupled to a spectrograph provides broad spectral coverage with excellent temporal resolution and sensitivity. However, the delay inherent in the electronics and the detector risetime impairs the recording of the initial tens of nanoseconds. This fact is not normally considered to be a major drawback, as the intense background occurring during the first nanoseconds of the plasma lifetime limits the quality of the recorded spectra. However, under femtosecond excitation, such a background is significantly reduced, opening up the possibility of studying events occurring in this early time window.[1,2] In such cases, ultrafast detectors are required, with sub-picosecond streak cameras in combination with spectrographs being the only (and expensive) option to perform such experiments. With an appropriate sweeping unit, temporal events as early as 100 fs can be recorded. The extraordinary time resolution of streak cameras is not in doubt, although the flexibility of such devices is limited due to the compromise between the sweep time

(temporal resolution) and the maximum time window that can be covered.

The prospect of simultaneously following several species within the expanding femtosecond laser plasma is interesting as it offers a means to elucidate the formation mechanisms of transient species. A laser-induced plasma is a highly reactive environment, with complex gas-phase reactions occurring early in its lifetime.[3,4] The characteristic spectra emitted by these plasmas evolve with time, and hence time-resolved studies can help understand the influence of the different reactions taking place on the final recorded spectrum.[5–7] Kinetic studies on molecular species are particularly interesting from a fundamental point of view, because the observed molecular species can either be due to native intramolecular bonds released directly from the sample or may derive from recombination in the gas phase.

The detection of molecular signatures in laser-induced plasmas has been a topic of deep study in recent years, not only by means of optical spectroscopy under different environmental conditions,[8,9] but also in combination with mass spectrometry.[10,11] The present work makes use of a different approach, combining femtosecond pump–probe microscopy with optical emission spectroscopy of a laser-induced plasma (LIBS). The approach described is based on the principle of performing acquisitions with sliding time windows. Several spectra are recorded before the starting of the laser excitation, with an identical spectral acquisition window being swept at fixed intervals during a time interval. By performing time-bracketing of the measurements, it is possible to obtain information from a very narrow time window. This approach has been

Universidad de Málaga, Departamento de Química Analítica, UMALASERLAB, Jimenez Fraud 3, 29010 Málaga, Spain. E-mail: laserna@uma.es

This journal is © The Royal Society of Chemistry 2019

J. Anal. At. Spectrom., 2019, **34**, 2119–2125 | **2119**

CONCLUSIONS

CONCLUSIONS

Investigations within the present Doctoral Dissertation have been developed to elucidate several questions raised on temporal evolution of ablation of solids with femtosecond laser irradiation. It has been proven the capacity of pump-probe microscopy to exhibit the fundamental dynamics of materials under ultrashort irradiation and its power to be integrated with laser-induced breakdown spectroscopy (LIBS) to provide additional information to plasma dynamics. This section summarizes the most relevant conclusions drawn from this research.

- Femtosecond pump-probe microscopy has proven its efficiency in showing the surface dynamics during material ablation with ultrashort laser pulses. It can be distinguished according to the reflectivity changes on the irradiated target excitation, melting, and expansion, as well as the permanent damage produced in the target after irradiation.

- The dynamics of ablation is conditioned by the metallic or dielectric nature of materials and excitation is induced by different mechanisms of the electronic subsystems. Materials show a general increase of its reflectivity during this stage, showing temporal differences in excitation stage related to the nature of materials, which remains from 100 fs up to 5 ps under our experimental conditions.

- Melting of irradiated samples is observed as a decrease of the reflectivity in materials, reaching values below their natural reflectivity and last for several hundreds picoseconds. This stage is induced by the de-excitation of the electronic subsystem by electron-phonon collisions which generates a temperature gradient through the irradiated volume, followed by a rarefaction wave.

- Expansion stage is started by the reflection of the rarefaction wave on the molten-non molten material interface. This reflection provokes a density gradient on the molten volume, characterized by a liquid-gas mixture of material encapsulated by a solid-liquid layer of material at the air interface. This layer is pushed outwards the sample by the rarefaction wave and the mixture.

- During expansion the bulk material, the gas-liquid mixture, the solid-liquid layer, and air create a multilayer optical system. Under probe light illumination an interference pattern is generated, or Newton's rings according to the symmetry of the irradiated area which evolves with the expansion of the gas-liquid mixture.

- Time-resolved measurements were performed on silicon samples, all except one presenting a high degree of polish. Newton's rings could not be observed in the

sample with surface roughness, as the interference pattern cannot develop under this condition.

- Newton's rings evolve in number and time as expansion of the gas-liquid mixture pushes the solid-liquid layer. The contrast of this pattern is dependent of the optical properties of the irradiated material, while their onset, number and width depend on the irradiated material and the fluence of the laser pulse.

- Lateral expansion of Newton's rings can be measured with pump-probe technique. The first ring showed an average radial expansion velocity of 2 Mach, while the second ring expanded faster, which an average velocity of 4 Mach. The faster expansion of the second ring is in accordance with a progressive deformation of the dome.

- The energy of photons used as pump pulses for sample ablation induces temporal differences in excitation stage, in agreement with the higher excitation at shorter wavelengths.

- Melting and deformation of material surface as manifested by Newton's rings start earlier with higher photon energy of pump pulses. Transmission of energy from electrons to phonons results in a faster melting and expansion of the gas-liquid mixture of material.

- The observation of surface dynamics can present differences according to the relation between optical properties of the sample and probe beam. Pump-probe microscopy of gold films with probe light at 400 nm showed increase of reflectivity according to electrons excitation while this was not observed using probe light at 800 nm. Excitation was not observed with probe light at 800 nm due to the 98% reflectivity of gold at that wavelength.

- Combination of pump-probe microscopy and optical emission spectroscopy of laser-produced plasmas has permitted to relate the dynamics of ablation processes in ultrashort laser irradiation to the formation, evolution and emission of plasmas.

- The combination of these techniques has achieved a temporal resolution of 100 ps for spectra acquisition. To our knowledge, this temporal resolution has not been achieved previously with LIBS experiments. This provides a detailed information concerning to stages of plasma formation and the onset of plasma emission lines.

- It has been observed that there exists a time gap between the break of the dome formed with expanding material and plasma emission. It can be concluded that ejected material is at a high temperature and only continuum emission is observed.

- Onset of Si (I) emission at 390.55 nm is observed 6 ns after pump irradiation. Pump-probe micrographs showed that at 1.5 ns after irradiation the dome is already broken. This means that the ejected gas-liquid mixture ejected spends 4.5 ns until emission lines can be observed.

- It has been corroborated with optical emission spectroscopy that CN molecular emission presents temporal differences in its onset. It was observed earlier in nylon, 10 ns after irradiation due to fragmentation route, while it could not be distinguished in Teflon until 20 ns due to recombination of carbon with surrounding nitrogen.
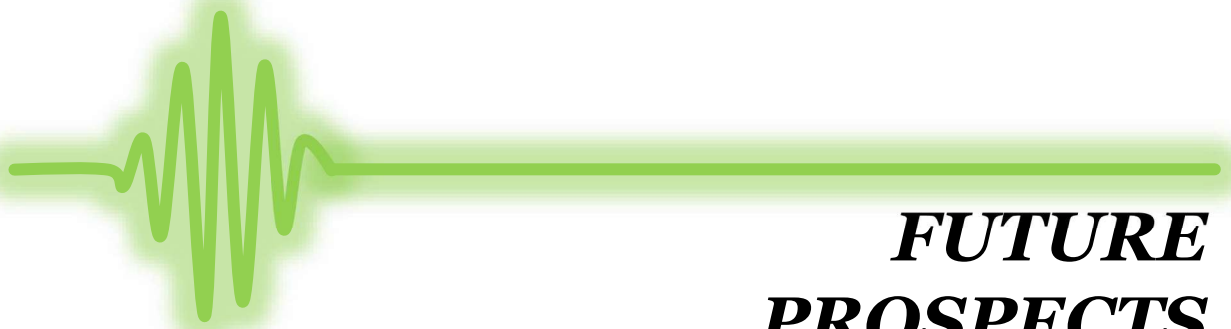
FUTURE
PROSPECTS

FUTURE PROSPECTS

In this doctoral Thesis it has been studied the surface dynamics of materials under femtosecond laser irradiation prior to plasma formation, and the evolution of plasmas. Many different experimental configurations, data processing and further studies have been left for future works mainly due to the lack of time. In this section some ideas are described that could be exploited to obtain further and more detailed knowledge.

It would be interesting to implement some modifications in the experimental set up to improve the energy of pump beam when using different harmonics from the laser system. The sample holder only allows studying the reflectivity of irradiated samples, while other studies have shown that pump-probe can also be applied on the study of transmitted probe light through the sample. From my point of view, this could supply very precious information concerning to the temporal evolution of transparent samples and tissues.

Another complementary study to pump-probe microscopy is the addition of holographic filters both in front and side views. This experimental configuration would contribute to a further understanding of the dynamic Newton's rings and the expansion of irradiated materials. In addition, the combination of all these techniques with hyperspectral imaging using filters centred in a specified region of the electromagnetic spectrum would be of high interest, as it could be supported with results provided using the LIBS experimental procedure which has been described in this thesis.

One the most time-consuming work I have found in the development of this dissertation has been image processing. Despite the hand-made script written to analyse pump-probe micrographs allowed selecting the required images, it was not optimized for an automatic processing. This improvement requires to study which are the most plausible solutions and select the best implementation in the script. This would ease the analysis of the experimental results. However, this can present a drawback related to the computer specifications as RAM memory or graphic card, but the problem can be overcome by selecting a time interval of time-resolved studies.

Concerning to the formation of molecular emission observed with the combined pump-probe and LIBS experimental set up, a promising study would consist on performing this experimental procedure under different ambient conditions. The emission of CN molecules would be only attributed to fragmentation under Argon or Helium atmospheres, and a comparison with ambient atmosphere could be determined.

In summary, the efficient combination of these techniques would result in a detailed description and better understanding of the surface dynamics and plasma formation on materials under femtosecond laser irradiation.
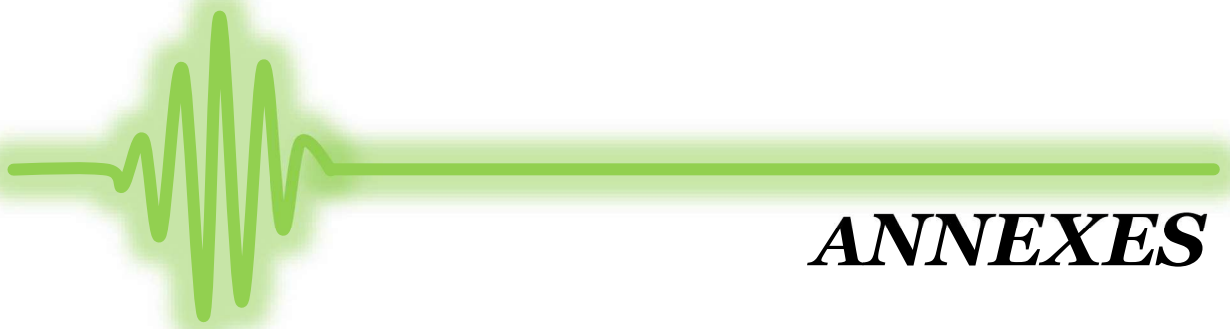
ANNEXES
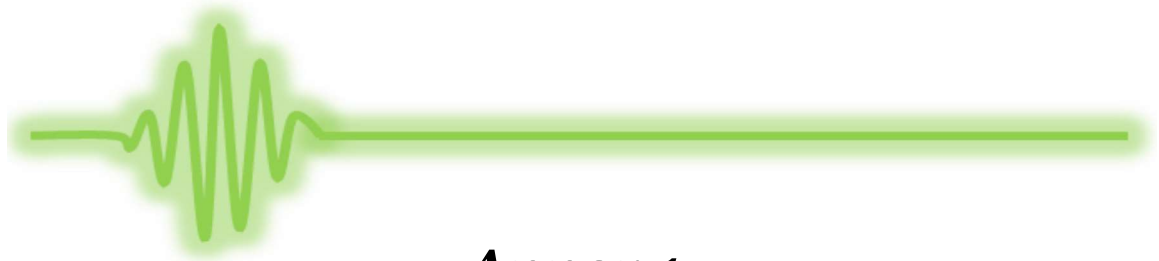
Annex 1.
Temporal evolution of laser-produced colliding plasmas: fluence-dependent dynamics

ANNEX 1. TEMPORAL EVOLUTION OF LASER-PRODUCED COLLIDING PLASMAS: FLUENCE-DEPENDENT DYNAMICS

In this annex is presented the experimental set up and some results obtained during the research stay at National Centre for Plasma Science and Technology, at Dublin City University, under the supervision of John T. Costello and Patrick Hayden.

There exist two opposite phenomena which can be found out when two plasmas collide, depending on the ion-ion mean free path. Interpenetration is undergone when the two plasmas pass through each other and the main heating processes are attributed to binary collisions among species. On the other hand, under the right conditions, stagnation layer is formed at the collision front of the two plasmas and is characterized by a rapid accumulation of a dense layer of plasma material between the two plasmas [1-3]. Colliding laser-produced plasmas can be originated by splitting a laser beam into two beams, and focusing these beams on to two close areas of the same target, with typical distances between 1-10 mm. The plasmas produced at each point are referred as "seed plasmas" and the expansion of their plumes results in interpenetration of their species or the formation of a stagnation layer.

In this sense, it was introduced the "collisionality parameter" ξ to establish which of these mechanisms is the dominant under the interaction of two colliding plasmas, given by the following expression [3]

$$\xi = \frac{D}{\lambda_{ii}} \qquad\qquad (A1.1)$$

$$\lambda_{ii} = \frac{m_i^2 v_{12}^4}{4\pi e^4 Z^4 n_i ln\Lambda_{12}} \qquad\qquad (A1.2)$$

In this expression, D is the separation between the two colliding plasmas in the target, and λ_{ii} is the ion-ion mean free path [4]. The parameters which determines the ion-ion mean free path are introduced: m_i is the ion mass, v_{12} is the relative collision velocity of the ions from each of the plumes, e is the electronic charge, Z is the average ionization state of the plasma, n_i is the average plasma ion density, and $ln\Lambda_{12}$ is the so-called Coulomb logarithm for collisions between the seed plasmas.

In colliding plasmas, the higher the collisionality parameter, the more probable it is to observe the stagnation layer between the seed plasmas. This can be performed

experimentally on a target by increasing the distance between the seed plasmas or decreasing the ion-ion mean free path according to the characteristics of the laser pulse [4].

In addition, it has been reported that heating a plasma with a second laser pulse can enhance the emission intensity due to an increase of laser absorption in applications as LIBS, so it could also be applied in an enhancement of the stagnation layer [2, 3]. It is of interest studying stagnation and interpenetration in colliding plasmas due to possible applications in a broad range of research areas [1].

We report here a study of the interaction between two colliding plasmas on a tin sample. As tin (Sn) presents a heavier atomic weight in comparison with other metals studied under these experimental conditions, it could be interesting the research on how these conditions could affect to related phenomena associated to colliding plasmas. We provide a combination of Faraday cup analysis and broadband imaging for energy and time-resolved measurements of colliding plasmas which allows us to understand the formation and evolution of stagnation layers. The configuration of the set up for this experiment has the goals of monitoring the particle density at the collision front with the CCD and checking whether the Faraday Cup traces could be improved by adding the probing beam

Experimental setup

The experimental set up used in this work is schematically represented in figure A1.1. Laser colliding plasmas were produced by a Nd:YAG laser of 6 ns FWHM operating at its second harmonic. The optical path led the laser light through a polarizer which controlled the energy of the laser beam, and a wedge prism, which divided the beam in two parts. Then, both beams were sent into a vacuum chamber at a 10^{-6} Pa, and focused onto the target was located by a 1 m planoconvex lens. The sample consisted on a piece of Sn which into the vacuum chamber. The distance between both plasmas was measured and resulted in 87 mm. Single plasma observations could also be performed by blocking one of the branches of the split beam and comparing the results with the ones obtained with colliding plasmas.

A Faraday Cup was set in front of the target at a distance of 0.9 m, which detected the Sn ions produced by seed and colliding plasmas, and sent the resulted signal to an oscilloscope which provided the current distribution of the produced species. In addition, a CCD camera with 1 ns gate window (Andor) was also set in the experimental set up, which recorded spectrally integrated images of the formation of the plasmas.
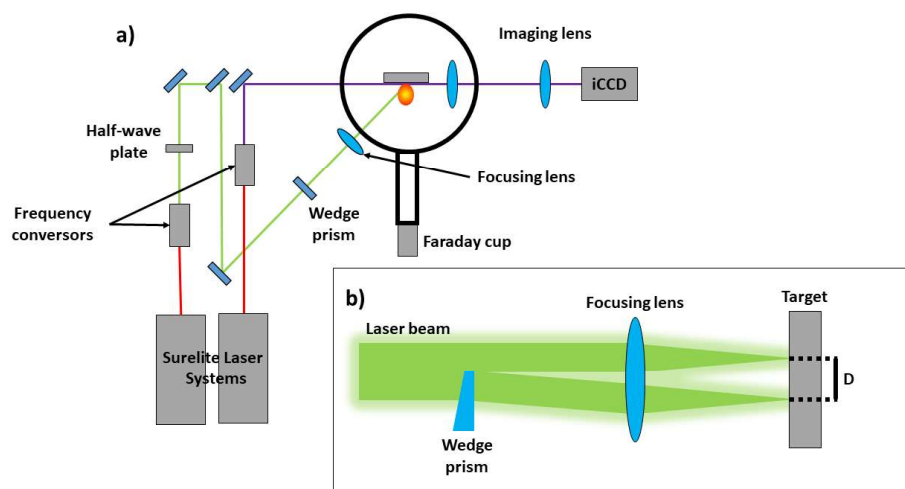
Figure A1.1: *a) Experimental set up for colliding laser plasmas experiments. b) Detail of the formation of colliding laser plasmas on the target.*

The experimental set up was triggered by a pulse delay generator, which controlled the laser firing and synchronized the CCD shutter to obtain a time-resolved study of the evolution of colliding laser-produced plasmas.

The energy of laser pulses was increased in steps of 50 mJ at each experiment, from 50 to 200 mJ and it was measured by the powermeter before the laser beam was split. Three measurements were taken at each position of the sample, and then a new area of the target was selected until it five sets of measurements were acquired. A second set of measurements used a second Nd:YAG laser as re-excitation source of the plasmas working at its fourth harmonic (266 nm) in a way that went through the colliding plasmas and straight to the iCCD. This second laser was also triggered by the delay pulse generator, and the delay was increased in steps of 20 ns, from 0 to 200 ns with respect to the first laser pulse to study the effect of reheating. The probe light was recorded first without plasma formation to establish a comparison of the effect of this second laser pulse, and was carried out for the same energy regimes applied in the first part of the experiment

<u>Results</u>

Results of the experiment are divided into two sections: In the first section energy dependent current traces and CCD images for both single and colliding are presented. Measurements of Faraday Cup traces were obtained for the energy intervals which have been mentioned for colliding plasmas, and both seed plasmas. Figure A1.2 represents some
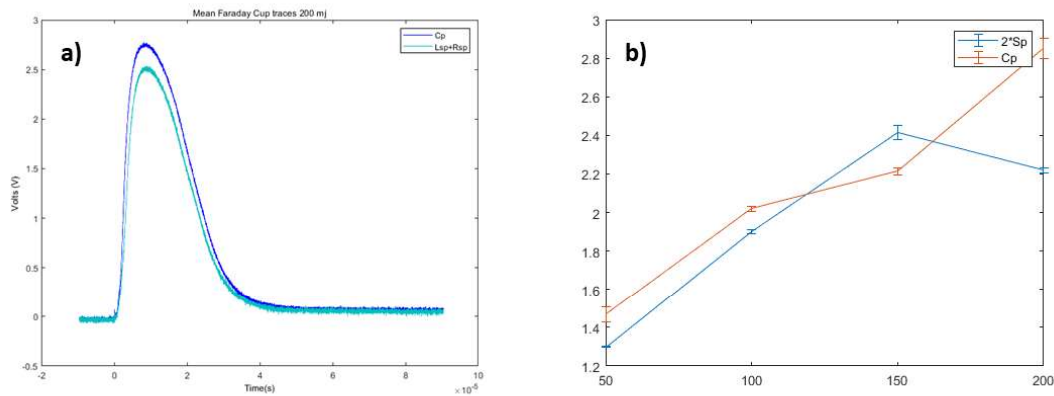
Figure A1.2: *a) Faraday Cup traces of colliding laser-produced plasmas compared to the sum of both seed plasmas at a laser energy of 200 mJ. b) Maxima of Faraday Cup traces of colliding plasmas and the sum of seed plasmas as a function of the laser pulse energy*

results obtained. In figure A1.2 a) are represented the Faraday cup traces obtained at an energy of 200 mJ for colliding plasmas, and the seed plasma multiplied by two. This comparison is realized to verify the formation of the stagnation layer in agreement to the Charge Yield Ratio (CYR) parameter [5]. This parameter establishes that stagnation layer has formed when the colliding plasma trace is greater than twice the seed plasmas trace. It is observed from figure A1.2 b) that only at 150 mJ the stagnation layer in colliding plasmas measurements was not observed, as its maximum value was below the expected trend when the pulse energy was increased. The maximum of seed plasmas at 200 mJ also does not follow the observed trend for the rest of measurements. Individual traces corresponding to these measurements were compared, and the outliers are explained by the irradiation of an area close to previous craters with deposition of particles from plasma plumes. This was confirmed during colliding plasmas imaging acquisition presented in figure A1.3. It can be observed the formation of stagnation layers at different intensities in all studied energies.

A second set of measurements at the studied energies was performed, with the addition of a second UV laser pulse in orthogonal configuration to the stagnation layer, and excited the space between the seed plasmas. The arrival of this second laser pulse was delayed in steps, as it has been mentioned previously. These measurements were carried out to evaluate whether the Faraday Cup signal from the stagnation layer could be improved. To visualize this goal, it was firstly measured the signal produced by the UV laser pulse without any interaction, and then, the contribution of the excited stagnation layer at each selected delay. The results from this temporal evolution of colliding laser-produced plasmas are presented in figure A1.4 a). It can be observed that there is only a decreasing trend at 50 and 200 mJ,
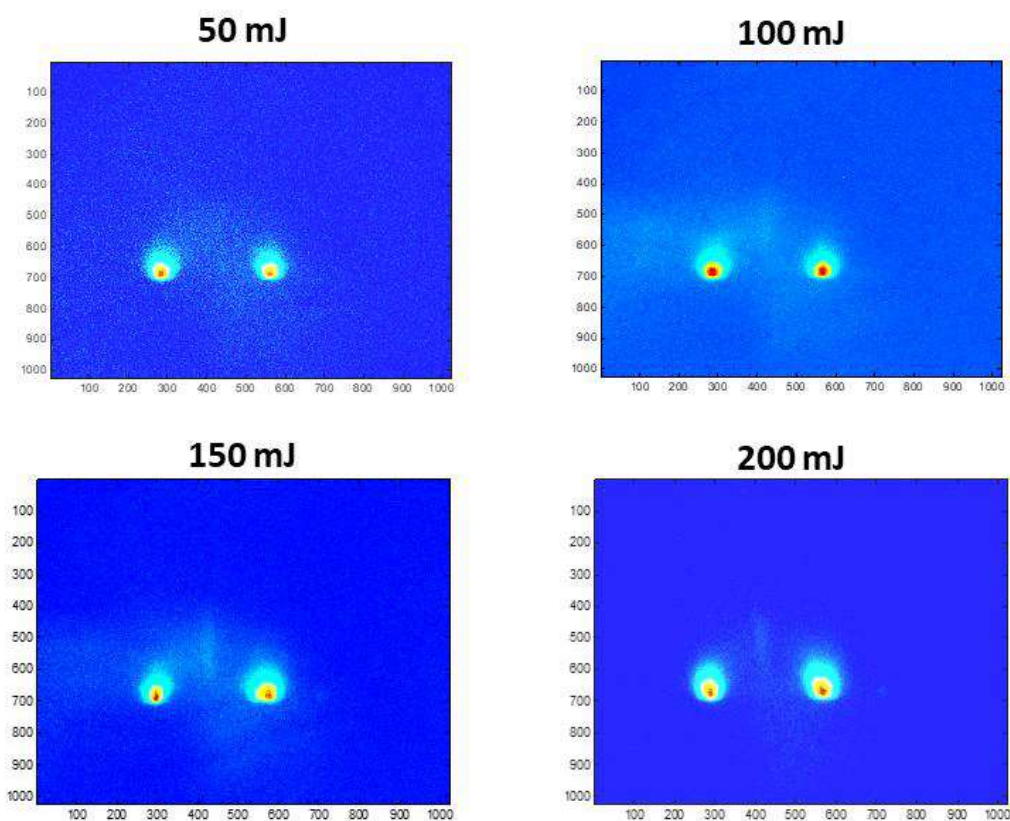
Figure A1.3: *Observation of the formation of stagnation layer between colliding plasmas on a tin sample at different irradiation energies with iCCD integrated images.*

while at 100 and 150 mJ it is negligible the decrease of the trace. It can be concluded that excitation of the stagnation layer with a second laser pulse maintains it at a constant value at 100 and 150 mJ.

It was also compared whether the temporal evolution of colliding laser-produced plasmas with the excitation of a second laser pulse provided higher traces than the reported during the first experiments. At 200 mJ, it was observed during the colliding plasmas measurements without additional laser excitation that the stagnation layer was well defined, so the contribution of a second laser pulse would not affect considerably the evolution of this system. At 50 mJ, however, it is observed that the maximum of the Faraday Cup traces was higher respect to the first set of measurements during 100 ns after irradiation, as it can be seen in figure A1.4 b). Despite it was proven the formation of a stagnation layer at this applied energy, the system would be in a softer regime of stagnation compared to results at higher laser energies. This means that the supplied energy with the second laser pulse contributed to enhance the formation of the stagnation layer.
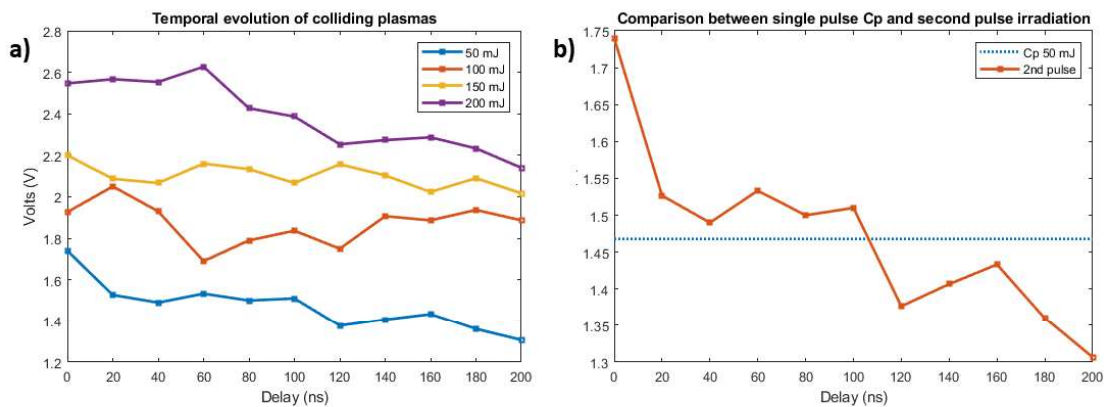
Figure A1.4*: a) Maxima from Faraday Cup traces after excitation with a second laser pulse at different delays respect to the first laser pulse. b) Comparison of the Faraday Cup traces at different delays (solid line) with the maximum obtained without excitation from a second laser pulse (dotted line) at 50 mJ*

These results should be complemented in order to provide a complete explanation with the analysis of kinetic energy distribution of all measurements. Moreover, images can be analyzed in more detail and the displacement and formation of the stagnation layer can be also studied. These further results are expected to be satisfactory to present a research article.

References

[1] H. Luna, K. D. Kavanagh, and J. T. Costello, Study of a colliding laser-produced plasma by analysis of time- and space-resolved image spectra, J. Appl. Phys. 101 (2007) 033302. http://dx.doi.org/10.1063/1.2431685

[2] P. Hough, C. McLoughlin, T. J. Kelly, P. Hayden. S. S. Harilal, J. P. Mosnier, J. T. Costello, Electron and ion stagnation at the collision front between two laser produced plasmas, J. Phys. D: Appl. Phys. 42 (2009) 055211. http://dx.doi.org/10.1088/0022-3727/42/5/055211

[3] P. Hough, C. McLoughlin, S. S. Harilal, J. P. Mosnier, and J. T. Costello. Emission characteristics and dynamics of the stagnation layer in colliding laser produced plasmas, J. Appl. Phys. 107 (2010) 024904. http://dx.doi.org/10.1063/1.3282683

[4] P. Hough. Laser, optical and electrical diagnostics of colliding laser-produced plasmas, Ph. D. Thesis (2010).

[5] P. Yeates, C. Fallon, E. T. Kennedy, and J. T. Costello, Charge resolved electrostatic diagnostic of colliding copper laser plasma plumes, Phys. Plasmas 18 (2011) 103104. http://dx.doi.org/10.1063/1.3633486
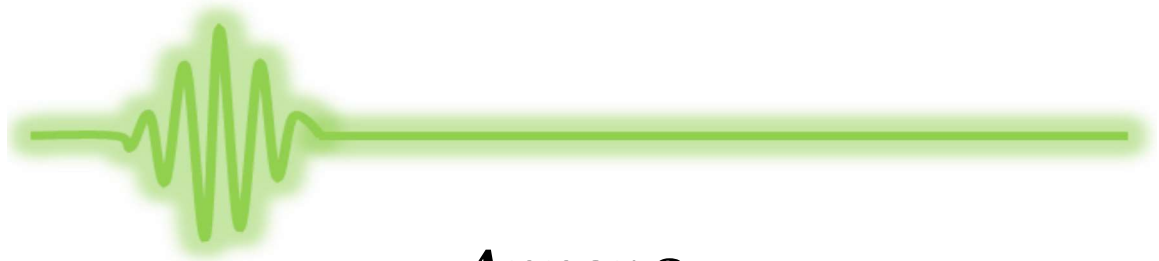
Annex 2.
Study on time-resolved pump-probe microscopy on porcine ocular tissues

ANNEX 2. STUDY ON TIME-RESOLVED PUMP-PROBE MICROSCOPY ON PORCINE OCULAR TISSUES

There is a great interest in the use of lasers in biological and medical applications. One of the most relevant application of lasers in medicine involves laser ablation of tissues in surgery. There are some remarkable properties of biological tissues which are relevant concerning to laser ablation. The composition and morphology of tissues define the optical properties and energy distribution during ablation mechanisms and final response to phase transformations. It should be noted that soft tissues are characterized by a high content of water and other components as proteins or chemical elements which vary their concentration depending on the type of tissue, as it has been demonstrated in studies using spectroscopic techniques to identify differences in tissues [1] or comparing models between water and human tissues [2-4].

In this sense, ocular surgery with laser has become very popular, as lasers enable manipulation and destruction of tissues with high precision. Despite the obvious increasing medical use of lasers, interaction of laser with biological tissues is still a topic of research, since it is the result of a complex mixture of processes and involves multidisciplinary areas of knowledge as thermodynamics, photochemistry or tissue biomechanics [5, 6].

Nevertheless, time-resolved studies of the processes induced in laser ablation are challenging for a deeper understanding and improving applications in surgery. Imaging techniques has proven their efficiency and are a useful tool to visualize these processes [7] and provide a high versatility to be adapted to the experimental conditions as temporal resolution or tissues.

Many studies have in laser ablation of biological tissues have been performed in animal tissues to ensure their validity in human tissues. It can be found in that ablation of ocular tissues have been studied in bovine cornea [8].

Pump-probe time-resolved microscopy have been used successfully in ultrashort laser-matter interaction. In this study, this technique was used to observe differences in morphological dynamics in different porcine ocular tissues, as sclera, cornea and lens, due to their similarity to human eye [9], which are remarked in figure A2.1. First results of this study are provided here, which can be used in further investigations to improve the experimental procedure, as well as image and data acquisition.
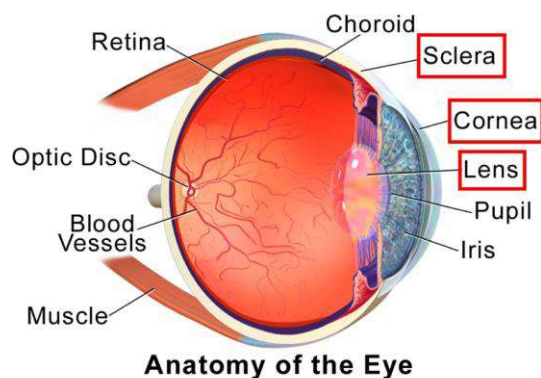
Figure A2.1: *Anatomy of the human eye. The tissues of interest studied on porcine eyes have been remarked in red squares. Image adapted from Wikimedia commons.*

These tissues were chosen in the study as they are responsible of focusing objects in the retina. The cornea is the transparent front part of the eye which covers the iris, pupil and anterior chamber. In humans, it has a fixed focusing power of approximately 43 dioptres. Its transparency is of relevant importance, as it is the most powerful focusing element, so a healthy cornea does not need blood vessels, and the oxygen and nutrients are supplied by tears through the outside surface, and by aqueous humour through the internal surface. The sclera is the white and opaque external layer of the eye. Cornea and sclera have a high and continuous content in type I collagen, but sclera presents an irregularity on their fibres, while cornea has a uniform distribution. The lens is a transparent tissue with biconvex form behind the iris and helps in the image formation in the retina by changing its shapes, so the eye can focus on objects at different distances. It is mainly composed by type IV collagen and transparent as the cornea, so it is absent of blood vessels.

Experimental details and results

In this experiment it was used tissues from porcine eye, as it is very similar to the human eye, and were studied the evolution of ablation by pump-probe technique which has been described in this thesis. Pump beam worked at 800 nm, and a fluence of 5 J/cm^2 while probe beam worked at 400 nm with a fluence below the ablation threshold of tissues. Porcine tissues were supplied and dissected by researchers of the Laboratory of Biomaterials Optics group from University of Granada, Spain. In this study, measurements were performed with dehydrated and hydrated tissues. The latter ones were conserved in aqueous solution to avoid osmosis processes. However, the vertical position of the sample holder was not adequate to observe hydrated tissues despite different attempts to solve this drawback, as
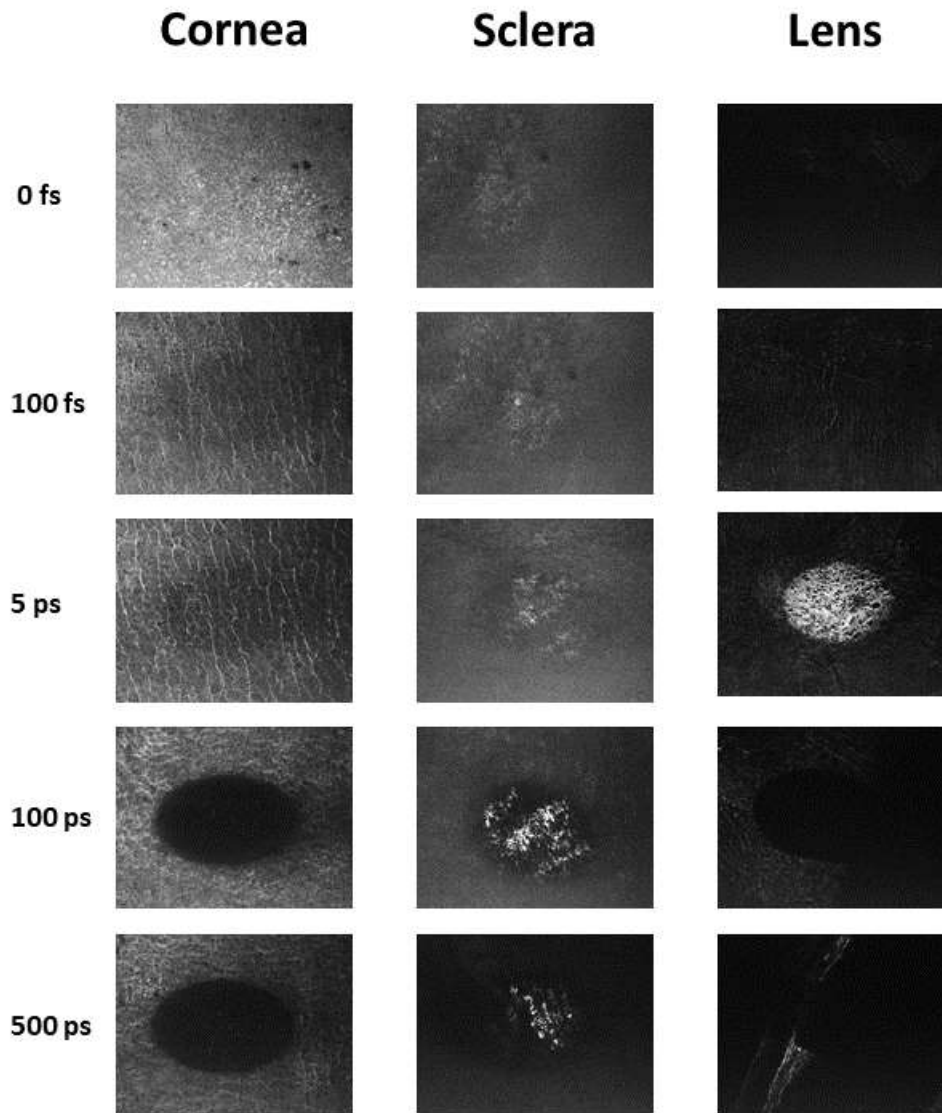
Figure A2.2: *Time-resolved micrographs of the three studied tissues under pump-probe microscopy at different delays after femtosecond laser irradiation at 5 J/cm². Brightness and contrast have been enhanced at identical levels to more detailed comparison.*

using microscope coverslips, and the experiment was finally carried out with dehydrated tissues.

It can be observed that tissues under the same experimental conditions followed a different temporal evolution, as seen in figure A2.2. Corneal tissues showed an early transformation after irradiation with ultrashort laser pulses in less than 1 ps. It is noteworthy that the

increase of reflectivity which has been reported in a wide variety of materials, as well as in results presented in this work in this case is not present. In a temporal lapse of 20 ps the irradiated area has been completely molten, associated to the decrease of the native reflectivity of the sample, and remains for all temporal delays measured. The sclera in opposition showed a light increase of reflectivity which remains for hundreds of picoseconds with an irregular distribution. These remarkable differences in the evolution of both tissues is due to the irregularities in the distribution of collagen fibres in the sclera and probe light is consequently scattered. Another possibility could be the formation of cavitation bubbles, as it was reported in a previous study [8], which can be discarded due to the low content in water of the dehydrated tissue. In the evolution of the lens the previous increase of reflectivity is observed, which has been reported as a general stage during excitation, followed by a decrease of the natural reflectivity of the tissue. However, it is observer at a considerably longer delay compared to inorganic materials, while at longer delays it showed a similar trend than the one reported for the cornea.

These results are supported by the temporal evolution of the reflectivity, which is shown in figure A2.3, but due to the irregular reflection of probe light these measurements did not provide reliable results on the sclera and are not shown in this annex. The evolution of cornea did not present the expected increase of the normalized reflectivity during excitation but at 1 ps it is observed the decrease of reflectivity which is associated to melting which reaches its minimum value at a delay of 50 ps. It has been described that under high fluence irradiation with ultrashort laser pulses dielectrics could experience ultrafast melting [10],
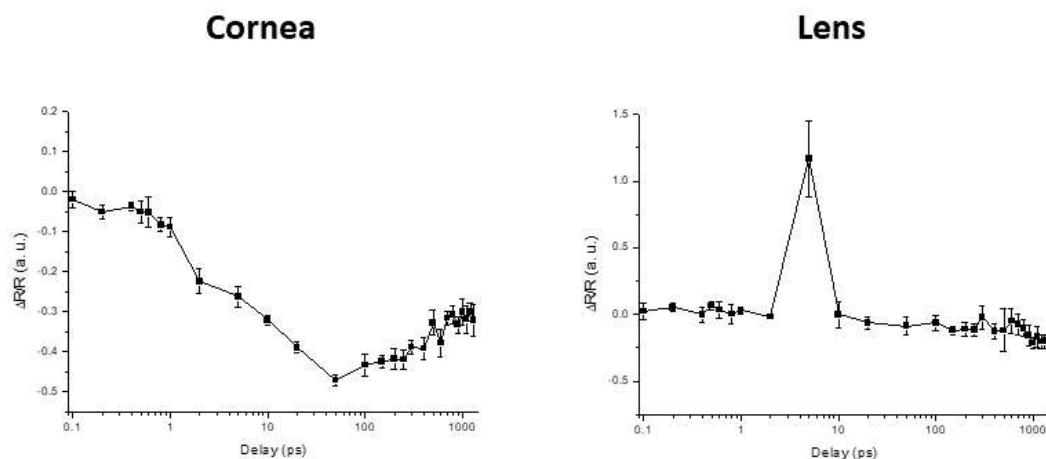
Figure A2.3: *Time-resolved normalized reflectivity of porcine cornea and lens at a fluence of 5 J/cm².*

Cornea **Sclera** **Lens**

Previous irradiation (only probe)

Permanet damage (∞)
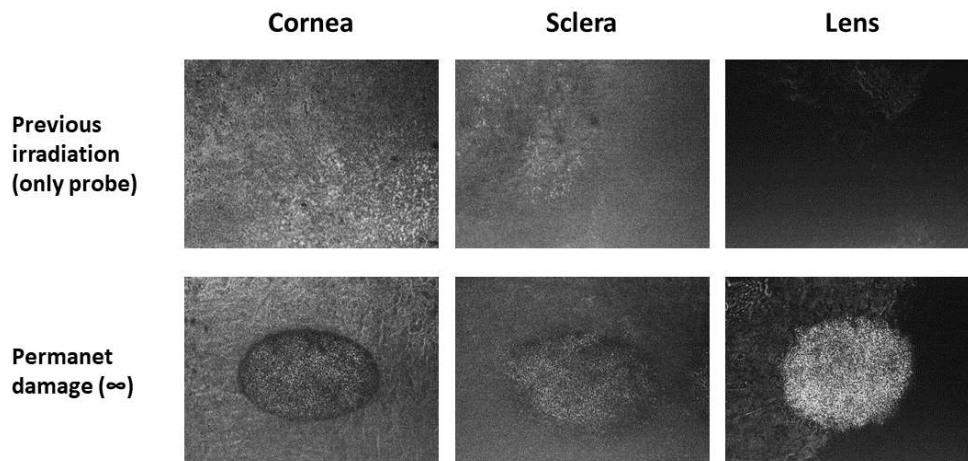
Figure A2.4: *Comparison of the three porcine eye tissues before and after irradiation with femtosecond laser pulses at 5 J/cm².*

but this assumption cannot be confirmed as it requires a more detailed study. Then it is observed a slight recovery but the normalized reflectivity remains at negative values.

On the other hand, lens presented a plateau in these measurements, but at 5 ps it is observed a high increase which has vanished at 10 ps, which is surprisingly delayed compared to excitation times observed in other materials. This effect should be further investigated to reveal whether this increase of reflectivity is attributed to electron excitation or a different process. After 10 ps, reflectivity goes negative values very close to 0, in opposition with the results related to corneal tissue.

The comparison of these three tissues before and after laser irradiation, once the permanent damage has appeared is shown in figure A2.4. In this figure strong differences can be observed. Cornea presented a well-defined crater and it can be observed that the texture of the tissue inside the crater is different. In contrast to these observations, sclera has a diffuse crater shape. Despite cornea and sclera have a similar composition, the orientation of collagen fibres could have had a crucial role during ablation process, and energy transport could have been affected. The most interesting result is shown again by lens, since its irradiated area presented a permanent damage with an increased reflectivity with the respect to rest of the sample, which means a strong change in the optical properties of this tissue during ablation process.

These results provided very interesting results which should be further investigated under a range of fluences to obtain a more detailed knowledge on their ablation dynamics.

Moreover, the study should be compared and integrated using additional techniques to clarify how their optical properties of the tissues have varied after irradiation and the role of their composition. An improvement in the experimental set up could also help to obtain information in hydrated tissues.

References

[1] S. Moncayo, F. Trichard, B. Busser, M. Sabatier-Vincent, F. Pelascini, N. Pinel, I. Templier, J. Charles, L. Sancey, V. Motto-Ros, Multi-elemental imaging of paraffin-embedded human samples by laser-induced breakdown spectroscopy, Spectrochim Acta B 133 (2017) 40–44. http://dx.doi.org/10.1016/j.sab.2017.04.013

[2] N. Nishirriura, C. B. Schaffer, E. H. Li, and E. Mazur, Tissue ablation with 100-fs and 200-ps laser pulses, Proceedings of the 20th Annual International Conference of the IEEE Engineering in Medicine and Biology Society. Vol.20 Biomedical Engineering Towards the Year 2000 and Beyond (Cat. No.98CH36286), Hong Kong, China, 4 (1998) 1703-1706. http://dx.doi.org/10.1109/IEMBS.1998.746912

[3] A. Hansen, R. Géneaux, A. Günther, A. Krüger, and T. Ripken, Lowered threshold energy for femtosecond laser induced optical breakdown in a water-based eye model by aberration correction with adaptive optics, Biomed. Opt. Express 4 (2013) 852-867. https://doi.org/10.1364/BOE.4.000852

[4] N. Linz, S. Freidank, X.-X. Liang and A. Vogel, Wavelength dependence of femtosecond laser-induced breakdown in water and implications for laser surgery, Phys. Rev. B 94 (2016) 024113. https://doi.org/10.1103/PhysRevB.94.024113

[5] A. Vogel, and V. Venugopalan, Mechanisms of Pulsed Laser Ablation of Biological Tissues, Chem. Rev. 103 (2003) 577–644. https://doi.org/10.1021/cr010379n

[6] K. Plamann, F. Aptel, C. L. Arnold, A. Courjaud, C. Crotti, F. Deloison, F. Druon, P. Georges, M. Hanna, J.-M. Legeais, F. Morin, É. Mottay, V. Nuzzo, D. A. Peyrot and M. Savoldelli, Ultrashort pulse laser surgery of the cornea and the sclera, J. Opt. 12 (2010) 084002. https://doi.org/10.1088/2040-8978/12/8/084002

[7] K. R. Rau, A. Guerra, A. Vogel, V. Venugopalan, Investigation of laser-induced cell lysis using time-resolved imaging, Appl. Phys. Lett. 84 (2004) 2940-2942. https://doi.org/10.1063/1.1705728

[8] T. Juhasz, G. A. Kastis, C. Suárez, Z. Bor, W. E. Bron, Time-resolved observations of shock waves and cavitation bubbles generated by femtosecond laser pulses in corneal tissue

and water. Lasers Surg. Med. 19 (1996) 23-31. https://doi.org/10.1002/(SICI)1096-9101(1996)19:1<23::AID-LSM4>3.0.CO;2-S

[9] J. Kampmeier, B. Radt, R. Birngruber and R. Brinkmann, Thermal and Biomechanical Parameters of Porcine Cornea, Cornea 19(3) (2000) 355-363.

[10] B. Rethfeld, A. Kaiser, M. Vicanek, and G. Simon, Ultrafast dynamics of nonequilibrium electrons in metals under femtosecond laser irradiation, Phys. Rev. B 65 (2002) 214303. https://doi.org/10.1103/PhysRevB.65.214303